

POLITECNICO DI TORINO

Master's Degree in Mechatronic Engineering
Dipartimento di Automatica e Informatica



**Politecnico
di Torino**

Master's Degree Thesis

**Design and Evaluation of a Fuzzy comfort-oriented
speed profile generator for autonomous passenger
cars**

Supervisors:

Prof. Andrea Tonoli

Prof. Nicola Amati

Co-supervisors:

Stefano Feraco

Sara Luciani

Candidate:

Giuseppe Mandraffino

Anno Accademico 2020 - 2021

Abstract

”During the past twenty years, autonomous driving has moved from the realm of science fiction to a very real possibility”. [1] With the growing interest in self-employed vehicles, the problem of motion sickness may be so important that not addressing it may limit the users’ acceptance, reducing the safety and environmental impact of autonomous vehicles.

The comfort of an autonomous vehicle is mostly related to the control algorithm. An autonomous vehicle’s control consists mainly of three interconnected modules: environment perception, path planning and vehicle control.

In view of this, the current study presents a method based on a Fuzzy Logic Controller aiming to compute a suitable reference speed profile in order to optimize the passengers’ comfort and control performances. To this end, the amount of vibration transmitted to the passengers and the probability to experience motion sickness are evaluated considering two comfort indexes extracted by ISO 2631.

This thesis work can be divided into four parts. After a deep analysis of the state of art and an investigation of the main modules that constitute the overall architecture of an autonomous vehicle, in the first part of the thesis the Fuzzy Logic Controller is designed. In the second part of the thesis work, a 3 degrees of freedom vehicle model is used to model the vehicle dynamics and simulations are conducted in virtual scenarios created using Automated Driving Scenario Toolbox[®] on MATLAB[®] and Simulink[®]. In the third part of the thesis work, the simulated experiments are performed on Simscape Vehicle Template where the vehicle dynamics are modeled using a complete vehicle model with 15 degrees of freedom. In the last part, the comfort indexes of driver and passengers are evaluated.

The study focuses on three different scenario; an highway scenario where the path is straight and the maximum speed is set to 130 km/h, an interurban scenario with fairly straight road and slight curves with maximum speed set to 70 km/h and a competition race track with sharp curves and maximum speed set to 70 km/h.

The effectiveness of the comfort optimization method results in a lower percentage of people who may experience nausea and in a lower value of equivalent acceleration perceived by the passengers compared to the classical approach.

Contents

1	Introduction	1
1.1	History of Autonomous Vehicle Technologies	2
1.2	SAE autonomous vehicle standard levels	7
1.2.1	Driving-Assistance Systems	9
1.2.2	Advanced Driving-Assistance Systems	11
1.3	State of Art	14
1.4	Thesis outline	18
2	Perception	21
2.1	Sensors	22
2.1.1	LIDAR	22
2.1.2	RADAR	23
2.1.3	Ultrasonic sensor	23
2.1.4	GPS	24
2.1.5	Camera	25
2.2	Lanes detection	26
3	Trajectory and velocity planning	28
3.1	Reference path generator	28
3.2	Reference velocity generator	32
3.2.1	Fuzzy Logic Controller	33
3.2.2	Membership functions	36
3.2.3	Rules	38
3.3	Motion sickness state of art	39
3.3.1	Comfort coefficients computation	40
3.3.2	a_{eq} comfort coefficient	40
3.3.3	Motion sickness dose value	45
4	Modelling	48
4.1	Reference frame and vehicle coordinates	49
4.2	3 DOF vehicle model	51
4.2.1	Kinematic Model	51
4.2.2	Dynamic Model	55
4.2.3	Parameterized Vehicle Model for Adaptive MPC	60

4.3	15 DOF vehicle model	65
4.4	Model Predictive Control	71
5	Validations and results	74
5.1	Driving Scenario Simulator	74
5.2	3 Degrees of Freedom vehicle model validation and results	78
5.3	15 Degrees of Freedom vehicle model validation and results	88
5.4	Passengers' comfort results	98
6	Conclusions and future works	102

CHAPTER 1

Introduction

According to the United States Department of Transportation (USDOT) "With 94 percent of fatal vehicle crashes attributable to human error, the potential of autonomous vehicle technologies to reduce deaths and injuries on our roads urges us to action. It's estimated that autonomous vehicle can reduce accidents by up to 90%, saving 30,000 lives a year. Less accidents mean less traffic congestion. This will most likely result in a reduction of CO2 emissions as well." [2]

As stated in the Ohio University's Future of Driving report: "Since software will drive the car, the modern vehicle can now be programmed to reduce emissions to the maximum extent possible. The transition to the new-age cars is expected to contribute to a 60% fall in emissions." [3]

Moreover, "Autonomous vehicles may cut travel time by up to 40 percent, recover up to 80 billion hours lost to commuting and congestion, and reduce fuel consumption by up to 40 percent" according to KPMG. [2]

These and many more are the advantages that the autonomous technologies can bring to our society. Considerable work and research have been done to develop reliable and performing control strategies, however, the latter do not address exhaustively the optimization of the passengers' comfort. To this end, in this thesis work a Fuzzy comfort-oriented speed profile generator has been design in order to optimize the passengers' comfort and control performances of autonomous vehicles.

A brief history of autonomous vehicle technologies, autonomous driving levels and nowadays technologies are presented in this chapter. Finally, an overview of the state of art of autonomous vehicles and Fuzzy Logic Controller are provided.

1.1 History of Autonomous Vehicle Technologies

”Autonomous technology is transforming industries ranging from automotive to insurance to healthcare. The opportunity to realize passive yet intelligent control is enabling innovation almost as fast as its creators can dream it up. However, the speed of advancement makes us wonder how the revolution started.” [4]

In the following section, a timeline of the most important technologies that led to the appearance of autonomous vehicles is presented.

Even if it may seem a recent topic, the prospect of autonomous transportation followed a progressive path that started with Leonardo da Vinci in the sixteenth century.

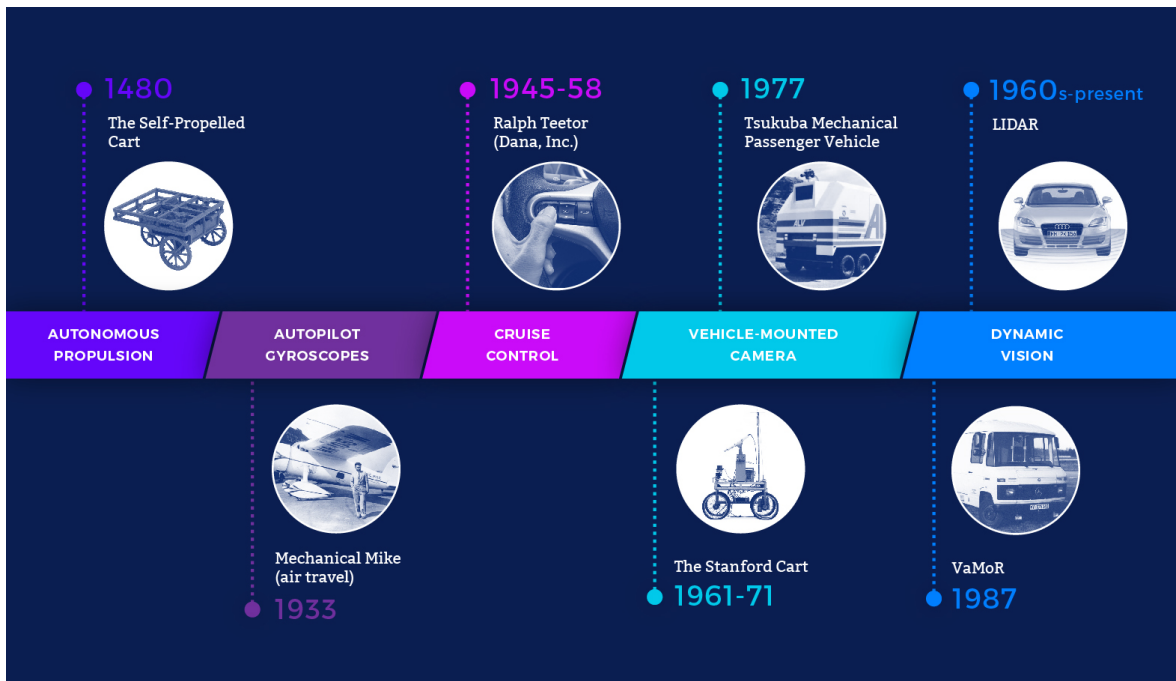


Figure 1.1: History of Autonomous Vehicle Technologies [4]

Leonardo da Vinci – The Self-Propelled Cart, 1480 In the sixteenth century, Leonardo da Vinci designed a self-propelled cart that was intended to be used in the theater. The cart could move without external stimuli since the power was generated by torsional springs under high tension and the steering command was set in advance given a pre-programmed path.[4]

The cart is considered, by the automotive community, the world’s first robot.



Figure 1.2: A self-propelled cart replica at museum Clos Lucé [5]

Wiley Post – Mechanical Mike (air travel) ”Mechanical Mike” was a prototype autopilot designed by Sperry Gyroscope Co., and used by Wiley Post during an around-the-world flight in 1933. It employed gyroscopes that were used to collect data from all three dimensions. One of these was a directional gyroscope, which provided data for the heading control of the airplane. The other was a horizontal gyroscope, that provided data for longitudinal and lateral control of the airplane. These data were used to calculate the position and motion of the plane.[4]

Gyroscopes have made a great contribution to the development of autonomous technologies and still remain an important part of autonomous vehicles.



Figure 1.3: Wiley Post’s Autopilot “Mechanical Mike” [6]

Ralph Teetor Cruise Control(Dana, Inc.), 1945-1958 The first cruise control system was developed by the German engineer Ralph Teetor in 1945. Cruise control takes over the mechanical throttle of a vehicle to maintain a steady speed that the driver can set.

Developments over the following decade led to commercialization of the device in 1959, when, GM was the first company who installed the device in its Cadillac model.

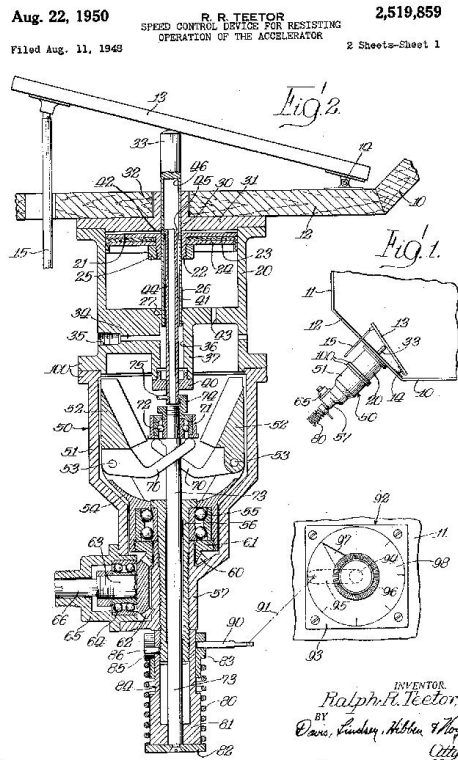


Figure 1.4: Ralph R. Teetor’s Cruise Control [7]

James Adams and Les Earnest Stanford Cart, 1961-71 To validate the assumption that a car could drive on the moon while being remotely controlled on Earth, James Adams, a Stanford University student, built "The Cart", as it was called. However, the 2.5 seconds delay in the timing of signal communication from Earth to the moon put an end to Adams’s research. Few years later, Les Earnest proposed to convert the cart into a road vehicle equipped with a video camera on the top to navigate. Based on images received through the camera, the vehicle was able to detect and autonomously follow a solid white line on the ground. Nowadays, cameras are a crucial elements of autonomous vehicle.

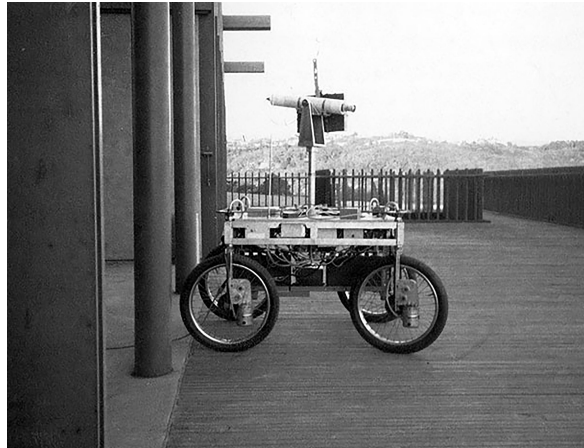


Figure 1.5: James Adams and Les Earnest Stanford Cart [8]

Tsukuba Mechanical – Passenger Vehicle, 1977 Improving the work developed by James Adams and Les Earnest in Stanford Cart, Japanese firm Tsukuba built an autonomous passenger vehicle able to travel at a speed of 20 miles per hour that could detect lane road boundaries using two vehicle-mounted cameras. It is considered the first truly autonomous vehicle.



Figure 1.6: Tsukuba Mechanical, Passenger Vehicle, 1977 [9]

Ernst Dickmanns – VaMoR, 1987 German engineer Ernst Dickmanns and his team equipped a Mercedes van with a bank of video cameras and a series of micro processor in order to sense the surrounding environment of the vehicle and to detect object and lane markers on the road. The key innovation of Dickmanns was the so called "dynamic vision", a processing images algorithm that was able to emphasize the relevant feature of the image and filter out the less important information. VaMoR was able to navigate Germany's highway at speeds up to 100 kilometer per hour.



Figure 1.7: Ernst Dickmanns – VaMoR, 1987 [10]

LIDAR, 1960s-present The outspread use of lasers in the last decades facilitated the invention of LIDAR (light detection and ranging). It is a remote sensing technique that allows to discover the distance of an object or surface using a laser pulse. The time that the laser takes to return to the origin is used to create a three-dimensional map of the environment around the vehicle.

The main difference between LIDAR and its predecessors SONAR (sound detection and ranging) and RADAR (radio detection and ranging), is that LIDAR uses ultraviolet wavelengths, in the visible or near infrared. This makes it possible to locate and obtain images and information on very small objects, of a size equal to the wavelength used.

”Coupled with modern GPS systems, LIDAR represents the most enabling technology for the recent momentum in the autonomous vehicle industry.” [4].

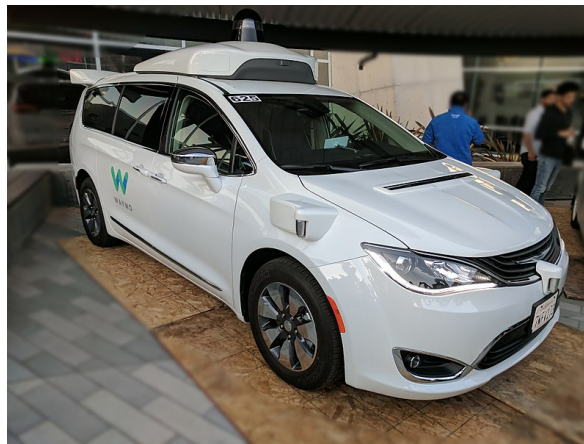


Figure 1.8: A LIDAR sensor mounted to an autonomous car [4]

1.2 SAE autonomous vehicle standard levels

The Society of Automotive Engineers (SAE) developed a classification system that defines the degrees of driving automation, ranging from 0 (fully manual) to 5 (fully autonomous). These six levels have been adopted by the U.S. Department of Transportation and the document is considered a global standard in automated vehicle technology.

Moreover, “SAE J3016™: Taxonomy and Definitions for Terms Related to On-Road Motor Vehicle Automated Driving Systems” was delivered to guide the manufacturers in the design, testing and development of highly automated vehicles.[11]

In the following, a brief explanation of the different levels of driving automation, illustrated in Figure 1.9, is presented

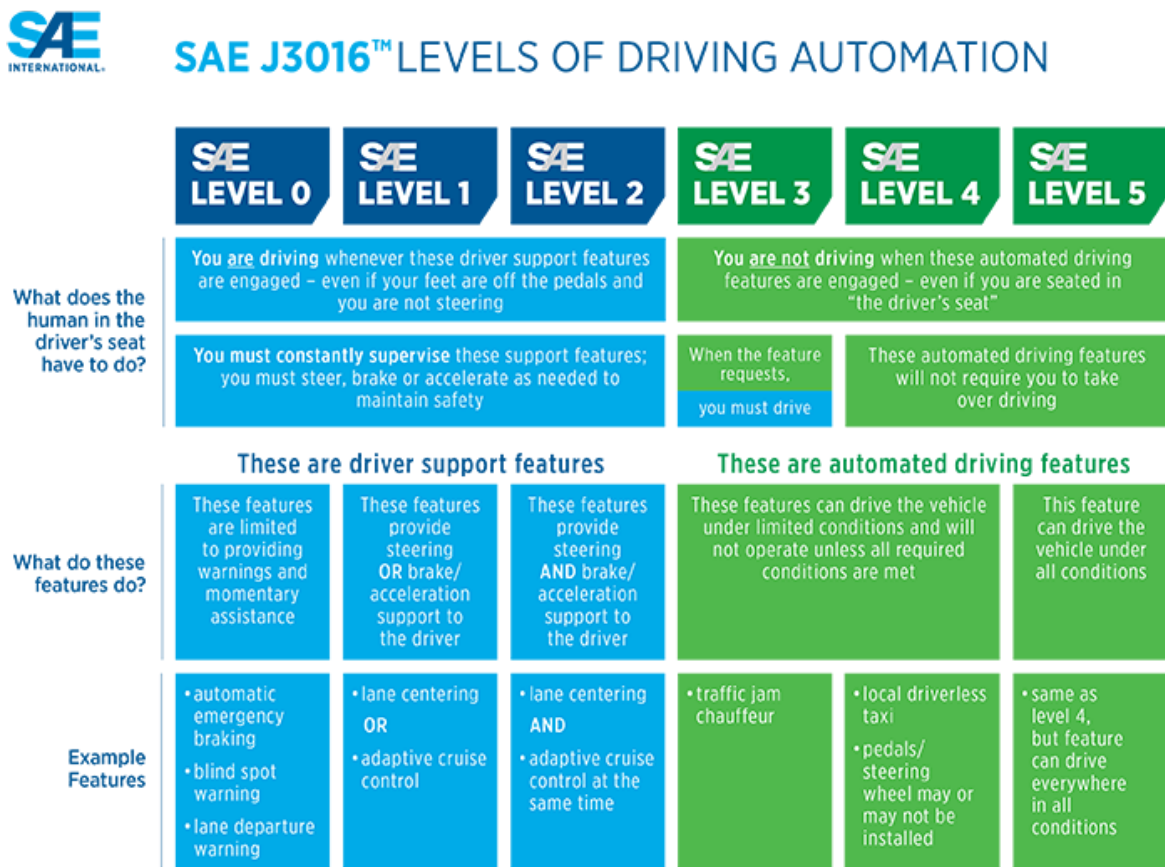


Figure 1.9: SAE autonomous vehicle standard levels [11]

- *Level 0*: Zero automation. The human driver takes care of all the aspects of the driving tasks, even if there may be systems in place to help the driver. An example would be the emergency braking system, since it actually does not "drive" the vehicle, and for this reason it is not certified as automation. Nowadays, the major on-road vehicles are Level 0.[12]
- *Level 1*: The human driver is sometimes assisted by a single advanced driver assistance system (ADAS) that manages either the steering or braking/accelerating command but not both simultaneously. A car equipped with a cruise control system is considered as Level 1 since the vehicle is able to maintain a safety distance from the preceding car but the driver monitors the other aspects of the driving task. This is the lowest level of automation.
- *Level 2*: An advanced driver assistance system (ADAS) is installed in the vehicle and it is able to control both the steering or braking/accelerating command. However, the human driver must continue to pay full attention at all times. "Tesla Autopilot and Cadillac (General Motors) Super Cruise systems both qualify as Level 2".[12]
- *Level 3*: From Level 2 to Level 3 there is a significant improvement from a technological point of view. Indeed, Level 3 vehicles have "environmental detection" capabilities. Under some circumstances the automated driving system (ADS) on the vehicle can perform all aspects of the driving task and make decisions for itself. Level 3 cars still require human override.
- *Level 4*: Level 4 vehicles can operate in self-driving mode since an automated driving system (ADS) on the vehicle can itself perform all driving tasks and monitor the driving environment. However, due to legislation and infrastructure limits, the Level 4 vehicle can go in self-driving mode only in limited areas where the speeds reach an average of 50 km/h.[17]
- *Level 5*: Human attention is not required at all times in Level 5 autonomous vehicles. The occupants are considered only passengers and they are not involved in the "dynamic driving tasks". Steering wheels or acceleration/braking pedals would not be present. "Currently there are no companies that are able to offer a fully autonomous ride in any conditions, on any road, with no human overseer".[13]

Level 4 technology has been achieved by the leaders in autonomous driving but only in limited area and under specific circumstances such as good weather and road conditions. Nowadays, autonomous cars available in the market are still stably at Level 3 technology.

1.2.1 Driving-Assistance Systems

In the following paragraph, the most important driving-assistance systems are illustrated and briefly explained. Driving assistance systems have the potential to save lives reducing traffic crashes. In Figure 1.10 is illustrated the timeline development of driving assistance technologies.



Figure 1.10: Timeline of driving assistance technologies[17]

Cruise control system: Cruise control takes over the mechanical throttle of a car to maintain a constant speed that can be set by the driver. However, the driver can always press the throttle pedal to increase the speed of the vehicle, if needed. This electronic system is particularly useful for long drives along highway or in poorly populated road, reducing driver fatigue and improving passenger's comfort.

Anti-lock Braking System (ABS) "Emergency braking or even braking on a wet or slippery surface can cause the wheels of the vehicle to lock. Locking wheels reduce the adhesion between tires and the road surface and make the vehicle unsteerable. The anti-lock braking system (ABS) prevents the wheels from locking and enables safe braking".[14] ABS system comprises an electronic control unit ECU, four wheel speed sensors, a return pump and hydraulic valves that manage the pressure of the breaking system in each wheel. If a wheel is about to lock the ECU reduces the pressure on the braking system on that wheel until it turns freely again, afterward the breaking pressure is increased again.

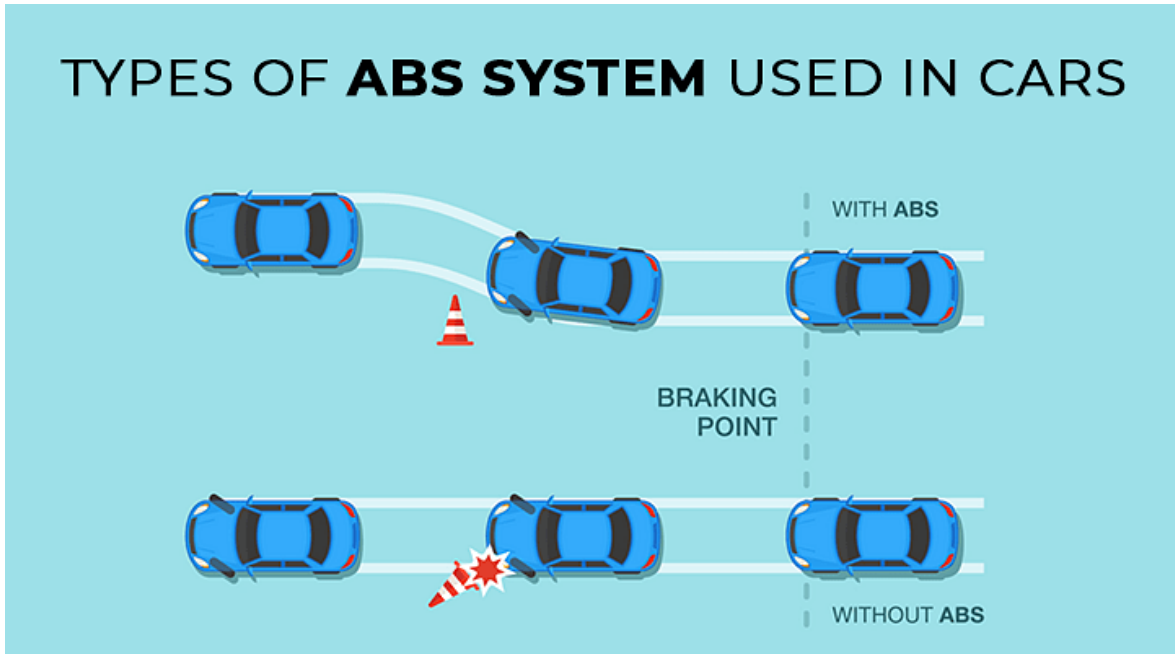


Figure 1.11: Anti-lock Braking System (ABS) [15]

Electronic Stability Control The electronic stability control system is able to correct oversteer and understeer situations that occur both in the case of incorrect cornering and in the case of a sudden change in trajectory. Moreover, the system detects vehicle skidding movements and actively counteracts them. Based on the data acquired from the wheels speed sensors, ABS system, steering angle and other sensors, the electronic stability control system intervenes to re-stabilize the vehicle by braking the individual wheels and acting on the engine delivery.[16]

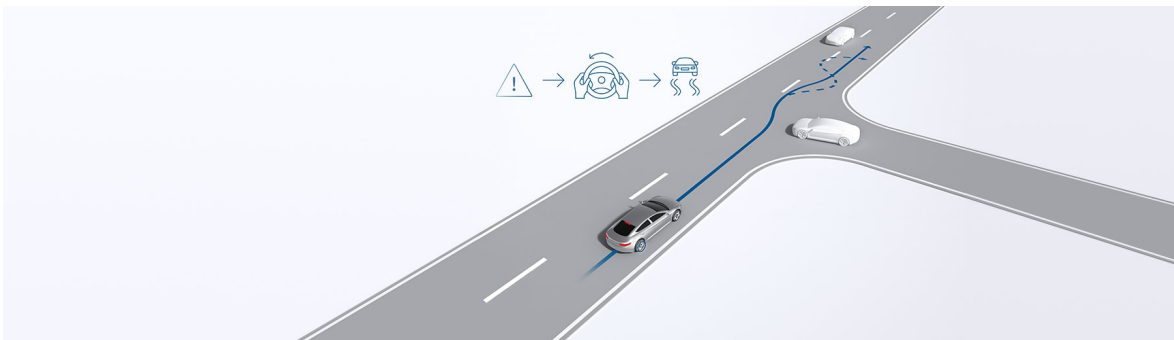


Figure 1.12: Electronic Stability Control [16]

Forward collision warning Based on the vehicle speed, the speed of the vehicle in front of the car and the distance between the vehicles, the Forward Collision Warning system warns the driver of a proximate crash if the distance between the two vehicles is under a certain threshold.[17]

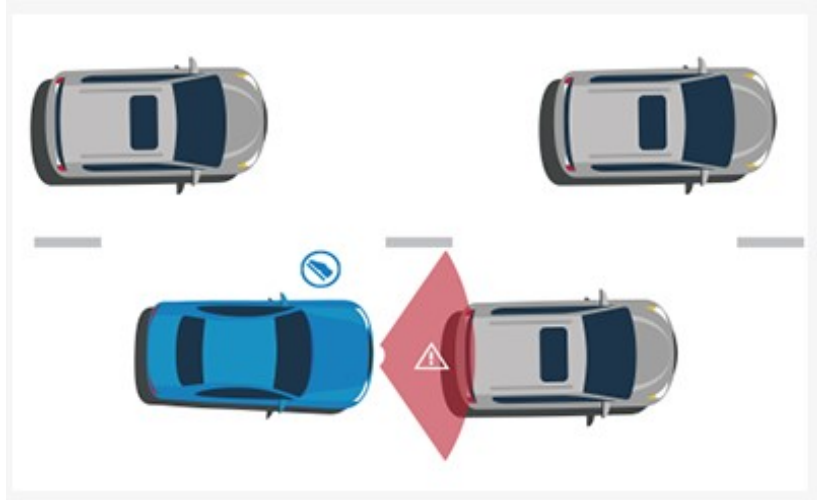


Figure 1.13: Forward collision warning [17]

Lane departure warning "Monitors the vehicle's position within the driving lane and alerts the driver as the vehicle approaches or crosses lane markers".[17]

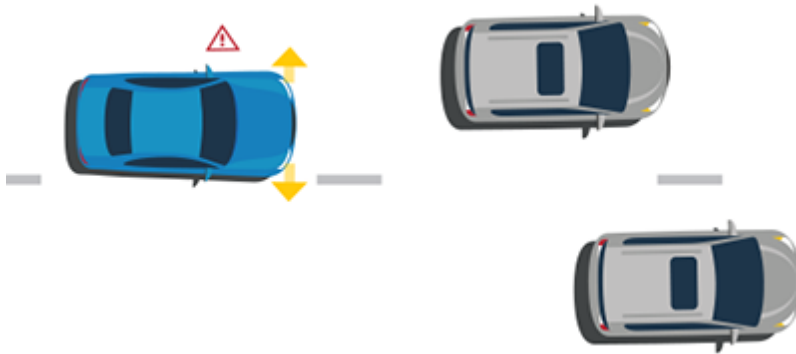


Figure 1.14: Lane departure warning [17]

1.2.2 Advanced Driving-Assistance Systems

The wide scale use of sensors and microprocessors in the last decade has facilitated the invention of new technologies that help the human driver in the driving tasks. Advanced Driving Assistance Systems (ADAS) are the evolution systems of Driving Assistance Systems (DAS).

In the following paragraph, the most important ADAS are illustrated and briefly explained.

Automatic Emergency Braking Rear-end crashes are common on our roadways. They are mostly due to distraction or inattentiveness when driving. Automatic emergency braking system applies the vehicle's brakes if it detects that the distance to the preceding vehicle is becoming critically short. First, the system warns the driver via an audible signal, then, if the driver doesn't apply a sufficient braking force or he brakes late, the system provides braking support. Moreover, if the system detects an unavoidable accidents, it prepares the vehicle and the seat belts to the collision. [18]

Recent Automatic emergency braking system are able to detect pedestrians in the vehicle's trajectory using information from forward sensors.

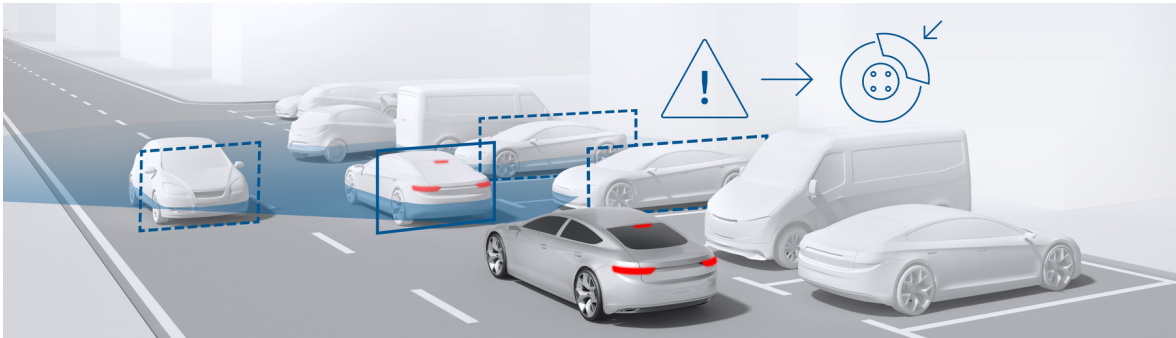


Figure 1.15: Automatic Emergency Braking [18]

Adaptive Cruise Control Unlike the standard Cruise Control, the Adaptive Cruise Control provides dynamical maintenance of the speed. The set speed will be automatically reduced or increased to maintain a predefined minimum distance from the preceding vehicle. The Adaptive Cruise Control uses a radar or laser sensor to monitor the distance to the vehicle traveling in front and, if this distance falls below the safety threshold, it reduces the speed of the car. When the road is clear again, Adaptive Cruise Control automatically brings the car back to the initially desired cruising speed. The adaptive cruise control can reduce stress for the driver and it is typically used for long drives along highway.

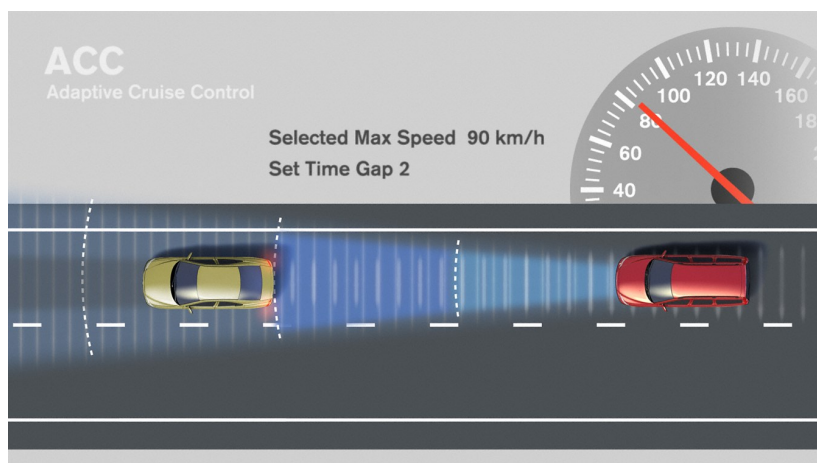


Figure 1.16: Adaptive Cruise Control [19]

Lane keeping assistance Lane assist limits the risk of unintentionally drifting out of lane, which is often source of road accidents. Through a sensor camera normally positioned behind the windshield, the Lane keeping assistance system detects the continuous and dotted lines on the road and identifies the lane in which the vehicle is travelling. When the car tends to diverge from the ideal trajectory, giving the sensors the idea that an unintentionally exit from the lane is taking place, the system intervenes promptly. In the case of the Lane departure warning, the electronic control unit (ECU) activates an acoustic signal or a vibration of the seat or steering wheel to bring the driver's attention back. In the case of Lane keep assist, the device also comes into play to bring the car back to the center of its lane thanks to commands to the steering and braking system, with an action that can be selective on each individual wheel. Moreover, the keeping assistance system intervenes with a slight resistance on the steer in case the driver is changing lane without using the indicator.[20]

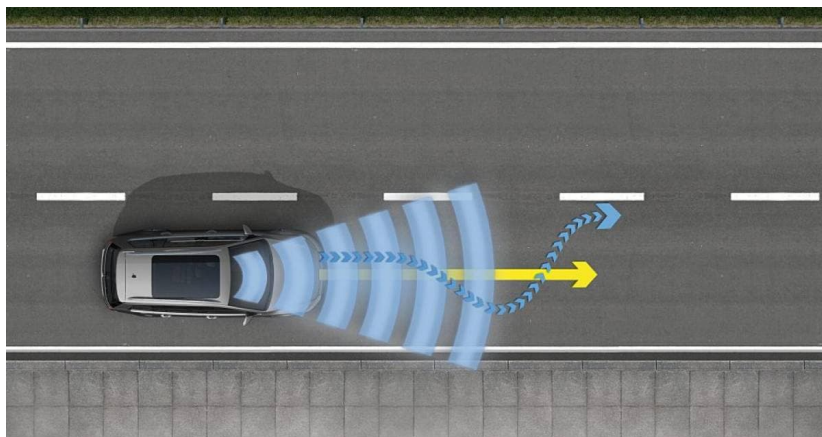


Figure 1.17: Adaptive Cruise Control [20]

1.3 State of Art

With the growing interest in self-employed vehicles, the problem of motion sickness may be so important that not addressing it may limit the users' acceptance, reducing the safety and environmental impact of autonomous vehicles.

State of the art regards the development of a method based on a Fuzzy Logic Controller aiming to compute a suitable reference speed profile in order to optimize the passengers' comfort and control performances. In the following paragraph, the progress of the thesis work is presented.

In the first part, an overview of the literature has been done. An investigation of the main modules that constitute the overall architecture of an autonomous vehicle is done in order to familiarized with the thesis' topic and to understand the formulas and symbols used in autonomous vehicle field. The global architecture of an autonomous vehicle is presented in the following figure together with a brief explanation of the main blocks that constitute it.

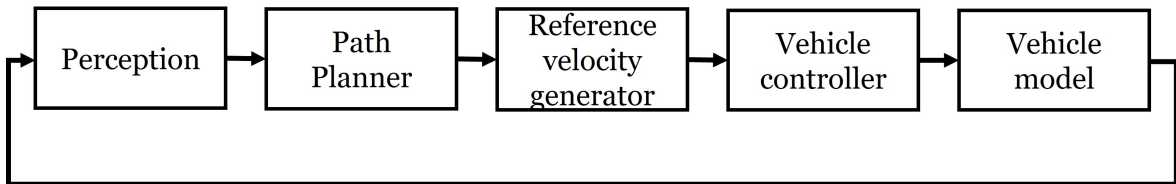


Figure 1.18: Autonomous vehicle architecture

- **Perception:** Meaningful information of the environment are acquired from camera LIDAR and RADAR sensor
- **Path planner:** Given the pose of the vehicle, the coordinates of the obstacles and the lane markings, an algorithm computes the reference trajectory.
- **Reference velocity generator:** Determines a suitable reference speed profile with satisfying control performances. In this thesis work a fuzzy comfort-oriented speed profile generator is used.
- **Vehicle controller:** The controller elaborates the input data and calculates the acceleration and steering commands to provide to the vehicle model.
- **Vehicle model:** The acceleration and steering commands are used by the vehicle model in order to modify its longitudinal and lateral dynamics

In the second part of the thesis, a deep review of the Fuzzy Logic and motion sickness topics present in the literature has been done. Afterwards, the Fuzzy Logic Controller was designed.

Fuzzy Logic Controller

Fuzzy logic is an extension of Boolean logic by Lotfi Zadeh in 1965 and it is a way to model logical reasoning where the truth of a statement is not binary, as in classical logic, but rather it is a degree of truth that ranges from zero (absolutely false) to one (absolutely truth). Fuzzy Logic allows to design Fuzzy Logic Controller which is a function that interprets the values of the input vector and, on the basis of sets of rules defined a-priori by the experimenter (if-then mechanism), assigns the value to the output vector. In this thesis work the main goal of the Fuzzy Controller is to determine a suitable reference speed profile combined with satisfying control and comfort performances.

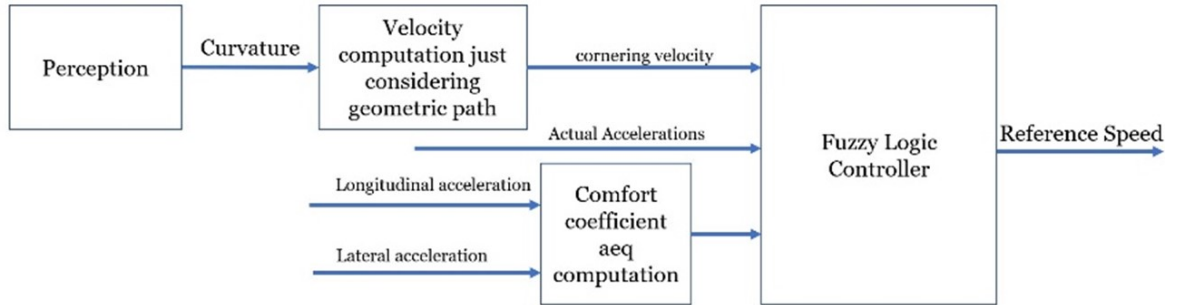


Figure 1.19: Fuzzy Logic Controller Architecture

The environment perception block receives the images data acquired in real-time from the sensors installed in the vehicle, namely Lidar, Radar and camera. The merging of these sensor data provides information on the surrounding environment, such as lane boundaries and obstacles location. Specifically, the path planning algorithm inside the perception block, processes the acquired data and returns the poses of the vehicle and the road curvature of the computed trajectory. From these information and the measurements of the vehicle's states in real-time, the reference trajectory and cornering velocity are computed. The cornering velocity, the actual accelerations of the vehicle and the comfort coefficient a_{eq} are the inputs of the Fuzzy Logic Controller that, based on sets of rules, computes the reference speed profile.

Comfort coefficients computation

The conflict theory by Reason and Brand (1975) is considered, in the recent past, the main theory that better explains Motion sickness: the acceleration perceived by the sense organs conflicts with the expected one determined on the basis of previous experience, generating a conflict leading to Motion sickness. ISO 2631 describes ways to evaluate vibration exposure to the human body. The quantified comfort measures of ISO2631-1 are based on frequency weighted root mean square ,RMS, computations of acceleration data. In this study, two indexes have been considered. The first index (a_{eq}) is computed as follows:

$$a_{W,i,RMS} = \left(\frac{1}{T} \int_{t_0}^{t_f} a_{W,i}^2(t) dt \right)^{\frac{1}{2}} \quad (1.1)$$

Where T_f is the exposure period time, $a_{W,i}$ the frequency weighted acceleration and W_i frequency weighted function.

The equivalent acceleration index is then calculated as follow:

$$a_{eq} = k_x^2 a_{x,W}^2 + k_y^2 a_{y,W}^2 \quad (1.2)$$

where, $k_x = k_y = 1$

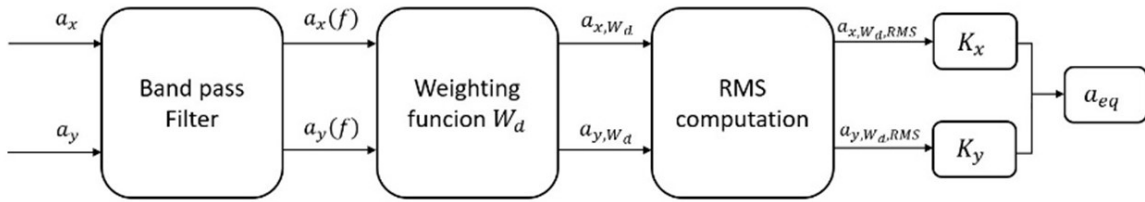


Figure 1.20: Comfort coefficient computation procedure

In Figure 1.20 it is shown the procedure to compute the comfort coefficient a_{eq} . A band pass filter is applied to the longitudinal and lateral acceleration. Then, the resulting accelerations are multiplied by a weighting function W_d and finally the root mean square is computed.

The second index called Motion sickness dose value ($MSDV$), indicates the percentage of people who may experience motion sickness. It is computed in the same way illustrated in Figure 1.20 but with a different weighting function (W_f).

In the third part of the thesis, the proposed optimization comfort method is validated using a three degrees of freedom vehicle model that is used to model the vehicle dynamics. Simulations are conducted in virtual scenarios created using Automated Driving Scenario Toolbox on MATLAB and Simulink. Then, the simulated experiments are performed on Simscape Vehicle Template where the vehicle dynamics are modeled using a complete vehicle model with fifteen degrees of freedom. The fifteen degrees of freedom vehicle model represents a sedan car.

In both cases, a Model Predictive Controller is used to manage the longitudinal and lateral dynamics of the vehicle. The Controller provides the wheel steering angle and the accelerating/breaking commands to the vehicle to maintain the center line and follow the desired reference trajectory.

In the last part of the thesis, the obtained results are presented together with an analysis of the front and rear passenger's comfort.

The study focuses on three different scenarios; an highway scenario where the path is straight and the maximum speed is set to 130 km/h, an interurban scenario with fairly straight road and slight curves with maximum speed set to 70 km/h and a competition race track (Berlin Track) with sharp curves and maximum speed set to 70 km/h. Together, they form a comprehensive set of key environments for the evaluation of the fuzzy comfort-oriented speed profile generator that is proposed in this thesis work.

1.4 Thesis outline

The thesis work is divided in six chapters, as follows:

- **Chapter 2 - Perception and path planning**

In this chapter the perception and path planning algorithm topics are discussed. In the first part, a brief overview of the most common sensors installed in nowadays autonomous vehicles is presented. Afterward, a more detailed explanation of the RADAR and LIDAR sensors are reported. In the end, the lane detection system is discussed.

- **Chapter 3 - Trajectory and velocity planning**

This is the main chapter of the thesis work. It aims to explain the problem formulation related to the reference velocity generator. The Fuzzy Logic Controller is extensively explained on all its details. In this thesis work the main goal of the Fuzzy Controller is to determine a suitable reference speed profile combined with satisfying control and comfort performances. Moreover, the motion sickness argument is considered. In particular, the procedure to compute the comfort coefficients extracted by ISO 2631 and used as performance evaluation of the proposed method is explained.

- **Chapter 4 - Modelling**

It aims to describe the vehicle models used to test the comfort-oriented method presented in the thesis work and to validate it. Moreover, the Model Predictive Control problem formulation is reported.

The chapter is divided in subsections:

- The convention used in the thesis work is introduced. In particular, the reference frame and vehicle coordinates.
- The description of the 3 degree of freedom vehicle model is extensively reported. Moreover, the linearized vehicle model for the Adaptive MPC control design is presented.
- The third subsection is related to the description of the complete vehicle model provided by Simscape Vehicle Template on MATLAB[®] and Simulink[®]. The vehicle has 15 degrees of freedom.
- In the last subsection, the Model Predictive Control problem formulation is presented.

- **Chapter 5 - Validations and results**

In this chapter the results obtained from simulations with the 3 degrees of freedom model and with the model provided by Simscape vehicle template are illustrated and discussed.

- In the first subsection, the scenarios created with Driving scenario simulator and used for simulations are illustrated. Moreover, results obtained with both the vehicle models are presented. In particular, the results obtained with the proposed method are compared with the classical one

– In the last subsection, the results of the comfort coefficients of the front and rear passengers are presented.

- **Chapter 6 - Conclusions and future works**

Final considerations of the proposed comfort-oriented method and possible improvements are discussed.

CHAPTER 2

Perception

An driverless vehicle software system can be generally divided into three main categories, namely perception, planning, and control. With the interactions between these competencies the vehicle is able to move autonomously.

The process of perception in self-driving cars uses a combination of sensors and cameras to collect information and extract relevant knowledge from the environment around the vehicle, such as detection of road markings, obstacles location and free drivable areas. The data provided by this process are exploited by the decision-making process that decides how the vehicle should move next. Sensors like radars and Lidars combined with a series of cameras are the vehicle's eyes.

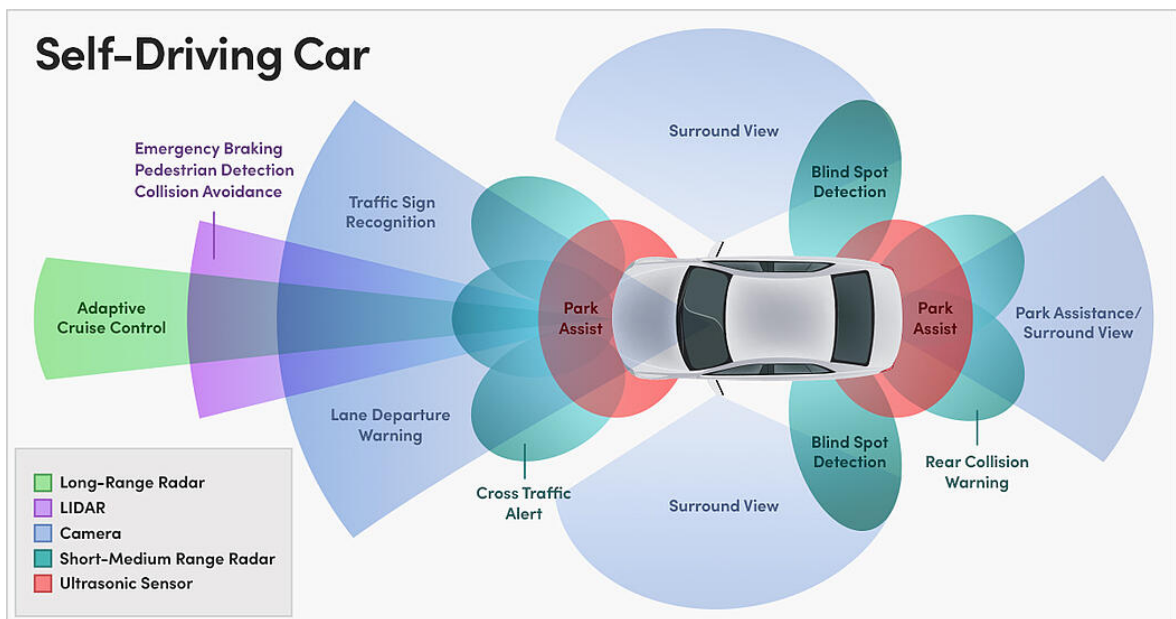


Figure 2.1: Sensors and their range in an autonomous vehicle [21]

2.1 Sensors

In the following section, the main sensors used in autonomous vehicles are described.

2.1.1 LIDAR

LIDAR is the crucial device for object detection for most of the existing autonomous vehicles. Light Detection and Ranging, or simply LIDAR, is a remote sensing technique that allows to discover the distance of an object or surface using a laser pulse. With its rotating axis, the device sends millions of light pulses per second. The time that the laser takes to return to the origin is used to create a dynamic, three-dimensional map of the environment around the vehicle. LIDAR uses ultraviolet wavelengths, in the visible or near infrared.[22] This makes it possible to locate and obtain images and information on very small objects, of a size equal to the wavelength.

The ideal detection result from a 3D LIDAR, with all the moving objects being identified, is illustrated in Figure 2.2

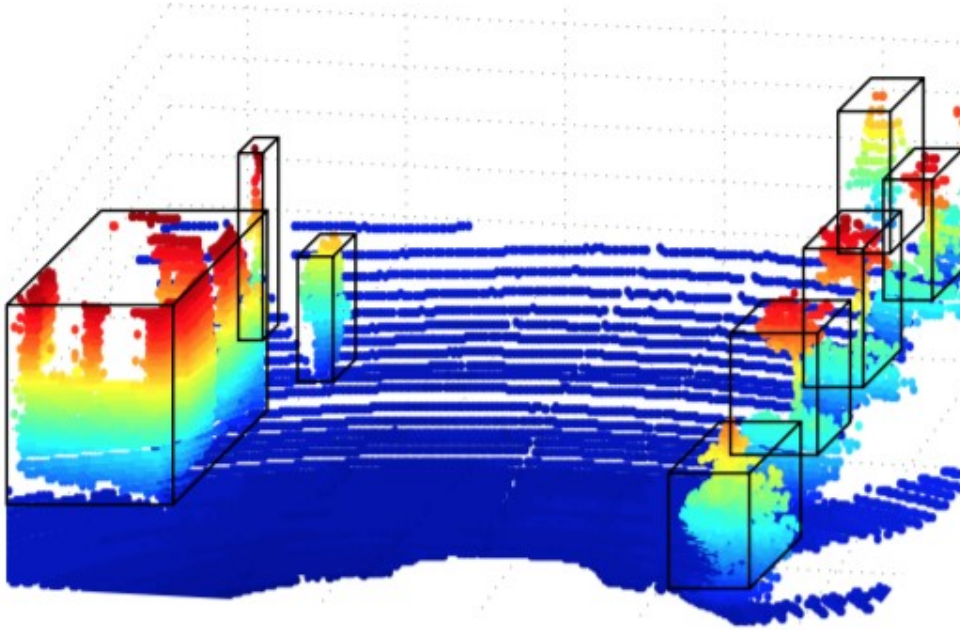


Figure 2.2: The ideal detection result from a 3D LIDAR [22]

The points returned by the LIDAR are not perfect in real scene. Missing points, scan point sparsity and unorganized patterns make difficult to handle LIDAR points. However, LIDAR makes data collection fast and with extremely high accuracy. It is not affected by light variations, such as darkness and light, and hard weather condition , such as snow, rain and dust. Moreover, LIDAR sensors are not affected by any geometrical distortions such as angular landscapes.

2.1.2 RADAR

Radio Detection And Ranging, or simply RADAR, is a device that is constituted of an antenna, that emits a radio signal in a specific direction and a radio receiver, that detects the radio signal once it has bounced off of objects in the environment. The time the radio signal takes to return is used to compute the relative distance between the vehicle and the object the signal bounced off. With this process occurring hundreds of times in all directions every second, vehicles can produce detailed point cloud maps of the environment.

Radio waves have less absorption compared to light waves when echoing off of other objects, so they work really well over a longer distance. However, radar sensors are less accurate than Lidar sensors and they provide too insufficient detail for self-employed vehicles.[23]

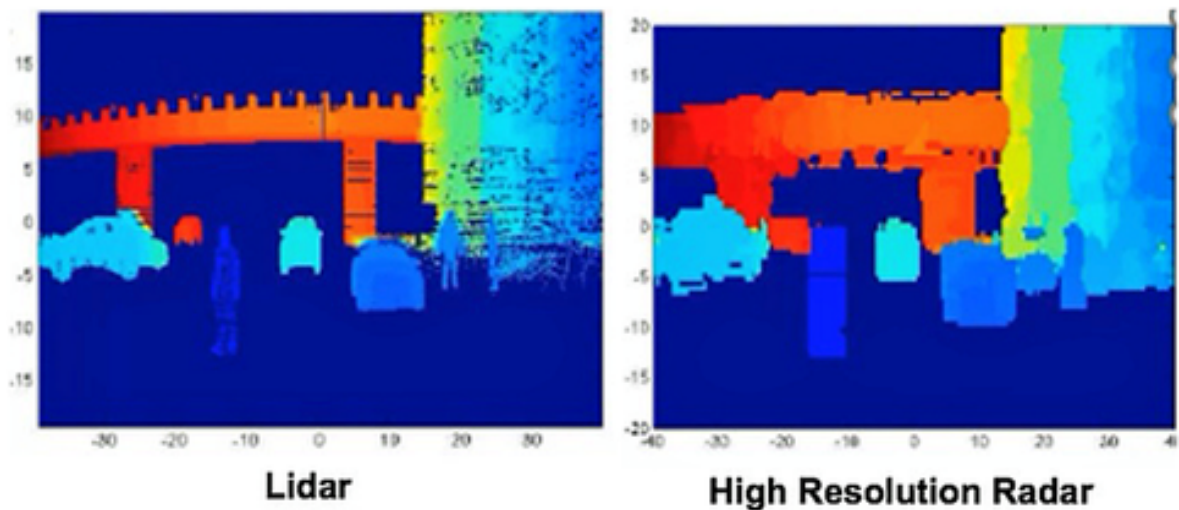


Figure 2.3: LIDAR and RADAR resolution comparison [23]

2.1.3 Ultrasonic sensor

The working principle of the ultrasonic sensor is similar to that of radar and lidar. In this case, an ultrasonic pulse is sent and reflected back in order to compute the distance between the vehicle and the object. Their range is very short (2m) but they are not affected by light and weather conditions. Ultrasonic sensors provide relatively precise measurements and are usually very inexpensive. They are commonly used in ADAS like parking assistant system and forward collision warning.

2.1.4 GPS

The Global Positioning System or GPS network consists of 29-32 global positioning satellites orbiting around the earth. The satellites are arranged in a way that four satellites are always positioned in each of six orbital planes, to ensure that the whole world is covered by the constellation of the GPS satellites.

The position of the satellites is generally described with the geocentric Cartesian reference frame, with origin in the Earth's centre, axes X and Y on the equatorial plane and the Z axis in the direction of the Earth rotation axis. Each satellite transmits radio signals that are processed by the GPS receiver in the vehicle and sent back to the satellites. From the time shift of the signal and the knowledge of signal speed, the distance from each satellite is computed. Four satellites are required to determine the location, direction of travel and travel speed of the vehicle (receiver) on the earth. Three satellites are necessary to trace the location, and then it is confirmed by the fourth satellite. This is done using a mathematical principle called trilateration that is illustrated in Figure 2.4. [24][25]

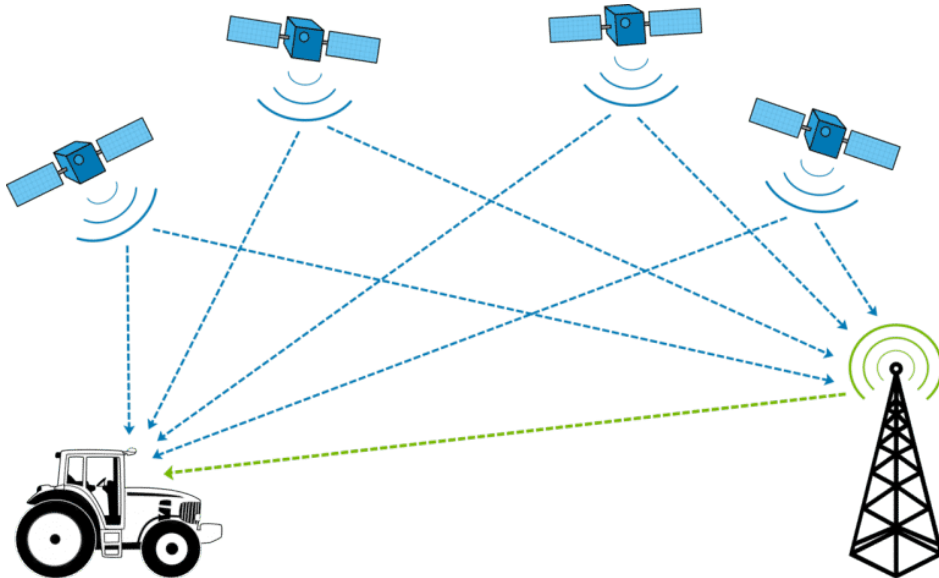


Figure 2.4: GPS trilateration principle [24]

Differential Global Positioning System (DGPS) is an enhancement of the GPS (Global Position System). GPS system based on the satellite technology has an accuracy of meters whereas DPGS accuracy is around 10 cm. DGPS uses the fixed ground based reference stations to broadcast the difference between the coordinates from the GPS and from the fixed position from the base station. DGPS rely on two stations, one is the base station and the other is the moving object (vehicle).[26]

2.1.5 Camera

The above described sensors such as Radar and Lidar use various types of waves to map the world based on how far objects are from them. Things like the colour of the traffic light or the road signs can't be determined by these sensors because these elements are depthless.

Cameras provide the richest information about the world around the vehicle and tend to replicate human vision. However, to confirm and label objects, cameras data are typically coupled with lidar and radar sensors data through a process called sensor fusion. In this way, the accuracy and reliability of the detection are improved.[26]

Cameras are used to identify four main attributes of the driving environment:

- Lane detection .
- Road sign detection.
- Traffic light detection.
- Object detection.

There are two type of camera, mono camera and stereo camera.

- **Mono camera:** Monocular vision system use one camera to estimate the distance from an object. To this end, two transformation matrices are used to map the pixel coordinates of the image in the world coordinate. The first one is a roto-translation matrix used to pass from world coordinates to camera coordinates. The second matrix allows to pass from camera coordinates to 2-D pixel coordinates and it is defined by intrinsic camera parameter such as optical center and focal length.
- **Stereo camera:** A stereo camera is a device made of two mono cameras placed at a predefined distance. This allows the vision system to simulate human binocular vision, and gives the system the ability to capture three-dimensional images.

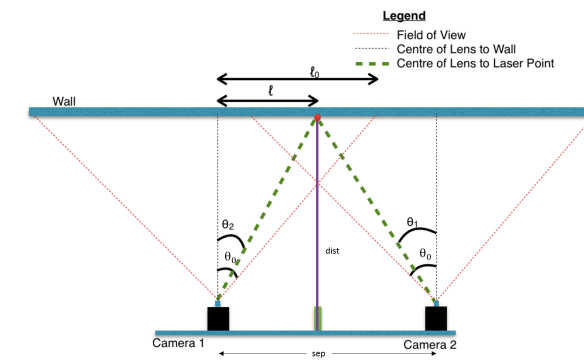


Figure 2.5: Stereo vision working principle [27]

2.2 Lanes detection

Lane line marking detection is related to the process of identifying the lane line markings on the road and estimate the vehicle pose with respect to the detected lines. The lines are used to compute the reference trajectory that corresponds to the center line of the lanes and in this thesis work is computed as the average between the left boundary of the lane and the right one.[22]

An extensive amount of research work has been done in this domain, however, it is yet to be completely solved and has remained a challenging problem due to the wide range of uncertainties in real traffic road conditions and road singularities, such as worn-out lane markings and variation of lighting conditions. Most of the lane line detection algorithms are based on three common steps:

- Lane line feature extraction.
- Fitting the pixels into different models.
- Estimating the center line and the vehicle pose.

The lane line feature extraction is related to the process of identifying the pixels that belong to the lane line markings and eliminate the meaningless pixels. Most of the detection algorithms that can be found in the literature exploit the high contrast of the lane line markings compared to road pavement. To this end, Sobel edge detector with symmetrical local threshold, adaptive thresholding and gradient-enhancing conversion are commonly used. Another set of algorithms, such as box filter, try to detect lane line markings searching for low-high-low intensity pattern along image rows. These types of algorithms are more reliable and less sensitive to noise compared with the ones cited before.[22]

Fitting the pixels into different models is the process to extract a compact high-level representation of the lane from the lane line detection results. Straight lines, parabolas, hyperbolas are parametric models typically used. Another category that are more flexible and can cover a wider type of road shapes are semi-parametric models. These mainly consist of splines, such as Cubic splines. However, they are more complex and computationally demanding.[22]

The last step is to estimate the center line and vehicle pose. In this thesis work the reference trajectory corresponds to the center line and it is computed as the average between the left boundary of the lane and the right one. The difference between the center line and the actual position of the vehicle, called cross-track error, is a piece of information served to the vehicle control system.[22]

CHAPTER 3

Trajectory and velocity planning

In this chapter a brief introduction about the motion planning problem is presented. The basic concepts of this wide topic are reported, focusing on the proposed path planning algorithm. Then, a detailed description of the Fuzzy Logic Controller used to generate a comfort oriented speed profile is presented. Finally, motion sickness problem and the related comfort coefficients used in this thesis work are reported.

3.1 Reference path generator

The aim of the trajectory planning algorithm is to generate a feasible reference path that the vehicle can follow implementing the acceleration/deceleration and steering commands that are provided by the control system. In short, the objective is to find a collision-free motion between the starting position and the goal position in a given environment. Before explaining the proposed path planning algorithm some basic concepts are introduced.

- **State space S :** The definition of the state space is an important component in the formulation of a planning problem. A state space capture all possible situations that could arise, for example, the position and orientation of a robot or the position and velocity of a car.

$$S = S_{free} + S_{obs} \quad (3.1)$$

- **Free space S_{free} :** It is the set of all the allowed configurations that avoid collision with the obstacles. Usually, it is extremely difficult to explicitly determine the shape of the free space.
- **Obstacles space S_{obs} :** It is the image of the obstacles in the State space S .
- **Target space:** It is a linear subspace of the free space which denotes the desired trajectory we want the vehicle to follow.

”In this thesis work, the path planning algorithm is based on a modified Rapidly-exploring Random Tree (RRT) algorithm for non-holonomic car-like mobile robots. A rapidly exploring random tree is an algorithm used to efficiently search non convex, high-dimensional spaces by randomly building a space-filling tree.”[28]

The tree is constructed incrementally from samples drawn randomly in the free space. The trees are grow towards unsearched areas of the environment. Due to differential constraints of non-holonomic car-like mobile robot, instead of using straight lines as in the classical RRT algorithm , Dubins curves are used to build the branches in the search tree.

The following set of equations describe the Dubins car model:

$$v_x = v_{CG} \cos \theta \quad (3.2)$$

$$v_y = v_{CG} \sin \theta \quad (3.3)$$

$$\dot{\theta} = r = \frac{v_{CG}}{L} \tan \delta \quad (3.4)$$

The two control variables are the velocity of the center of gravity v_{CG} and the steering angle δ . The following vector is used to indicate them:

$$u = [u_v \ u_\delta] \quad (3.5)$$

Therefore, the Dubins car model equations can be rewritten as:

$$v_x = u_v \cos \theta \quad (3.6)$$

$$v_y = u_v \sin \theta \quad (3.7)$$

$$\dot{\theta} = r = \frac{u_v}{L} \tan u_\delta \quad (3.8)$$

The maximum steering angle is indicated with δ_{MAX} .

$$|u_\delta| \leq \delta_{MAX} \quad (3.9)$$

By assumption, the vehicle can move only forward, so the velocity can assume only positive values. For simplicity, velocity is considered constant and can assume two possible values:

$$u_v \in \{0, 1\}$$

If u_v is equal to zero, the vehicle is still, while if it is equal to 1, the vehicle moves with a constant velocity. Finally, the Dubins car model can be simplified as follow:

$$v_x = \cos \theta \quad (3.10)$$

$$v_y = \sin \theta \quad (3.11)$$

$$\dot{\theta} = u \quad (3.12)$$

To compute the Dubins curves between two consecutive vertices, the shortest path is expressed as a combination of no more than three primitive curves.[29]

The cost function that looks for the shortest path is:

$$L_{curve}(\tilde{q}, \tilde{u}) = \int_0^{t_F} \sqrt{v_x(t)^2 + v_y(t)^2} dt \quad (3.13)$$

where \tilde{q} represents a general configuration, and t_F is the time needed to reach the final configuration.

In this thesis work three different primitive curves are considered and associated with the vector u .

- S, $u = 0$, drives the car straight ahead.
- L, $u = 1$, turns as sharply as possible to the left.
- R, $u = -1$, turns as sharply as possible to the right.

There exist ten possible combinations of primitive curves, but only six of them are optimal and are called Dubins curves.

$$\{ RSL, LSR, RSR, LSL, RLR, LRL \}$$

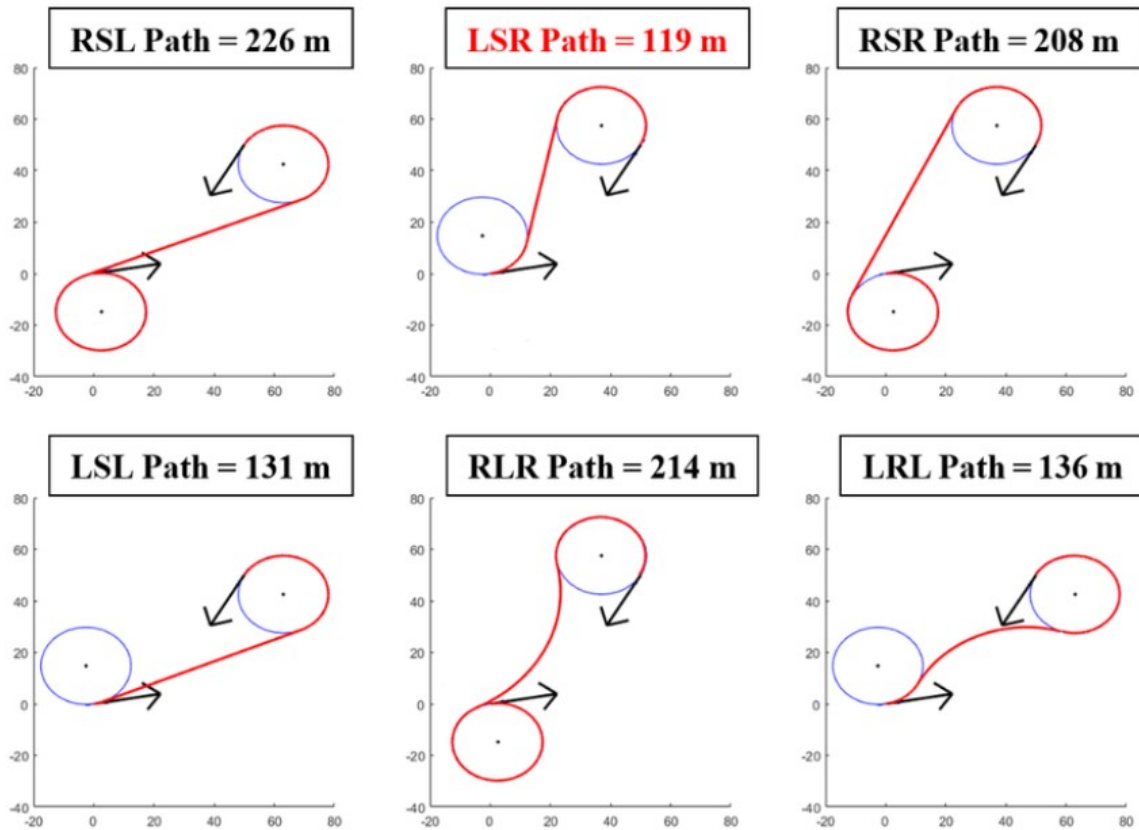


Figure 3.1: Dubins curves [30]

An arbitrary point $(x, y, \theta) \in \mathbb{R}^3$ is mapped into its corresponding image point in \mathbb{R}^3 by the following operators:

$$L_v(x, y, \theta) = (x + \sin(\delta + v) - \sin \delta, y - \cos(\delta + v) + \cos \delta, \delta + v) \quad (3.14)$$

$$R_v(x, y, \theta) = (x - \sin(\delta - v) + \sin \delta, y + \cos(\delta - v) - \cos \delta, \delta - v) \quad (3.15)$$

$$S_v(x, y, \theta) = (x + v \cos \delta, y + v \sin \delta, \delta) \quad (3.16)$$

where v indicates the length of the circular or straight segment.

The proposed path planning algorithm provides the road curvature every 0.1 seconds. It is defined as :

$$\kappa = \frac{d\Phi}{ds} \quad (3.17)$$

where Φ is the tangential angle and s is the arc length. Moreover, the radius of road curvature is defined as the inverse of road curvature:

$$R = \frac{1}{\kappa} \quad (3.18)$$

R is the radius of the osculating circle, which is the circle that best approximates the curve at a point.[31]

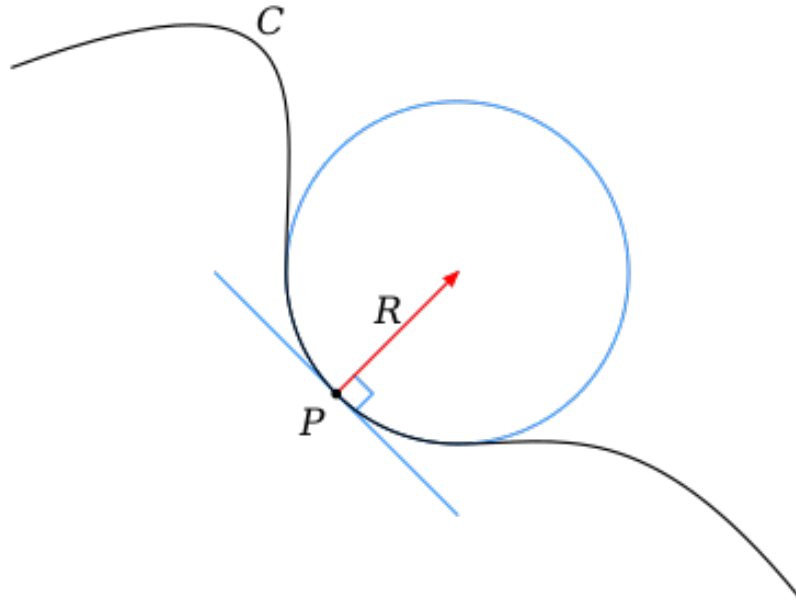


Figure 3.2: Osculating circle [31]

3.2 Reference velocity generator

This subsection is related to the determination of the reference speed profile. One of the criteria available in the literature is briefly discussed. The method is based on the information of the road provided by the path planning process. The main idea of this approach, developed by Daimler-Chrysler, is that the reference velocity must rise when the vehicle is driving in straight road and it must decrease when the vehicle is approaching a bend. In formula, the maximum admissible speed based on the road curvature information is:

$$V_{MAX} = \sqrt{\frac{g\mu}{\kappa}} \quad (3.19)$$

where g , μ and κ are respectively the acceleration of gravity, the friction coefficient and the road curvature.[32] The equation in 3.19 takes in consideration the maximum value of the curvature κ among the previewed curvature values computed in a fixed prediction horizon. In this way, the car will have time to brake before approaching a curve, resulting in a smooth driving. However, the description in model 3.19 is in some sense considered poor since it takes in consideration only the road curvature parameter neglecting other important characteristic of the road.

A more complete model is proposed by the National Highway Traffic Safety Administration (NHTSA). Indeed, the model considers also the road camber angle Φ_r .

$$V_{MAX} = \sqrt{\frac{g}{\kappa} \left(\frac{\Phi_r + \mu}{1 - \Phi_r \mu} \right)} \quad (3.20)$$

Therefore, the maximum acceleration needed by the vehicle in order to reach the reference speed must be less than:

$$a_{MAX} = \sqrt{\frac{V_x^2 - V_{MAX}^2}{2(d - t_r V_x)}} \quad (3.21)$$

where V_x is the vehicle speed, d is the distance to the bend and t_r is the time-delay related to driver reaction.

The determination of the reference speed profile is an essential aspect of the autonomous driving. The lateral acceleration is strictly dependent on the velocity of the vehicle and thus it will have an impact on the passengers' comfort. To this end, a fuzzy comfort oriented speed profile generator is designed to determine a suitable speed profile with satisfying control and comfort performances.

3.2.1 Fuzzy Logic Controller

Fuzzy logic is an extension of Boolean logic by Lotfi Zadeh in 1965 and it is a way to model logical reasoning where the truth of a statement is not binary, as in classical logic, but rather it is a degree of truth that ranges from zero (absolutely false) to one (absolutely truth).

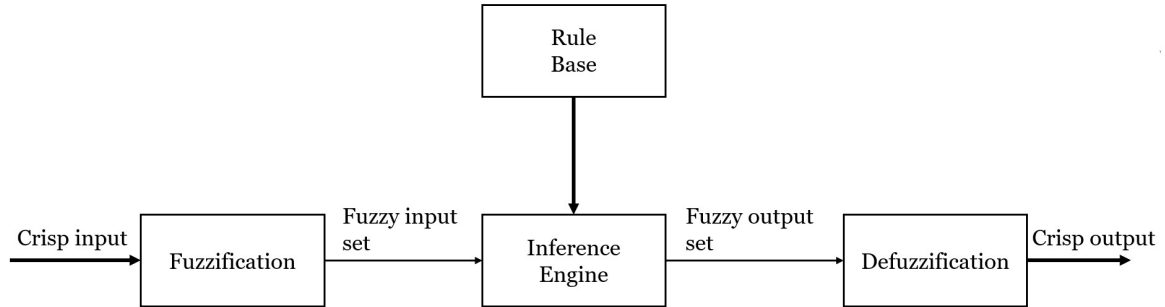


Figure 3.3: Fuzzy Logic architecture

Fuzzy Logic architecture is composed of four main parts as shown in Figure 3.3.

- **Fuzzification:** It is the process of converting the obtained crisp input data to a degree of membership for each fuzzy set.
- **Inference engine:** The inference engine looks up the membership grades for each rule and based on them generates a fuzzy output.
- **Rule base:** It contains all the rules built by the experiment. The rules have an if-then mechanism. Logical *and* and logical *or* are the most prominent logical operators used for the connectivity between inputs.
- **Defuzzification:** It is the final stage of a fuzzy logic system. This process converts the fuzzy set in a crisp output. There are different techniques available, in this thesis work the centroid method is used.

The following diagram illustrates the steps done in a mamdani inference system with max-min inferencing and centroid defuzzification in order to compute the crisp output. x, y and z are the inputs, n is the output and μ is the standard fuzzy-logic nomenclature for "truth value".[33]

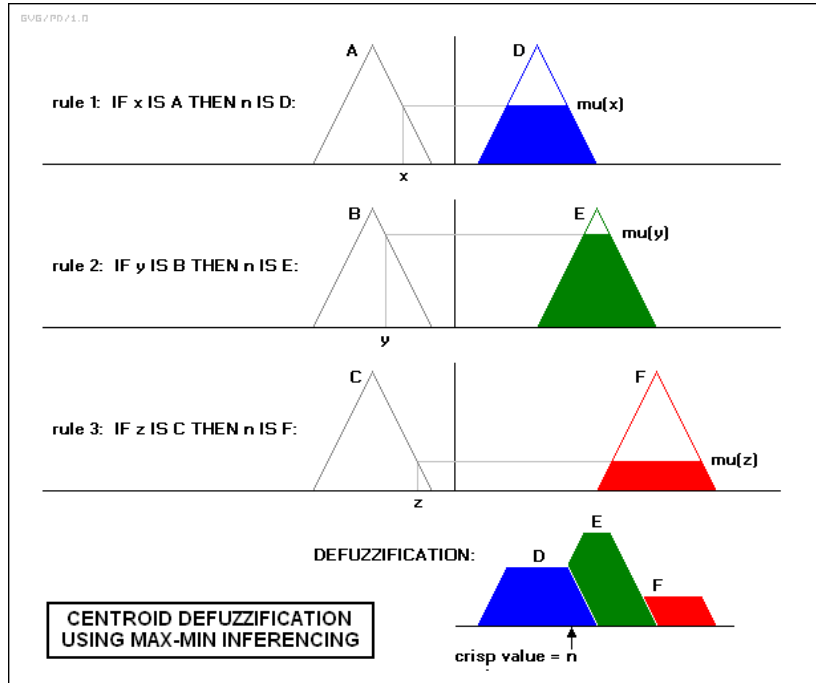


Figure 3.4: Steps for computing the output [33]

The Steps done to compute the output are:

1. Determination of the fuzzy rules.
2. Fuzzification of the inputs.
3. Determination of the degree of membership by combining the fuzzified inputs.
4. Determination of the degree of membership of the output according to the rules.
5. Defuzzification of the output.

Fuzzy Logic allows to design Fuzzy Logic Controller which is a function that interprets the values of the input vector and, on the basis of sets of rules defined a-priori by the experimenter (if-then mechanism), assigns the value to the output vector.

In this thesis work the main goal of the Fuzzy Controller is to determine a suitable reference speed profile combined with satisfying control and comfort performances. The Fuzzy Logic Controller architecture is illustrated in Figure 3.5

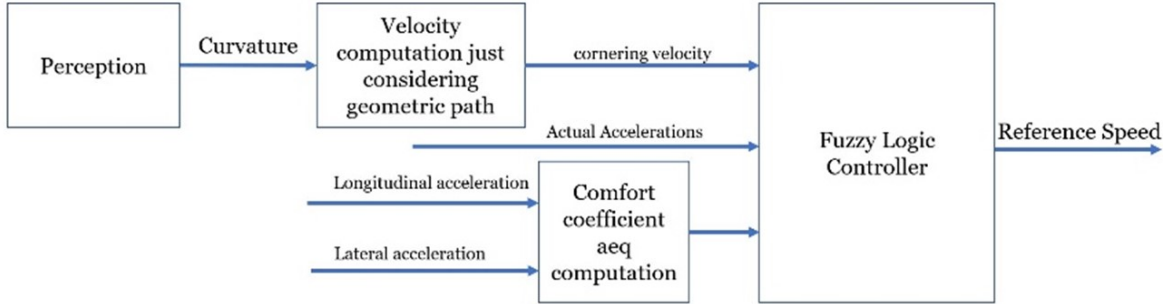


Figure 3.5: Fuzzy Logic Controller Architecture

The environment perception block receives the images data acquired in real-time from the sensors installed in the vehicle, namely Lidar, Radar and cameras. The merging of these sensor data provides information on the surrounding environment, such as lane boundaries and obstacles location. Specifically, the path planning algorithm inside the perception block, processes the acquired data and returns the pose of the vehicle and the road curvature of the computed path. From these information and the measurements of the vehicle's states in real-time, the reference trajectory and cornering velocity are computed.

The cornering velocity in equation 3.19, the actual longitudinal acceleration of the vehicle and the comfort coefficient a_{eq} are the inputs of the Fuzzy Logic Controller that, based on sets of rules, computes the reference speed profile.

In particular, the comfort coefficient a_{eq} is evaluated every forty seconds considering the last four hundred samples of the longitudinal and lateral acceleration data that are gathered using a buffer. The procedure used to compute the comfort coefficient is extensively described in the following subsection. However, the Fuzzy Logic Controller is updated every 0.1 seconds.

Fuzzy Logic Controller was designed using the Fuzzy Logic Toolbox on MATLAB[®] and Simulink[®].

3.2.2 Membership functions

The membership functions used in the Fuzzy Logic Controller are illustrated in the following figures. Fuzzy control system was designed based on a methodical approach to trial-and-error. After a significant amount of simulations, it was decided to use predefined Gaussian shape both for the inputs and the outputs. Even the range values of each function was decided according to the knowledge acquired during the experiments.

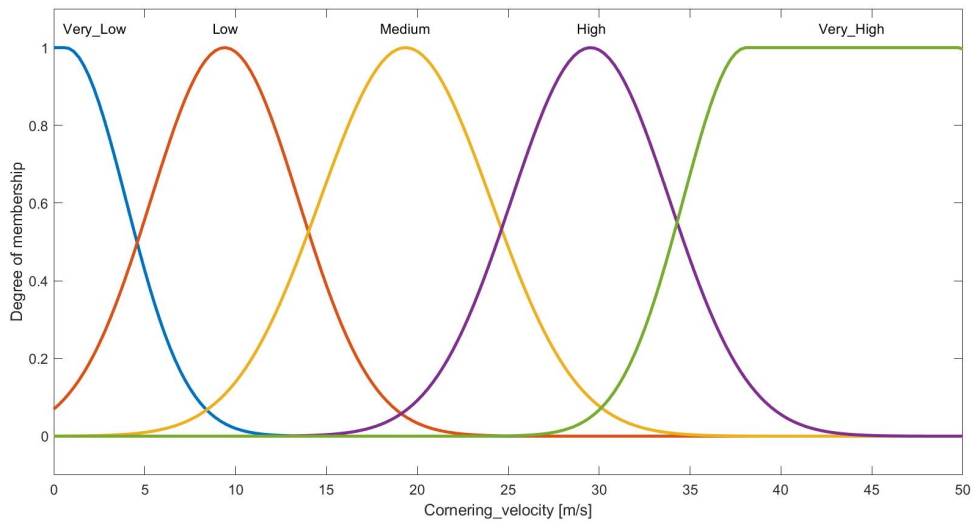


Figure 3.6: Membership function of the first input

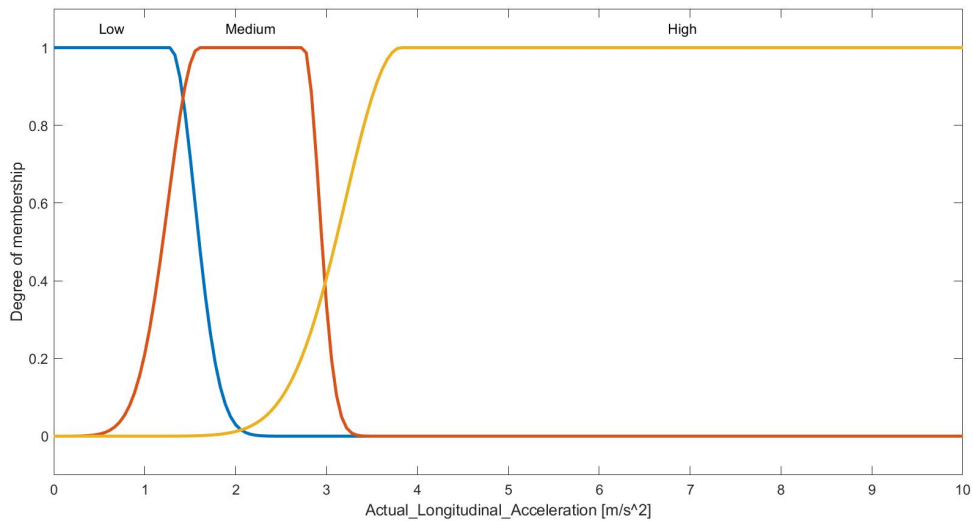


Figure 3.7: Membership function of the second input

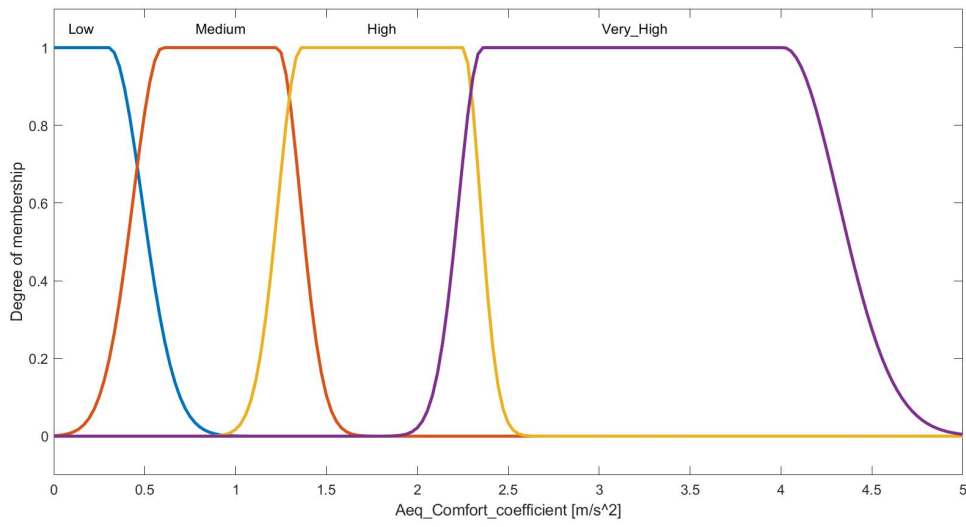


Figure 3.8: Membership function of the third input

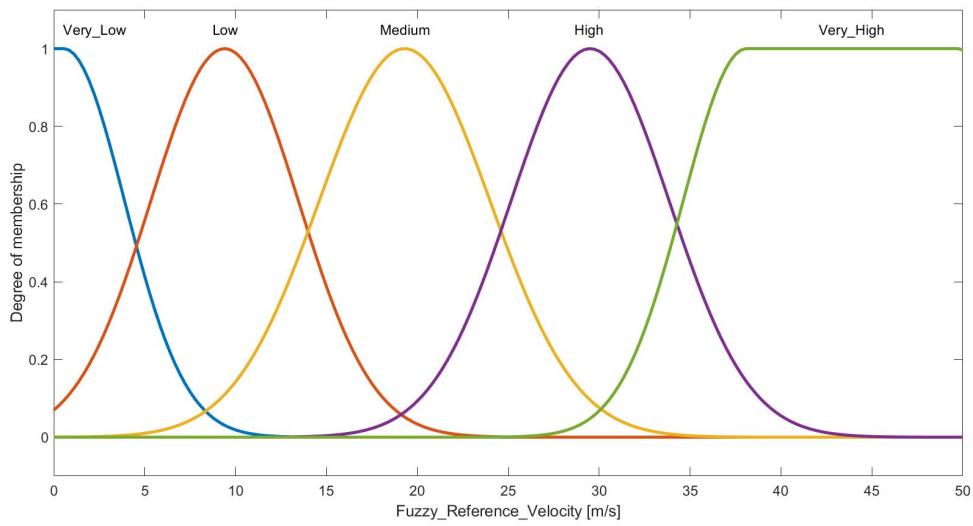


Figure 3.9: Membership function of the output

3.2.3 Rules

In this subsection, the rules used in the Fuzzy Logic Controller are presented. Like in the case of the membership functions, the rules were designed based on a trial-and-error methodical approach.

Each row represents a rule. An example of a rule is:

If Cornering velocity is *Medium* **and** Longitudinal Acceleration is *High* **and** a_{eq} coefficient is *High* **then** Reference velocity is *Low*.

Table 3.1: Rule base

n°	Input			Output
	Cornering velocity	Longitudinal Acceleration	a_{eq} coefficient	Reference velocity
1	Very Low	Low	Low	Low
2	Low	Low	Low	Low
3	Medium	Low	Low	Medium
4	High	Low	Low	High
5	Very High	Low	Low	Very High
6	Medium	Medium	Medium	Low
7	High	Medium	Medium	Medium
8	Very High	Medium	Medium	Medium
9	Medium	High	High	Low
10	High	High	High	Low
11	Very High	High	High	Medium
12	Very Low	-	Low	Very Low
13	Low	-	Low	Low
14	Medium	-	Low	Medium
15	High	-	Low	High
16	Very High	-	Low	Very High
17	Very Low	-	Medium	Very Low
18	Low	-	Medium	Low
19	Medium	-	Medium	Low
20	High	-	Medium	Low
21	Very High	-	Medium	Low
22	Very Low	-	High	Very Low
23	Low	-	High	Low
24	Medium	-	High	Low
25	High	-	High	Low
26	Very High	-	High	Low
27	Very Low	-	Very High	Very Low
28	Low	-	Very High	Low
29	Medium	-	Very High	Low
30	High	-	Very High	Low
31	Very High	-	Very High	Low

3.3 Motion sickness state of art

The term motion sickness has been coined by Irwin (1881) who suggested that seasickness might better be called motion sickness because “not only does it occur on lakes and even on rivers, but as is well known, a sickness identical in kind may be induced by various other motions than that of turbulent water, ...”. In 1949 Tyler and Bard described this disorder as “Motion sickness is a specific disorder which is evoked in susceptible persons and animals when they are subjected to movements which have certain characteristics”.[34]

The conflict theory by Reason and Brand (1975) is considered, in the recent past, the main theory that better explains Motion sickness: the acceleration perceived by the sense organs conflicts with the expected one determined on the basis of previous experience, generating a conflict leading to Motion sickness.

Motion sickness is typically caused by low frequency lateral, vertical, angular and rotary motion to which an individual has not adapted. Simultaneous movements along or about movement axes have also a high impact on the occurrence of motion sickness. The principal sensors used by our brain to sense motion are:

- **The vestibular system** : It is responsible for sensing motion, gravity and acceleration and help us to keep balanced.
- **The eyes**: Inform our brain to movements in relation to the surrounding environment.
- **Proprioceptors**: They are the deeper tissues of the human body surface. Pressure and vibration interactions with the environment help the brain to understand better the motion.

These three inputs are combined by our brain to create our spatial orientation, coordination and balance. When one of these senses provide information that do not match with the information perceived by the other senses the individual can experience motion sickness.

Motion sickness can be divided into three categories:

- **Motion felt but not seen**: In these situations, the motion is sensed by the vestibular system but it is not detected by the visual system.
- **Motion seen but not felt**: In these cases the visual system detects motion but the vestibular system does not. This typically occurs in space sickness, where zero gravity interferes with the vestibular system, or in virtual reality sickness.
- **Motion that is seen and felt**: ”When moving within a rotating reference frame such as in a centrifuge or environment where gravity is simulated with centrifugal force, the coriolis effect causes a sense of motion in the vestibular system that does not match the motion that is seen.”[35]

The most common symptoms related to motion sickness are nausea, dizziness, tiredness and loss of appetite.

3.3.1 Comfort coefficients computation

ISO 2631 describes ways to evaluate vibration exposure to the human body. The quantified comfort measures of ISO 2631-1 are based on frequency weighted root mean square, *RMS*, computations of acceleration data.

In this study, two indexes have been considered.

3.3.2 a_{eq} comfort coefficient

The first index (a_{eq}) is computed as follows:

$$a_{W,i,RMS} = \left(\frac{1}{T} \int_{t_0}^{t_f} a_{W,i}^2(t) dt \right)^{\frac{1}{2}} \quad (3.22)$$

Where T_f is the exposure period time, $a_{W,i}$ the frequency weighted acceleration and W_i is the frequency weighted function.

The equivalent acceleration index is then calculated as follow:

$$a_{eq} = k_x^2 a_{x,W}^2 + k_y^2 a_{y,W}^2 \quad (3.23)$$

$$k_x = k_y = 1 \quad (3.24)$$

Where $a_{x,W}$ and $a_{y,W}$ are the weighting *RMS* accelerations with respect to the orthogonal x and y axes respectively.

The ISO 2631-1 provides a classification of likely reactions in terms of comfort based on the rms values of the frequency-weighted equivalent acceleration, as illustrated in table 3.2.

Table 3.2: Classification of likely reactions in terms of comfort based on a_{eq} values. [36]

$a_{eq} \leq 0.315m/s^2$	Not uncomfortable
$0.315m/s^2 \leq a_{eq} \leq 0.63m/s^2$	A little uncomfortable
$0.5m/s^2 \leq a_{eq} \leq 1m/s^2$	Fairly uncomfortable
$0.8m/s^2 \leq a_{eq} \leq 1.6m/s^2$	Uncomfortable
$1.25m/s^2 \leq a_{eq} \leq 2.5m/s^2$	Very Uncomfortable
$a_{eq} \geq 2.5m/s^2$	Extremely uncomfortable

In Figure 3.10 it is shown the procedure to compute the comfort coefficient a_{eq} . A band pass filter is applied to the longitudinal and lateral acceleration. Then, the resulting accelerations are multiplied by a weighting function W_d and finally the root mean square is computed.

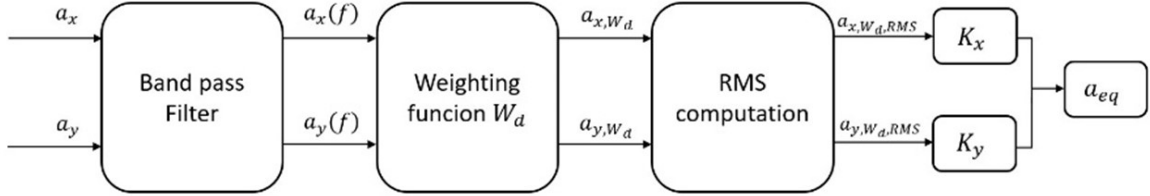


Figure 3.10: Comfort coefficient a_{eq} procedure computation

The procedure and the formulas used for the design of the band pass filters used for the *rms* analysis described above are presented in the following paragraph.

The design of the band pass filter is obtained merging together four different filters:

- High pass filter
- Low pass filter
- Transition acceleration-velocity
- Upward step

The transfer function of the high pass filter is the following:

$$H_h(s) = \frac{1}{1 + \sqrt{2}w_1/s + (w_1/s)^2} \quad (3.25)$$

where :

- $w_1 = 2\pi f_1$
- $s =$ Laplace Transform
- f_1 is the cut off frequency in Hz for which there is an amplitude attenuation of $-3dB$ and a phase shift of 90°

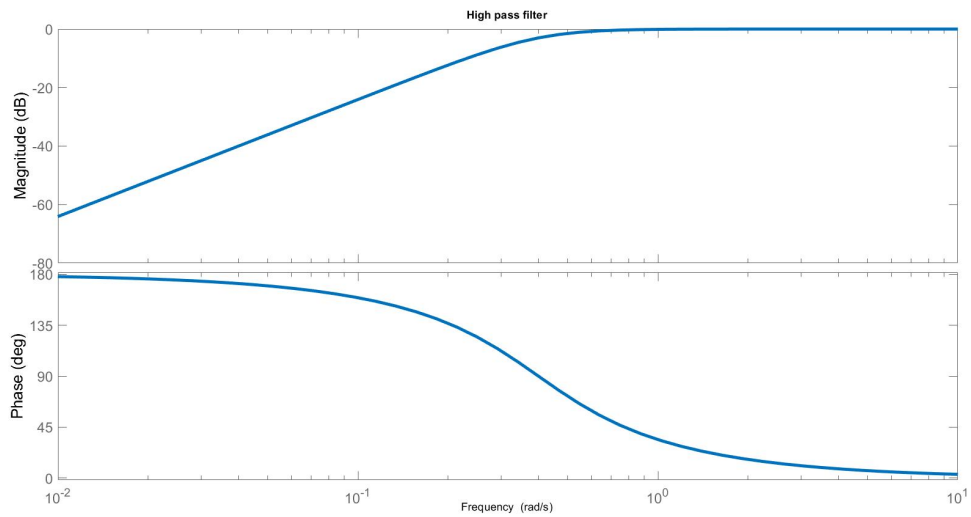


Figure 3.11: Bode of the High pass filter

The transfer function of the low pass filter is the following:

$$H_l(s) = \frac{1}{1 + \sqrt{2}s/w_2 + (s/w_2)^2} \quad (3.26)$$

where:

- $w_2 = 2\pi f_2$
- f_2 is the cut-off frequency (100 Hz)

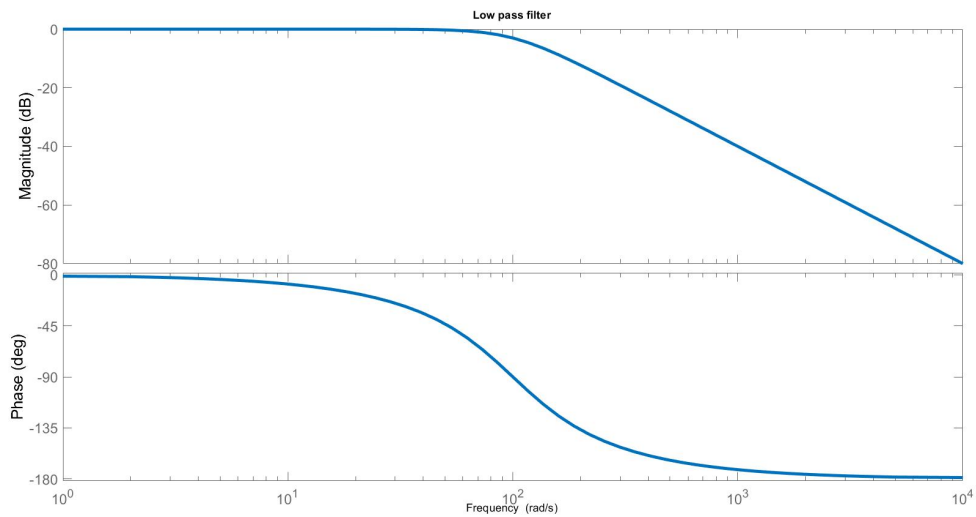


Figure 3.12: Bode of the Low pass filter

The acceleration-velocity transition function is a function proportional to the acceleration for low frequencies and proportion to the velocity for high frequencies.

The transfer function of the acceleration-velocity transition function is the following:

$$H_t(s) = \frac{1 + s/w_3}{1 + s/Q_4w_4 + (s/w_4)^2} \quad (3.27)$$

where:

- $w_3 = 2\pi f_3$
- $w_4 = 2\pi f_4$

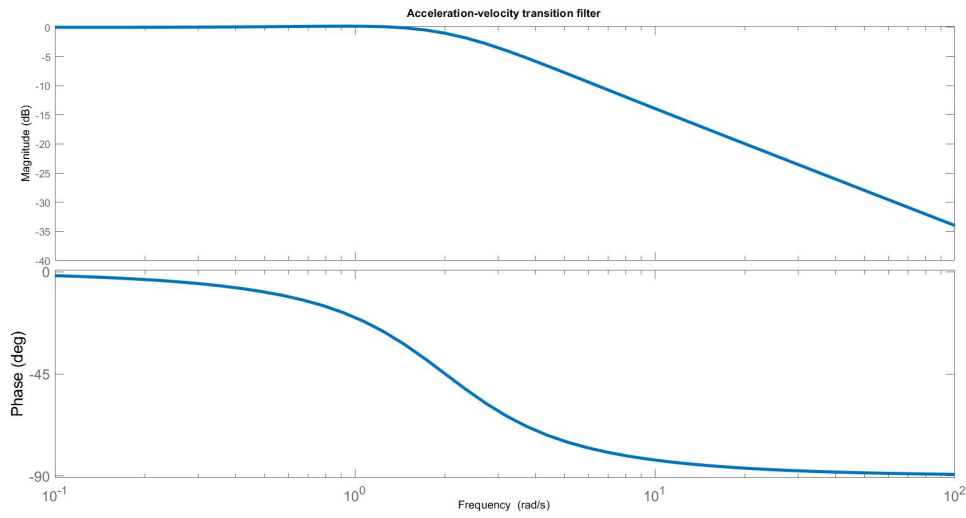


Figure 3.13: Bode of the Acceleration-velocity transition filter

The formula of the Upward step is the following:

$$H_s(s) = \frac{1 + \frac{s}{Q_5w_5} + \left(\frac{s}{w_5}\right)^2}{1 + \frac{s}{Q_6w_6} + \left(\frac{s}{w_6}\right)^2} \left(\frac{w_5}{w_6}\right)^2 \quad (3.28)$$

where:

- $w_5 = 2\pi f_5$
- $w_6 = 2\pi f_6$

Finally, the transfer function of the band pass filter used for the computation of the comfort coefficient a_{eq} is constructed using the following equation:

$$H_{W_i}(s) = H_h(s) H_l(s) H_t(s) H_s(s) \quad (3.29)$$

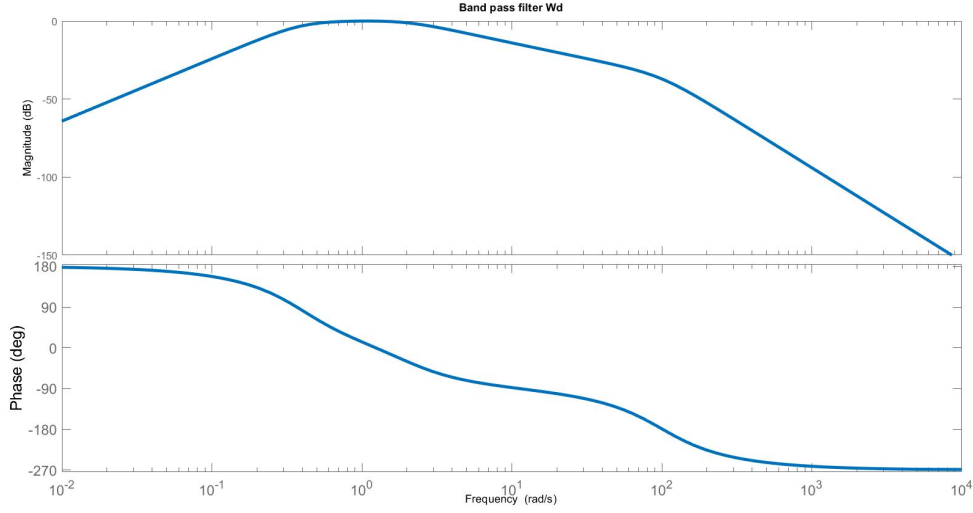


Figure 3.14: Bode of the band pass filter W_d

Depending on the parameters of $H_h(s)$, $H_l(s)$, $H_t(s)$ and $H_s(s)$ described above and the Table 3.3, the transfer function in equation 3.29 can be either H_{W_d} (for the a_{eq} coefficient) or H_{W_f} (for the $MSDV$ coefficient).[37]

Table 3.3: Parameters for the frequency weighting filters of ISO 2631-1

Weighting function	w_1	w_2	w_3	w_4	w_5	w_6	Q_4	Q_5	Q_6
a_{eq} (W_d)	2.51	628.31	12.56	12.56	∞	∞	0.63	-	-
$MSDV$ (W_f)	0.50	3.95	∞	1.57	0.39	0.62	0.86	0.80	0.80

3.3.3 Motion sickness dose value

The second index called Motion sickness dose value ($MSDV$) indicates the percentage of people who may experience motion sickness. It is computed in the same way of the comfort coefficient a_{eq} described above but with a different weighting function. The Motion sickness dose value ($MSDV$) is:

$$a_{MSDV} = \left(\int_{t_0}^{T_f} [a_{i,W_f}(t)]^2 dt \right)^{\frac{1}{2}} \quad (3.30)$$

where a_{i,W_f} is the instantaneous frequency weighted acceleration, T_f is the full period of exposure and W_f is the frequency weighting function shown in Figure 3.16 in solid line. Hence, the MSDV is accumulated over time, in correspondence with how most people experience motion sickness. However, to compare acceleration data of different time ranges it can be useful to compute the mean MSDV-rate, $MSDV/T_f$. This measure is independent of the time range of the measurement.[37]

$$a_{MSDV/T_f} = \frac{1}{T_f} \left(\int_{t_0}^{T_f} [a_{i,W_f}(t)]^2 dt \right)^{\frac{1}{2}} \quad (3.31)$$

According to ISO 2631, the percentage of people who may vomit is approximately given by :

$$a_{MSDV}[\%] = K_m a_{MSDV} \quad (3.32)$$

where K_m is equal to 1/3.

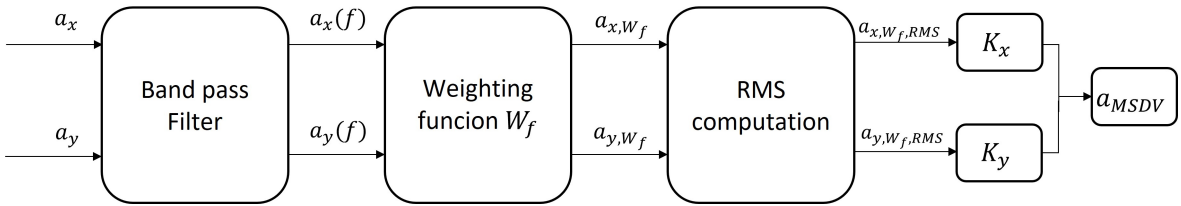


Figure 3.15: Comfort coefficient $MSDV$ procedure computation

where $K_x = K_y = 1$

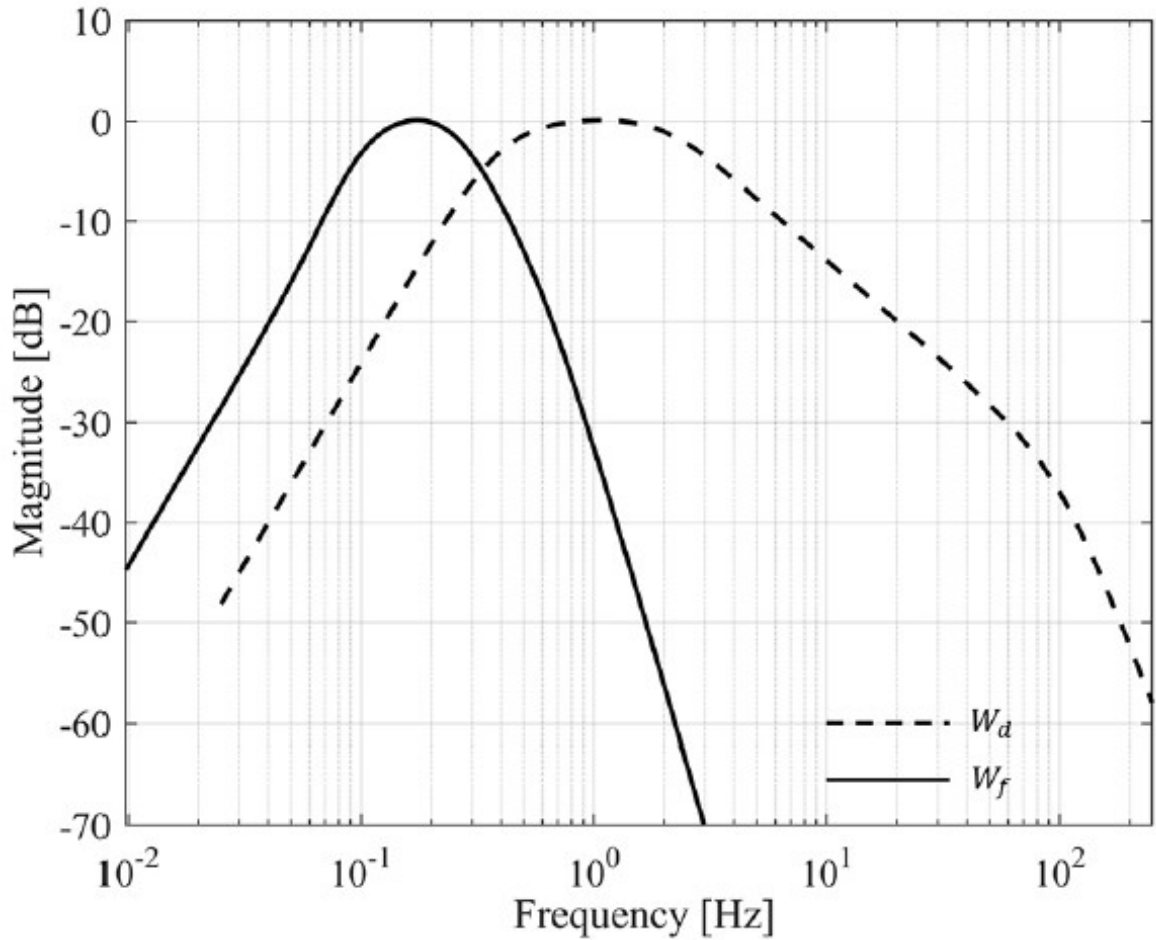


Figure 3.16: Weighting functions; W_f (solid line) for $MSDV$ and W_d (dashed line) for a_{eq} ; ISO 2631-1 [36]

The comfort indexes described above are used to evaluate the performance of the fuzzy comfort-oriented speed profile generator presented in this thesis work. Moreover, the comfort coefficient a_{eq} is also used as one of the inputs of the Fuzzy Logic Controller.

CHAPTER 4

Modelling

This chapter presents the mathematical vehicle models used for the simulation and evaluation of the proposed comfort-oriented speed profile generator.

Three vehicle models are described in this chapter, the first two models present the kinematic and dynamic model of a three degrees of freedom vehicle and the third model is a linearized model used in the Adaptive Model Predictive Control.

In the first part of the chapter, reference frame and vehicle coordinates are described to familiarize with the conventions and symbols typically used in literature. Afterwards, a detailed description of the three degrees of freedom model is presented. This simple model is used for the fuzzy logic controller's first design. Although the model provides less accurate prediction with respect to other more complex vehicle models, it is less computationally demanding and for this reason it was used as first approximation to have fast simulations.

In the second part of the chapter the linearized model used by the Adaptive MPC is presented together with a brief description of the control strategy used for the lateral and longitudinal dynamics of the vehicle.

The second part of the chapter aims to present a description of the fifteen degrees of freedom vehicle model which is imported from Simscape Vehicle Template on Matlab[®] and Simulink[®]. This complex model is computationally expensive but it is able to provide very accurate predictions. Finally, a brief description of the Model Predictive Control strategy is reported.

Both the simple three DOF model and the complex fifteen DOF model are used in the validation phase.

4.1 Reference frame and vehicle coordinates

The right-handed Cartesian world coordinate system defined in ISO 8855 is used to describe the vehicle axis system. The Vehicle coordinate system is illustrated in the following figure:

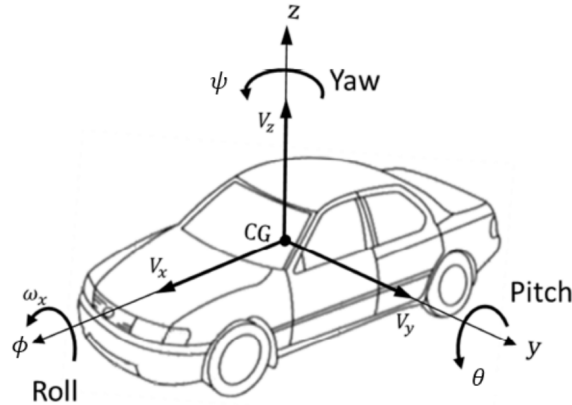


Figure 4.1: Vehicle Coordinates System [38]

The symbol **CG** indicates the Center of Gravity. It corresponds to the mean value of the system's mass distribution in space. The Center of Gravity is the origin of the vehicle reference frame.

The vehicle movements are divided into translational and rotational movements. The translational movements along the main axis are:

- Longitudinal movement along axis x
- Lateral movement along axis y
- Vertical movement along axis z

Velocities along the axes are indicated with v . Accelerations are indicated with a . The subscript represents the axis along which the velocity and acceleration propagate.

- Longitudinal velocity v_x, \dot{x}
- Lateral velocity v_y, \dot{y}
- Vertical velocity v_z, \dot{z}
- Longitudinal acceleration a_x, \dot{v}_x, \ddot{x}
- Lateral acceleration a_y, \dot{v}_y, \ddot{y}
- Vertical acceleration a_z, \dot{v}_z, \ddot{z}

The rotational movements around the main axes are:

- Roll. It is indicated with ϕ . It represents the rotation about the longitudinal axis x

- Pitch. It is indicated with θ . It represents the rotation about the lateral axis y
- Yaw. It is indicated with ψ . It represents the rotation about the vertical axis z

Angular velocities around the axes are indicated with ω , accelerations are indicated with α . The subscript represents the rotation axis.

- Angular velocity around longitudinal axis x is indicated with ω_x or $\dot{\phi}$
- Angular velocity around lateral axis y is indicated with ω_y or $\dot{\theta}$
- Angular velocity around vertical axis z is indicated with $\omega_z, \dot{\Psi}, \dot{\psi}, r$.
- Angular acceleration around longitudinal axis x is indicated with $\alpha_x, \dot{\omega}_x, \ddot{\phi}$
- Angular acceleration around lateral axis y is indicated with $\alpha_y, \dot{\omega}_y, \ddot{\theta}$
- Angular acceleration around vertical axis z is indicated with $\alpha_z, \dot{\omega}_z, \ddot{\Psi}, \ddot{\psi}, \dot{r}$.

The Vehicle reference frame is fixed in the Center of Gravity and it moves together with the vehicle. On the other hand, the World reference system does not move with the vehicle, it remains fixed on the ground.

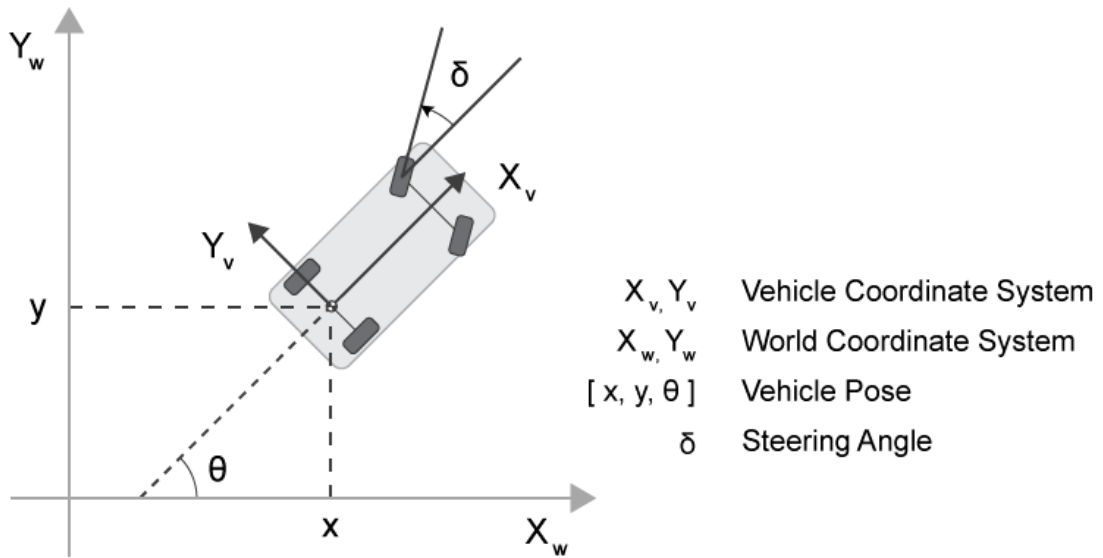


Figure 4.2: World Coordinates System [39]

The global coordinates are typically indicated with capital letters or with the subscript W. For now on, global coordinates are indicated with bold capital letter:

- Longitudinal global direction \mathbf{X}
- Lateral global direction \mathbf{Y}
- Vertical global direction \mathbf{Z}

4.2 3 DOF vehicle model

As said above, a three degrees of freedom vehicle model is used as simple approximation of the real vehicle behaviour in the first part of the design of the Fuzzy Logic Controller. Even if the model does not provide accurate predictions, it is low computationally demanding and the simulations performed with this model are low time consuming.

Only three directions are considered in this simple model:

- Longitudinal direction along axis x
- Lateral direction along axis y
- Yaw direction, rotation along axis z

In this section, both kinematic and dynamic model of a 3 DOF vehicle model are presented together with their constraints and assumptions.

4.2.1 Kinematic Model

The assumptions considered in this vehicle modelling are:

- The front and the rear tires are represented as one single tire on each axle. The imaginary tire contact points V and H are along the center of the axle.
- The pneumatic trail and the aligning torque are neglected.
- The longitudinal forces on the tires are not considered.
- The load distribution between front and rear axle is constant.
- The vehicle's mass is concentrated at the center of gravity S.
- The velocity of the vehicle's center of gravity is considered constant along the longitudinal direction.
- All Roll, Pitch and Lift movements are neglected.

The last two assumptions lead to three constraints for the six degree of freedom rigid body in the model. Hence, the six degree of freedom reduces to three. The only possible movements are the longitudinal movement along axis x, lateral movement along axis y and rotational movement along axis z defined by the yaw angle ψ_v and slip angle β . The latter represents the difference between the direction of the center of gravity and the vehicle's steering axis.[40]

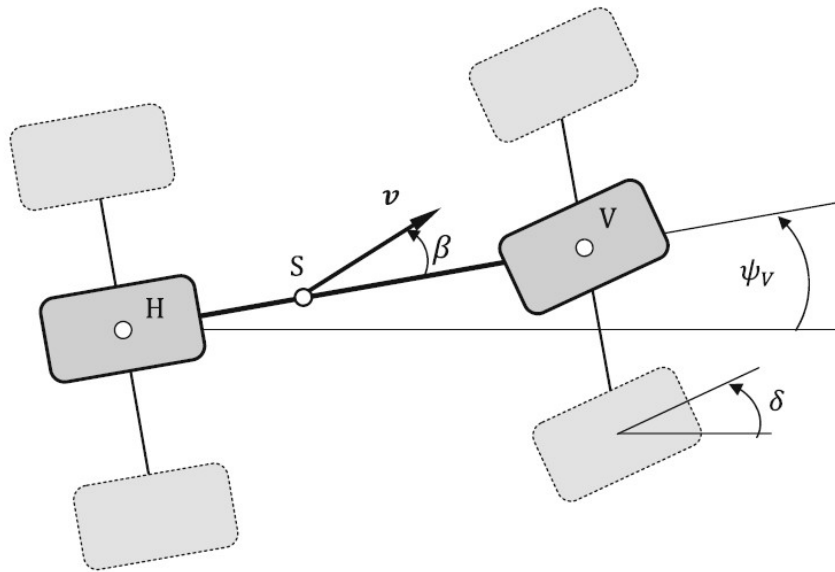


Figure 4.3: Linear single track model [40]

In order to compute the equations of motion of the presented rigid body, kinematics of the vehicle is reviewed. Kinematics is a branch of the mechanics that describes the motion of a point, body and groups of objects without considering the forces that influence the motion.

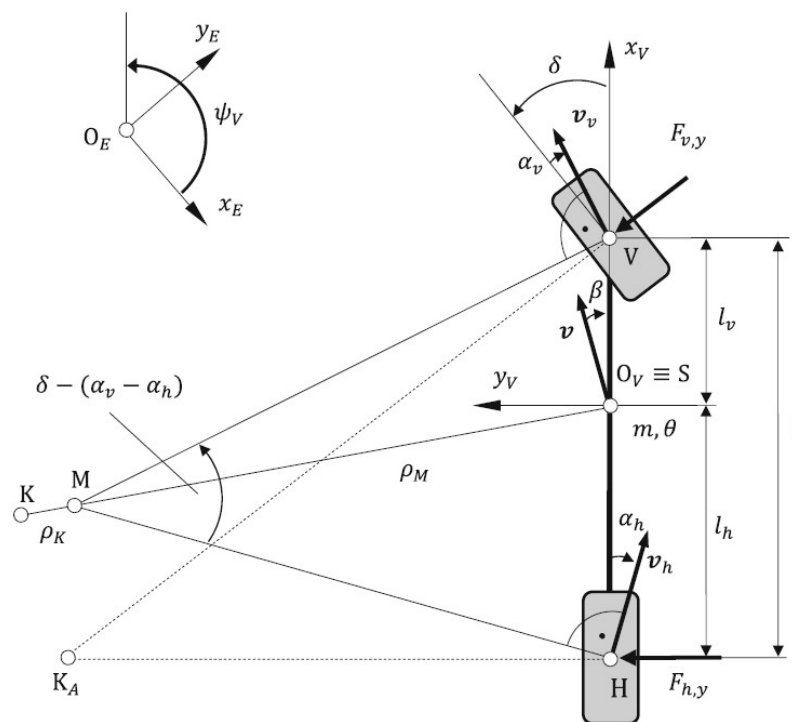


Figure 4.4: Kinematic of the single track model [40]

The kinematic of the vehicle is described considering the inertial system $\mathbf{K}_E = \{O_E; x_E; y_E; z_E\}$ as shown in Figure 4.4. Based on the assumption of very small velocities v of the center of gravity, indicated with the letter S, all the points of the rigid body move in a circle with center in K_A . The latter coincides with the instantaneous center of rotation M under this assumption. In order to execute this motion, the vehicle requires a steering angle computed according to the following equation:

$$\tan \delta_A = \frac{l}{\sqrt{\rho_M^2 - l_h^2}} \quad (4.1)$$

Under the assumption of small steering motion and large radii of curvature with respect to the dimension of the vehicle:

$$|\delta_A| \ll 1 \quad (4.2)$$

$$l \ll \rho_M \quad (4.3)$$

the steering angle can be approximated as follow:

$$\tan \delta_A \approx \frac{l}{\rho_M} \quad (4.4)$$

The distance between the rear axle and the center of gravity is defined as rear wheelbase and it is indicates with l_h . The distance between the center of gravity and front axle is defined as front wheelbase and it is indicate with l_v . The sum of the rear wheelbase and the front wheelbase is called simply wheelbase and it is indicated with l .

$$l = l_h + l_v \quad (4.5)$$

The steering angle of the front wheel is typically called Ackermann steering angle and it is computed as in Eq. (4.4).

The velocity of the vehicle is computed according to the local reference frame $K_v = \{O_V, x_V; y_V; z_V\}$. The origin of the local reference frame is the center of gravity S.

$$\mathbf{v}_v = \begin{bmatrix} v \cos \beta \\ v \sin \beta \\ 0 \end{bmatrix} \quad (4.6)$$

Hence, the acceleration of the vehicle's center of gravity is:

$$\mathbf{v}_a = \frac{d\mathbf{v}_v}{dt} + \mathbf{v}_\omega \times \mathbf{v}_v = \begin{bmatrix} -v \sin \beta \dot{\beta} \\ v \cos \beta \dot{\beta} \\ 0 \end{bmatrix} + \begin{bmatrix} 0 \\ 0 \\ \dot{\psi}_V \end{bmatrix} \times \begin{bmatrix} v \cos \beta \\ v \sin \beta \\ 0 \end{bmatrix} = \begin{bmatrix} -v (\dot{\psi}_V + \dot{\beta}) \sin \beta \\ v (\dot{\psi}_V + \dot{\beta}) \cos \beta \\ 0 \end{bmatrix} \quad (4.7)$$

Based on the assumption of constant longitudinal velocity, the acceleration is purely normal and perpendicular to the vehicle:

$$a_n = |a_n| = v \left(\dot{\psi}_V + \dot{\beta} \right) \quad (4.8)$$

The lateral acceleration of center of gravity, perpendicular to the longitudinal axis is:

$$a_y = v \left(\dot{\psi}_V + \dot{\beta} \right) \cos \beta \approx v \left(\dot{\psi}_V + \dot{\beta} \right) = \frac{v^2}{\rho_K} \quad (4.9)$$

under the assumption of small side slip angle β and according to the following equation:

$$\rho_K = \frac{v}{\left(\dot{\psi}_V + \dot{\beta} \right)} \quad (4.10)$$

The velocities of the tires contact points are needed to compute the horizontal tire forces, used afterward in the dynamic model.

Therefore, the velocity at the front wheel is :

$$v_{v_v} = \begin{bmatrix} v \cos \beta \\ v \sin \beta \\ 0 \end{bmatrix} + \begin{bmatrix} 0 \\ 0 \\ \dot{\psi}_V \end{bmatrix} \times \begin{bmatrix} l_v \\ 0 \\ 0 \end{bmatrix} = \begin{bmatrix} v \cos \beta \\ v \sin \beta + l_v \dot{\psi}_V \\ 0 \end{bmatrix} \quad (4.11)$$

The velocity at the rear wheel is:

$$v_{v_h} = \begin{bmatrix} v \cos \beta \\ v \sin \beta \\ 0 \end{bmatrix} + \begin{bmatrix} 0 \\ 0 \\ \dot{\psi}_V \end{bmatrix} \times \begin{bmatrix} -l_h \\ 0 \\ 0 \end{bmatrix} = \begin{bmatrix} v \cos \beta \\ v \sin \beta - l_h \dot{\psi}_V \\ 0 \end{bmatrix} \quad (4.12)$$

Expressing the front wheel current velocity as the side slip angle β and the steering angle δ we obtain:

$$v_{v_v} = \begin{bmatrix} v \cos \beta \\ v \sin \beta + l_v \dot{\psi}_V \\ 0 \end{bmatrix} = \begin{bmatrix} v_v \cos (\delta - \alpha_v) \\ v_v \sin (\delta - \alpha_v) \\ 0 \end{bmatrix} \quad (4.13)$$

The front slip angle α_v with the assumption of small steering angle δ is:

$$\tan (\delta - \alpha_v) = \frac{v \sin \beta + l_v \dot{\psi}_V}{v \cos \beta} \approx \beta + l_v \frac{\dot{\psi}_V}{v} \quad (4.14)$$

$$\alpha_v \approx \delta - \beta - l_v \frac{\dot{\psi}_V}{v} \quad (4.15)$$

The same can be done to the rear axle:

$$v_{v_h} = \begin{bmatrix} v \cos \beta \\ v \sin \beta - l_h \dot{\psi}_V \\ 0 \end{bmatrix} = \begin{bmatrix} v_h \cos \alpha_h \\ -v_h \sin \alpha_h \\ 0 \end{bmatrix} \quad (4.16)$$

The rear slip angle α_h with the assumption of small steering angle δ is:

$$-\tan \alpha_h = \frac{v \sin \beta - l_h \dot{\psi}_V}{v \cos \beta} \approx \beta - l_h \frac{\dot{\psi}_V}{v} \quad (4.17)$$

$$\alpha_h \approx -\beta + l_h \frac{\dot{\psi}_V}{v} \quad (4.18)$$

4.2.2 Dynamic Model

Dynamics is a branch of the mechanics that study the motion of a system with regard to the forces and torques that govern it. This models tend to be more complex and computationally demanding with respect to the kinematic model described above. However, it provides accurate predictions of the vehicle dynamics. Indeed, it is typically used for high performance scenario like racing. The method used to describe the dynamic model is based on the Newton-Euler approach.[41]

Longitudinal vehicle dynamics

In Figure 4.5 it is illustrated the free-body diagram of the vehicle.

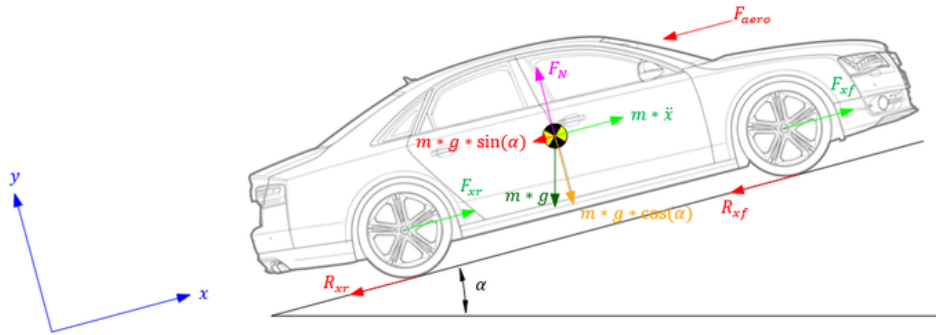


Figure 4.5: Longitudinal vehicle dynamics free-body diagram.[41]

According to the second law of Newton we have:

$$m\ddot{x} = F_{xf} + F_{xr} - F_{aereo} - R_{xf} - R_{xr} - mg \sin \alpha \quad (4.19)$$

where:

- $m\ddot{x}$: Vehicle inertial term.
- F_{xf} : Front tire force.
- F_{xr} : Rear tire force.
- R_{xf} : Front rolling resistance.
- R_{xr} : Rear rolling resistance.
- $mg \sin \alpha$: Component of the gravitational force.

To simplify the equation we can represent the front and rear tire forces as unique traction force F_x and the front and rear rolling resistance as unique rolling resistance R_x . Moreover, under the assumption of small angle α we have $\sin \alpha \approx \alpha$. Hence, the resulting simplified equation is:

$$m \ddot{x} = F_x - F_{aereo} - R_x - m g \alpha \quad (4.20)$$

- **Traction Force F_x :** It depends on the angular acceleration of the wheel $\ddot{\theta}_{wheel}$, the wheel radius r_{wheel} and the vehicle mass m .

$$F_x = m r_{wheel} \ddot{\theta}_{wheel} \quad (4.21)$$

- **Aerodynamic drag force:** This force interferes with the longitudinal movement of the vehicle and it is due to the relative motion between the vehicle and the gas in which the vehicle is immersed.

$$F_{aereo} = \frac{1}{2} C_\alpha \rho A v^2 \approx C_\alpha v^2 \quad (4.22)$$

where:

- ρ : air density.
- A: Frontal surface area of the vehicle.
- C_α : Drag coefficient, it is related to the shape of the vehicle and to the Reynolds number of the fluid.
- v : Longitudinal velocity of the vehicle.
- **Rolling Resistance:** Depends on the tire pressure P (function of the vehicle velocity) and on the tire normal force N.

$$R_x = NP(v) \quad (4.23)$$

$$P(v) = C_{r,0} + C_{r,1}|v| + C_{r,2}v^2 \quad (4.24)$$

$$R_x = NC_{r,0} + C_{r,1}|v| + C_{r,2}v^2 \approx C_{r,1}|v| \quad (4.25)$$

Finally, the resulting equation for the longitudinal dynamic is:

$$\ddot{x} = r_{wheel} \ddot{\theta}_{wheel} - \frac{C_\alpha v^2}{m} - \frac{C_{r,1} |v|}{m} - g \alpha \quad (4.26)$$

Lateral vehicle dynamics

In Figure 4.6 it is shown the free-body diagram along the lateral direction.

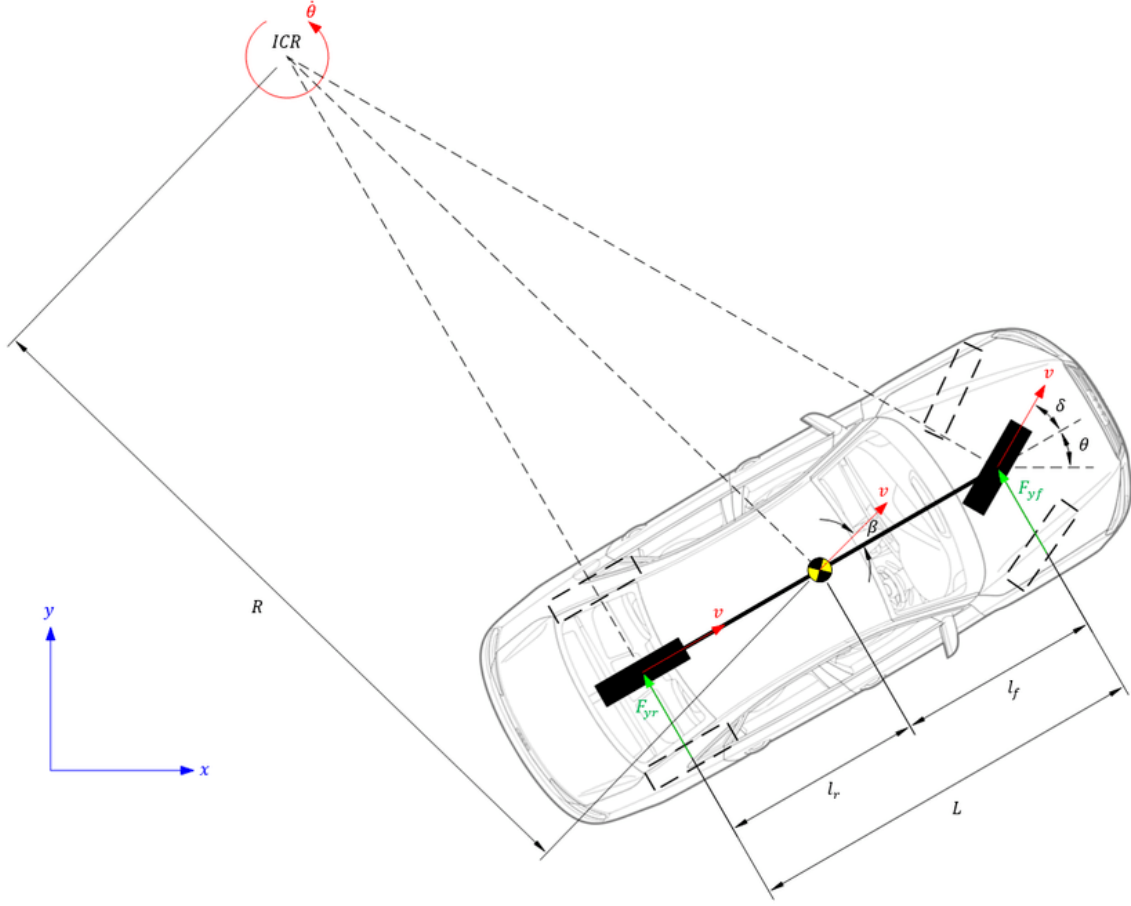


Figure 4.6: Lateral vehicle dynamics free-body diagram [41]

According to Newton's second law we obtain:

$$m a_y = F_{yf} + F_{yr} \quad (4.27)$$

$$I_z \ddot{\theta} = l_f F_{yf} - l_r F_{yr} \quad (4.28)$$

The forces in the lateral direction considered are the front and rear tire forces, F_{yf} and F_{yr} respectively, and the inertial term $m a_y$. The vehicle torque about instantaneous center of rotation $I_z \ddot{\theta}$ and the moments of front and rear tire forces, $l_f F_{yf}$ and $l_r F_{yr}$ respectively, are the torques that act on the vehicle.

The total acceleration is computed as follow:

$$a_y = \ddot{y} + R \dot{\theta}^2 = \ddot{y} + v \dot{\theta} \quad (4.29)$$

Hence, substituting Eq. 4.29 in Eq. 4.27 we have:

$$m(\ddot{y} + v\dot{\theta}) = F_{yf} + F_{yr} \quad (4.30)$$

The front and rear lateral tire forces F_{yf} , F_{yr} also called cornering forces, can be computed with the help of the diagram in Figure 4.7 and with the following equations:

$$F_{yf} = C_f \alpha_f = C_f \left(\delta - \beta - \frac{l_f \dot{\theta}}{v} \right) \quad (4.31)$$

$$F_{yr} = C_r \alpha_r = C_r \left(-\beta + \frac{l_r \dot{\theta}}{v} \right) \quad (4.32)$$

where C_f and C_r are the cornering stiffness of the front and rear tires and α_f and α_r are the front and rear tire slip angle respectively.

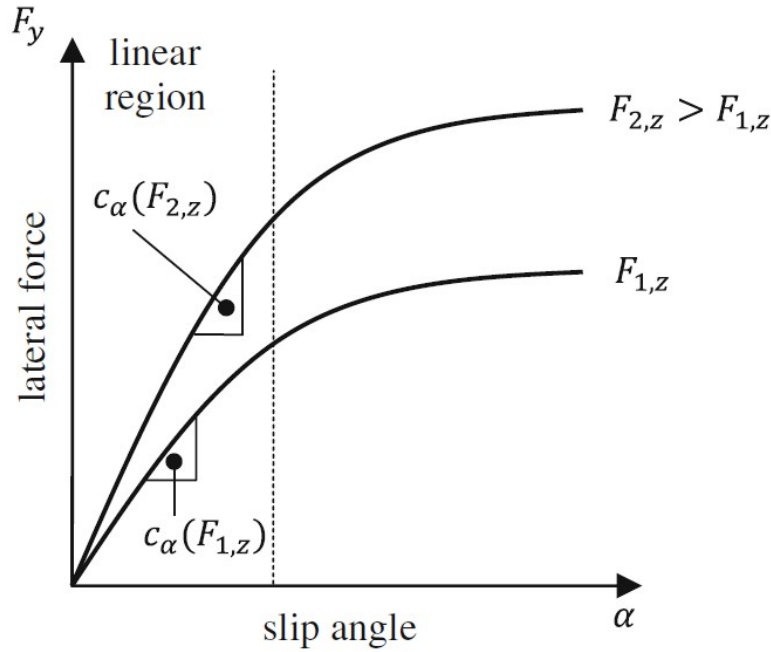


Figure 4.7: Relationship between the tire lateral forces and the slip angle [40]

Finally, substituting Eq. 4.31 and 4.32 in Eq. 4.30 and 4.28 we get:

$$\ddot{y} = -\frac{C_f + C_r}{m} \beta + \left(\frac{C_r l_r - C_f l_f}{m v} - v \right) \dot{\theta} + \frac{C_f}{m} \delta \quad (4.33)$$

$$\ddot{\theta} = \frac{C_r l_r - C_f l_f}{I_z} \beta - \frac{C_r l_r^2 + C_f l_f^2}{I_z v} \dot{\theta} + \frac{C_f l_f}{I_z} \delta \quad (4.34)$$

Tires load distribution

In the following figure it is illustrated the static load distribution of the vehicle when the velocity is equal to zero.

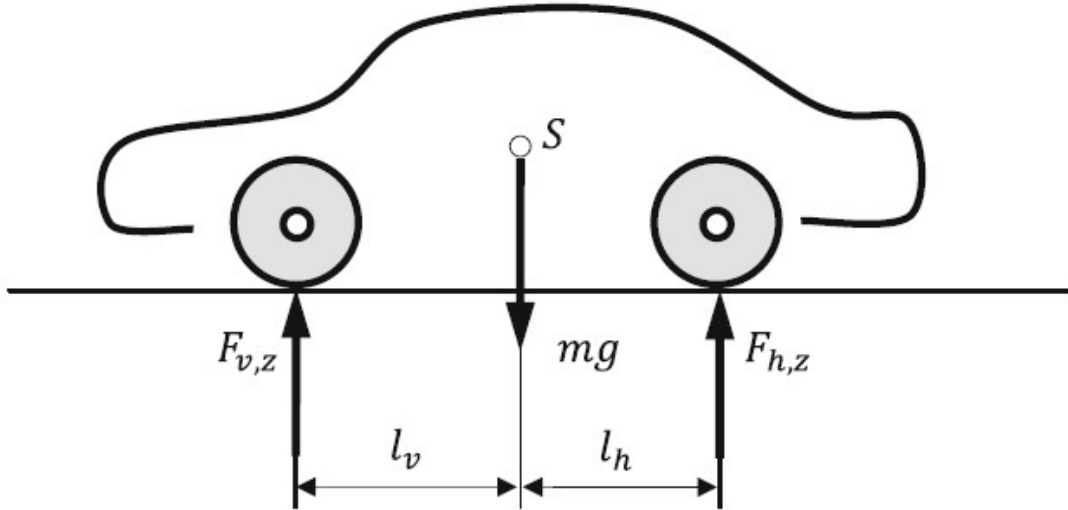


Figure 4.8: Tires load distribution [40]

The following equations describe the equilibrium in the vertical direction z and the rotation equilibrium around the rear tire contact point.

$$F_{v,z} + F_{h,z} - m g = 0 \quad (4.35)$$

$$m g l_h - F_{v,z} l_v = 0 \quad (4.36)$$

The normal forces acting on the front and rear tire $F_{v,z}$ and $F_{h,z}$ respectively, are given by:

$$F_{v,z} = m g \frac{l_h}{l} \quad (4.37)$$

$$F_{h,z} = m g \frac{l_v}{l} \quad (4.38)$$

$$l = l_v + l_h \quad (4.39)$$

4.2.3 Parameterized Vehicle Model for Adaptive MPC

In this thesis work, an Adaptive Model Predictive Control has been used to manage the longitudinal and lateral dynamics of the autonomous vehicle. To this end, the equations of motion of a two degrees of freedom vehicle model, used to define the lateral and longitudinal dynamics of the car, are written in terms of the lateral deviation error e_1 and the relative yaw angle error e_2 .

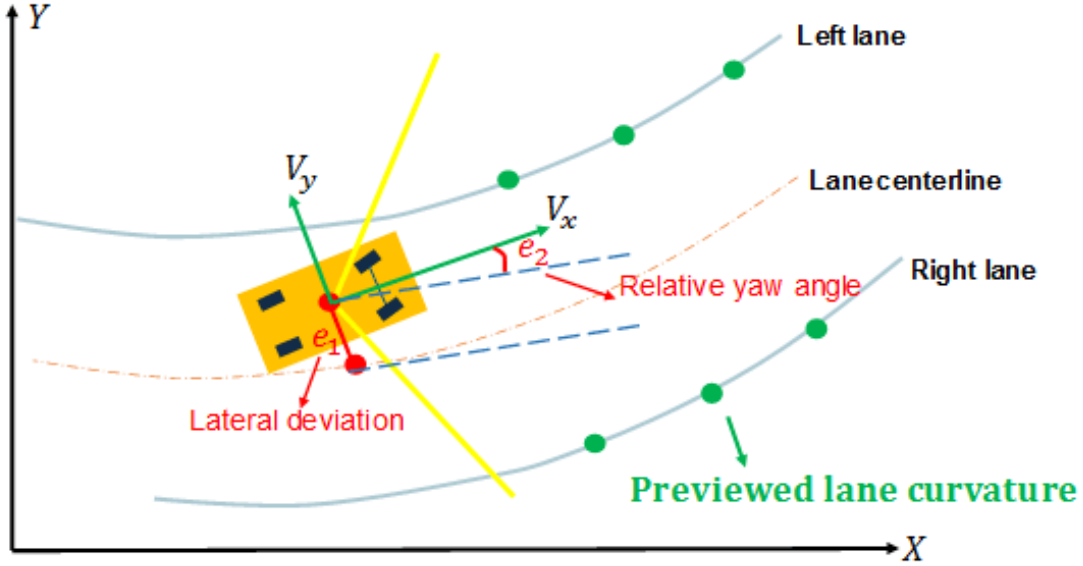


Figure 4.9: Lateral deviation and relative yaw angle errors. [42]

- **Lateral deviation error e_1** : It is defined as the distance between the centerline of the reference trajectory and the center of gravity of the vehicle.
- **Relative yaw angle e_2** : It is defined as the deviation of the yaw angle of the vehicle from the desired yaw angle provided by the reference trajectory.

Lateral deviation error e_1 and relative yaw angle e_2 are described in mathematical form as follow:

$$e_1 = y - y_{cl} \quad (4.40)$$

$$e_2 = \psi - \psi_{des} \quad (4.41)$$

and their derivatives are:

$$\dot{e}_1 = V_y + V_x e_2 \quad (4.42)$$

$$\dot{e}_2 = \dot{\psi} - \dot{\psi}_{des} \quad (4.43)$$

- \mathbf{y}_{cl} : is the position of the lane centerline.
- ψ_{des} : is the desired yaw angle provided by the reference trajectory.
- $\dot{\psi}_{des}$: is the desired yaw rate and it is computed as follow:

$$\dot{\psi}_{des} = V_x \kappa \quad (4.44)$$

where κ is the road curvature

The transfer function between the desired acceleration and the actual vehicle speed is given by:

$$P(s) = \frac{1}{s(\tau s + 1)} \quad (4.45)$$

It accounts for the longitudinal dynamics of the vehicle. In matrix form we have:

$$\begin{bmatrix} \dot{V}_x \\ \dot{V}_x \end{bmatrix} = \begin{bmatrix} -\frac{1}{\tau} & 0 \\ 1 & 0 \end{bmatrix} \begin{bmatrix} \dot{V}_x \\ V_x \end{bmatrix} + \begin{bmatrix} \frac{1}{\tau} \\ 0 \end{bmatrix} \ddot{V}_x \quad (4.46)$$

$$y = \begin{bmatrix} 0 & 1 \end{bmatrix} \begin{bmatrix} \dot{V}_x \\ V_x \end{bmatrix} \quad (4.47)$$

τ is the time constant, \ddot{V}_x is the longitudinal jerk.

The state space model for the lateral dynamics is:

$$\begin{bmatrix} \dot{V}_y \\ \ddot{\psi} \end{bmatrix} = \begin{bmatrix} -\frac{(2C_f + 2C_r)}{mV_x} & -V_x - \frac{(2C_f l_f - 2C_r l_r)}{mV_x} \\ -\frac{(2C_f l_f - 2C_r l_r)}{I_{zz}V_x} & -\frac{(2C_f l_f^2 + 2C_r l_r^2)}{I_{zz}V_x} \end{bmatrix} \begin{bmatrix} V_y \\ \dot{\psi} \end{bmatrix} + \begin{bmatrix} \frac{2C_f}{m} \\ \frac{2C_f l_f}{I_{zz}} \end{bmatrix} \delta \quad (4.48)$$

and the state space form of the lateral deviation and relative yaw angle is:

$$\begin{bmatrix} \dot{e}_1 \\ \dot{e}_2 \end{bmatrix} = \begin{bmatrix} 1 & 0 & 0 & V_x \\ 0 & 1 & 0 & 0 \end{bmatrix} \begin{bmatrix} V_y \\ \dot{\psi} \\ e_1 \\ e_2 \end{bmatrix} + \begin{bmatrix} 0 \\ -\kappa \end{bmatrix} V_x \quad (4.49)$$

Merging together Eq. 4.48 and 4.49 we obtain the linearized model for the lateral control used by the Adaptive MPC.

$$\begin{bmatrix} \dot{V}_y \\ \dot{\psi} \\ \dot{e}_1 \\ \dot{e}_2 \end{bmatrix} = \begin{bmatrix} -\frac{(2C_f + 2C_r)}{mV_x} & -V_x - \frac{(2C_f l_f - 2C_r l_r)}{mV_x} & 0 & 0 \\ -\frac{(2C_f l_f - 2C_r l_r)}{I_{zz}V_x} & -\frac{(2C_f l_f^2 + 2C_r l_r^2)}{I_{zz}V_x} & 0 & 0 \\ 1 & 0 & 0 & V_x \\ 0 & 1 & 0 & 0 \end{bmatrix} \begin{bmatrix} V_y \\ \psi \\ e_1 \\ e_2 \end{bmatrix} + \begin{bmatrix} 2\frac{C_f}{m} \\ 2\frac{C_f l_f}{I_{zz}} \\ 0 \\ 0 \end{bmatrix} \delta + \begin{bmatrix} 0 \\ 0 \\ 0 \\ -\kappa \end{bmatrix} V_x \quad (4.50)$$

$$y = \begin{bmatrix} 0 & 0 & 1 & 0 \\ 0 & 0 & 0 & 1 \end{bmatrix} \begin{bmatrix} V_y \\ \dot{\psi} \\ e_1 \\ e_2 \end{bmatrix} \quad (4.51)$$

The Adaptive MPC uses a fixed model structure, but allows the models parameters to evolve with time. The plant model is updated at each time step as the operating point keeps changing. Therefore, the adaptive MPC, differently from the standard MPC, uses a suitable model for the current condition.

The plant model used in the Adaptive MPC is an LTI discrete-time, state-space model with a sampling time T_s equal to 100 ms. The state space model that accounts for the combined longitudinal and lateral dynamics used in the internal plant model of the Adaptive MPC is the following:

$$\begin{aligned} x(k+1) &= Ax(k) + B_u u(k) + B_d v(k) \\ y(k) &= Cx(k) \end{aligned} \quad (4.52)$$

where:

- k is the time index (current control interval).
- x represents the plant model states.
- u are the manipulated input variables.
- v are the measured input disturbances.
- y represents the output vector.
- A is the state matrix
- B_u is the input matrix
- B_d is the disturbance input matrix
- C is the output matrix

$$\underbrace{\begin{bmatrix} \ddot{V}_x \\ \dot{V}_x \\ \dot{V}_y \\ \ddot{\psi} \\ \dot{e}_1 \\ \dot{e}_2 \end{bmatrix}}_{\mathbf{x}(k+1)} = \underbrace{\begin{bmatrix} -\frac{1}{\tau} & 0 & 0 & 0 & 0 & 0 \\ 1 & 0 & 0 & 0 & 0 & 0 \\ 0 & 0 & -\frac{(2C_f+2C_r)}{mV_x} & -V_x - \frac{(2C_f l_f - 2C_r l_r)}{mV_x} & 0 & 0 \\ 0 & 0 & -\frac{(2C_f l_f - 2C_r l_r)}{I_{zz}V_x} & -\frac{(2C_f l_f^2 + 2C_r l_r^2)}{I_{zz}V_x} & 0 & 0 \\ 0 & 0 & 1 & 0 & 0 & V_x \\ 0 & 0 & 0 & 1 & 0 & 0 \end{bmatrix}}_{\mathbf{A}} \underbrace{\begin{bmatrix} \dot{V}_x \\ V_x \\ V_y \\ \psi \\ e_1 \\ e_2 \end{bmatrix}}_{\mathbf{x}(k)} +$$

$$+ \underbrace{\begin{bmatrix} \frac{1}{\tau} & 0 \\ 0 & 0 \\ 0 & 2\frac{C_f}{m} \\ 0 & 2\frac{C_f l_f}{I_{zz}} \\ 0 & 0 \\ 0 & 0 \end{bmatrix}}_{\mathbf{B}_u} \underbrace{\begin{bmatrix} \dot{V}_x \\ \delta \end{bmatrix}}_{\mathbf{u}(k)} + \underbrace{\begin{bmatrix} 0 \\ 0 \\ 0 \\ 0 \\ 0 \\ -\kappa \end{bmatrix}}_{\mathbf{B}_d} \underbrace{V_x}_{\mathbf{v}(k)}$$

$$\underbrace{\begin{bmatrix} V_x \\ e_1 \\ e_2 \end{bmatrix}}_{\mathbf{y}(k)} = \underbrace{\begin{bmatrix} 0 & 1 & 0 & 0 & 0 & 0 \\ 0 & 0 & 0 & 0 & 1 & 0 \\ 0 & 0 & 0 & 0 & 0 & 1 \end{bmatrix}}_{\mathbf{C}} \underbrace{\begin{bmatrix} \dot{V}_x \\ V_x \\ V_y \\ \psi \\ e_1 \\ e_2 \end{bmatrix}}_{\mathbf{x}(k)}$$
(4.53)

The state vector is composed of longitudinal acceleration, longitudinal velocity, lateral velocity, angular velocity, lateral deviation and relative yaw angle:

$$\begin{bmatrix} \dot{V}_x & V_x & \dot{V}_y & \dot{\psi} & e_1 & e_2 \end{bmatrix} \quad (4.54)$$

The manipulated variables are the longitudinal acceleration \dot{V}_x and the steering angle δ .

$$\begin{bmatrix} \dot{V}_x & \delta \end{bmatrix} \quad (4.55)$$

The measured outputs are:

$$\begin{bmatrix} V_x & e_1 & e_2 \end{bmatrix} \quad (4.56)$$

The vehicle model used in this thesis work is an autonomous car characterized by the following parameters:

Table 4.1: 3 DOF vehicle model parameters

3 DOF Parameters

$m = 1500$ [kg]	Mass of the vehicle
$I_{zz} = 95.81$ [kgm ²]	Moment of inertia about vertical axis Z [kg m ²]
$l_f = 1.2$ [m]	Front wheelbase, distance between center of gravity and front axle
$l_r = 1.624$ [m]	Rear wheelbase, distance between center of gravity and rear axle
$C_f = 132000$ [N/rad]	Cornering stiffness of the front tire
$C_r = 132000$ [N/rad]	Cornering stiffness of the rear tire
$\tau = 0.5$ [s]	Time constant
$v_0 = 0.001$ [m/s]	Initial longitudinal velocity
$f = 0.0182$	Rolling resistance coefficient
$\mu = 0.8$	Friction coefficient.

4.3 15 DOF vehicle model

The three degrees of freedom simple model described above is used for the fuzzy logic controller's first design. Although the model provides low accurate prediction, it is low computationally demanding and for this reason it was used as first approximation to have fast simulations during the validation phase.

After completing the evaluation of the proposed comfort-oriented speed profile generator with this model, a fifteen degrees of freedom vehicle model, which is imported from Simscape Vehicle Template, was used to obtain very accurate data from simulations. However, the simulations performed with this model were more time consuming.

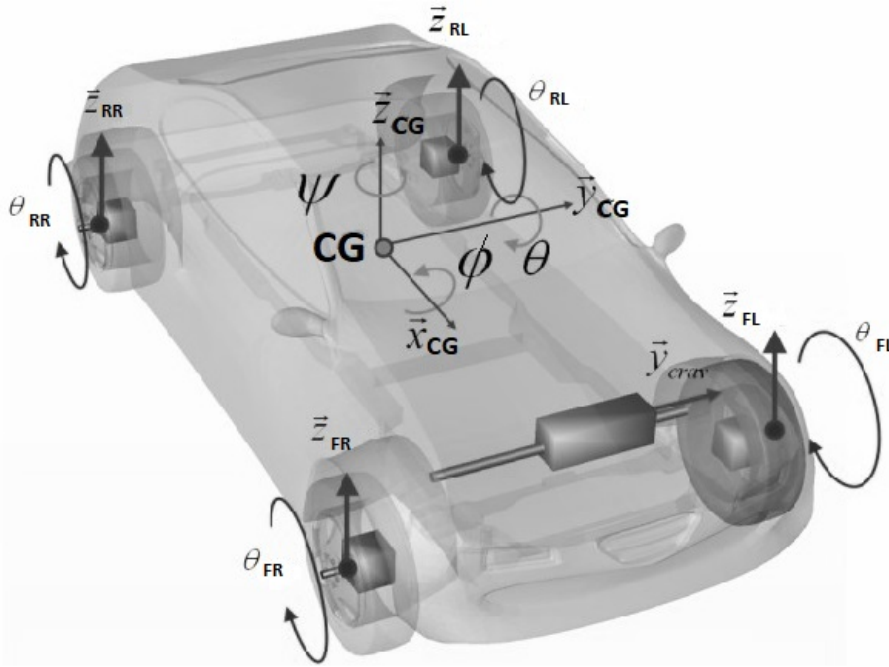


Figure 4.10: Simscape 15 DoF vehicle model

The model represents a four wheel full electric vehicle model powered by two independent electric motors. The coil spring and the shock absorber installed on the double wishbone suspensions are responsible to manage the vertical motion of the car.

The anti-roll bar that is connected to the wishbones limits the body roll, keeping the vehicle more stable when cornering.

The steering wheel rack system accounts for the steering system of the vehicle and it aims to steer the front wheels in the correct direction.

The fifteen degrees of freedom considered in the vehicle model illustrated in figure 4.10 are listed below:

- \mathbf{x}_{CG} , Longitudinal movement along local axis x
- \mathbf{y}_{CG} , Lateral movement along local axis y
- \mathbf{z}_{CG} , Vertical movement along local axis z
- \mathbf{z}_{FL} , Vertical movement of the front left wheel
- \mathbf{z}_{FR} , Vertical movement of the front right wheel
- \mathbf{z}_{RL} , Vertical movement of the rear left wheel
- \mathbf{z}_{RR} , Vertical movement of the rear right wheel
- **Roll** ϕ , Rotation around longitudinal local axis \mathbf{x}_{CG}
- **Pitch** θ , Rotation around lateral local axis \mathbf{y}_{CG}
- **Yaw** ψ , Rotation around vertical local axis \mathbf{z}_{CG}
- θ_{FL} , Rotation of the front left wheel
- θ_{FR} , Rotation of the front right wheel
- θ_{RL} , Rotation of the rear left wheel
- θ_{RR} , Rotation of the rear right wheel
- \mathbf{y}_{crav} , Movement of the front wheel angle

The translational and rotational motions of the center of gravity (CG) of the vehicle are described by the following equations.

Longitudinal movement:

$$m(\dot{v}_x - v_y r + v_z \dot{\theta}) = F_{xfl} + F_{xfr} + F_{xrl} + F_{xrr} \quad (4.57)$$

Lateral movement:

$$m(\dot{v}_y - v_z \dot{\phi} + v_x r) = F_{yfl} + F_{yfr} + F_{yrl} + F_{yrr} \quad (4.58)$$

Vertical movement:

$$m(\dot{v}_z - v_x \dot{\theta} + v_y r) = F_{sfl} + F_{sfr} + F_{srl} + F_{srr} - m_s g \quad (4.59)$$

Rotational movement around the longitudinal x-axis:

$$I_{xx} \ddot{\phi} = \frac{L}{2} (F_{sfl} + F_{srl} - F_{sfr} + F_{srr}) + h_r (F_{yfl} + F_{yfr} - F_{yrl} + F_{yrr})$$

Rotational movement around the lateral y-axis:

$$I_{yy} \ddot{\theta} = l_r (F_{srl} + F_{srr}) - l_f (F_{sfl} + F_{sfr}) + h_p (F_{xfl} + F_{xfr} + F_{xrl} + F_{xrr})$$

Rotational movement around the vertical z-axis:

$$I_{zz} \dot{r} = \frac{L}{2} (F_{xfr} + F_{xrr} - F_{xfl} + F_{xrl}) + l_f (F_{yfl} + F_{yfr}) - l_r (F_{yrl} + F_{yrr})$$

where:

- \mathbf{F}_{xfl} , driving force of front left wheel
- \mathbf{F}_{xfr} , driving force of front right wheel
- \mathbf{F}_{xrl} , driving force of rear left wheel
- \mathbf{F}_{xrr} , driving force of rear right wheel
- \mathbf{F}_{yfl} , yaw force of front left wheel
- \mathbf{F}_{yfr} , yaw force of front right wheel
- \mathbf{F}_{yrl} , yaw force of rear left wheel
- \mathbf{F}_{yrr} , yaw force of rear right wheel
- \mathbf{F}_{sfl} , suspension force of front left wheel
- \mathbf{F}_{sfr} , suspension force of front right wheel
- \mathbf{F}_{srl} , suspension force of rear left wheel
- \mathbf{F}_{srr} , suspension force of rear right wheel
- \mathbf{I}_{xx} , moment of inertia around longitudinal local axis x_{CG}
- \mathbf{I}_{yy} , moment of inertia around lateral local axis y_{CG}
- \mathbf{I}_{zz} , moment of inertia around vertical local axis z_{CG}
- l_r , distance from the center of gravity to rear axle
- l_f , distance from the center of gravity to front axle
- r , wheel radius

- \mathbf{h}_r , distance from the center of mass to roll axle
- \mathbf{h}_p , distance from the center of mass to pitch axle
- \mathbf{m}_{ufl} , mass of front left wheel
- \mathbf{m}_{ufr} , mass of front right wheel
- \mathbf{m}_{url} , mass of rear left wheel
- \mathbf{m}_{urr} , mass of rear right wheel
- \mathbf{m}_u , unsprung mass
- \mathbf{m}_s , sprung mass

$$m_u = m_{ufl} + m_{ufr} + m_{url} + m_{urr} \quad (4.60)$$

$$m = m_s + m_{ufl} + m_{ufr} + m_{url} + m_{urr} = m_s + m_u \quad (4.61)$$

The equations of vertical dynamics for each wheel are equal to:

Vertical movement of rear left wheel:

$$m_{url} \ddot{z}_{url} = k_{url} (z_{rl} - z_{url}) - F_{srl} \quad (4.62)$$

Vertical movement of rear right wheel:

$$m_{urr} \ddot{z}_{urr} = k_{urr} (z_{rr} - z_{urr}) - F_{srr} \quad (4.63)$$

Vertical movement of front left wheel:

$$m_{ufl} \ddot{z}_{ufl} = k_{ufl} (z_{fl} - z_{ufl}) - F_{sfl} \quad (4.64)$$

Vertical movement of front right wheel:

$$m_{ufr} \ddot{z}_{ufr} = k_{ufr} (z_{fr} - z_{ufr}) - F_{sfr} \quad (4.65)$$

where:

- \mathbf{z}_{ufl} , Vertical position of the front left unsprung mass
- \mathbf{z}_{ufr} , Vertical position of the front right unsprung mass
- \mathbf{z}_{url} , Vertical position of the rear left unsprung mass
- \mathbf{z}_{urr} , Vertical position of the rear right unsprung mass
- \mathbf{k}_{ufl} , Vertical stiffness of the front left wheel
- \mathbf{k}_{ufr} , Vertical stiffness of the front right wheel
- \mathbf{k}_{url} , Vertical stiffness of the rear left wheel

- \mathbf{k}_{urr} , Vertical stiffness of the rear right wheel

The equations that describe the rotational equilibrium of the wheels are equal to:

Equilibrium of front left wheel:

$$T_{xfl} - F_{xfl} r_{wheel} - T_{bfl} - R = I_{fl} \dot{\omega}_{fl} \quad (4.66)$$

Equilibrium of front right wheel:

$$T_{xfr} - F_{xfr} r_{wheel} - T_{bfr} - R = I_{fr} \dot{\omega}_{fr} \quad (4.67)$$

Equilibrium of rear left wheel:

$$T_{xrl} - F_{xrl} r_{wheel} - T_{brl} - R = I_{rl} \dot{\omega}_{rl} \quad (4.68)$$

Equilibrium of rear right wheel:

$$T_{xrr} - F_{xrr} r_{wheel} - T_{brr} - R = I_{rr} \dot{\omega}_{rr} \quad (4.69)$$

where:

- \mathbf{T}_{xfl} , Driving torque of the front left wheel
- \mathbf{T}_{xfr} , Driving torque of the front right wheel
- \mathbf{T}_{xrl} , Driving torque of the rear left wheel
- \mathbf{T}_{xrr} , Driving torque of the rear right wheel
- \mathbf{T}_{bfl} , Braking torque of the front left wheel
- \mathbf{T}_{bfr} , Braking torque of the front right wheel
- \mathbf{T}_{brl} , Braking torque of the rear left wheel
- \mathbf{T}_{brr} , Braking torque of the rear right wheel
- \mathbf{I}_{fl} , moment of inertia of the front left wheel
- \mathbf{I}_{fr} , moment of inertia of the front right wheel
- \mathbf{I}_{rl} , moment of inertia of the rear left wheel
- \mathbf{I}_{rr} , moment of inertia of the rear right wheel
- \mathbf{M} , Rolling resistance torque of the wheels

The vehicle parameters used in this model are listed below:

Table 4.2: 15 DOF vehicle model parameters

15 DOF Parameters	
$m = 1500$ [kg]	Mass of the vehicle
$I_{xx} = 432$ [kgm ²]	Moment of inertia about longitudinal axis
$I_{yy} = 1922.7$ [kgm ²]	Moment of inertia about lateral axis
$I_{zz} = 2066$ [kgm ²]	Moment of inertia about vertical axis
$C_f = 132000$ [N/rad]	Front cornering stiffness
$C_r = 132000$ [N/rad]	Rear cornering stiffness
$f = 0.0182$	Rolling resistance coefficient
$\mu = 0.8$	Friction coefficient
$l_f = 1.2$ [m]	Front wheelbase
$l_r = 1.624$ [m]	Rear wheelbase
$r_{\text{wheel}} = 0.35$ [m]	Wheel radius
$m_u = 7$ [kg]	Mass of each wheel
$T = 1.869$ [m]	Vehicle track
$\tau = 0.5$ [s]	Time constant
$v_0 = 0.001$ [m/s]	Initial longitudinal velocity
$k_u = 66000$ [N/m]	Vertical stiffness of the wheel
$k_s = 140000$ [N/m]	Suspension stiffness
$b_s = 140000$ [N·s/m]	Suspension damping of the wheels
$A_{\text{cross}} = 2.81$ [m ²]	Cross-sectional area of the vehicle

4.4 Model Predictive Control

In this section, a brief description of the problem formulation and theory behind the Model Predictive Control is presented. The MPC aims to manage the longitudinal and lateral dynamics of the vehicle to allow autonomous driving. This advanced control method was chosen due to its abilities to work with constraints both on the inputs and outputs. This is important for the control of a vehicle since the car is not only constrained by mechanic limits but also by environment ones such as obstacles and other cars.

MPC is a feedback control algorithm that uses a model to make predictions about future outputs. The MPC control strategy tries to find the best solution among all the possible ones through an optimization problem that minimizes a cost function.

In this thesis work the MPC controller solves a multistep optimization problem and feedback correction based on the following recursive procedure:

- obtain the state vector $x(k) = x(k|k)$
 $x(k|k)$ is the state vector at time instant k
- solve the quadratic optimization problem with respect to $U(k|k)$
 $U(k|k)$ is the input vector at time instant k
- compute the optimal input vector $U^*(k|k)$ that minimizes the cost function in a finite prediction horizon H_p

$$U^*(k|k) = [u^*(k|k) \quad u^*(k+1|k) \quad \dots \quad u^*(k+H_p-1|k)]^T$$

- apply as present control action $u(k|k) = u^*(k|k)$, the first input of the optimal input vector $U^*(k|k)$
- the time instant is updated to $k+1$ and the procedure is repeated

The state space model used as the internal plant model for MPC is:

$$\begin{aligned} x(k+1) &= Ax(k) + B_u u(k) + B_d v(k) \\ y(k) &= Cx(k) \end{aligned}$$

where:

- k is the time index (current control interval)
- x is the state vector
- u is the manipulated variables input vector
- v is the measured disturbance input vector
- y is the output vector
- A is the state matrix

- B_u is the input matrix
- B_v is the disturbance input matrix
- C is the output matrix

The cost function to minimize in order to solve the optimization problem is:

$$\begin{aligned} \min_u J &= \sum_{j=1}^{H_p} \|y(k+j|k) - y_{ref}(k+j|k)\| Q_y + \sum_{j=0}^{H_c-1} \|u(k+j|k)\| R_u \\ \text{subject to } &u(k+j+1|k) = Ax(k+j|k) + B_u u(k+j|k) + B_d v(k+j|k) \\ &x(k|k) = x(k) \\ &y(k+j|k) = Cx(k+j|k) \\ &|u(k+j|k)| \leq u_{limit} \end{aligned} \tag{4.70}$$

where:

- Q_y weighting matrix for the output
- R_u weighting matrix for the manipulated variables
- H_p is the prediction horizon
- H_c is the control horizon

These parameters must be tuned to obtain a suitable control of the vehicle.

The **inputs** to the MPC are:

- previewed curvature, that is the sequence of upcoming road curvature values
- lateral deviation error e_1
- relative yaw angle error e_2
- reference velocity V_{ref} , computed by the proposed fuzzy comfort-oriented speed profile generator.

The **outputs** of the MPC are the front-wheel steering angle δ and the desired longitudinal acceleration a_x . The goal of the MPC controller is to compute the optimal steering angle and throttle/brake commands, minimizing the lateral deviation e_1 and relative yaw angle e_2 , that are provided to the vehicle to maintain the center line and follow the reference trajectory.

CHAPTER 5

Validations and results

In this chapter three different driving scenarios used for simulations are presented. Afterwards, the simulation results are presented and discussed both for the simple three degrees of freedom model and for the more complex fifteen degrees of freedom vehicle model provided by Simscape Vehicle template on MATLAB[®] and Simulink[®]. The results obtained with the fuzzy comfort-oriented speed profile generator are compared to the ones obtained with the classical approach. Finally, an analysis of passengers' comfort seated in different position of the car are presented.

5.1 Driving Scenario Simulator

Three different simulation scenarios, represented in the following figures, have been considered to validate the proposed comfort-oriented speed profile generator. The virtual scenarios are created using Automated Driving Scenario Toolbox[®] on MATLAB[®] and Simulink[®].

- **Scenario 1, Highway:** The path has mainly straights and low curvature turns. The vehicle can drive at the maximum speed according to the speed limits of the highway (130km/h for Italian Highways). The lanes are separated by a dashed line and each lane has a width of 4m. At the beginning of the simulation, the car is placed in the middle of the lane with an initial longitudinal velocity equal to 0 km/h.
- **Scenario 2, Inter Urban:** The path considers rural and suburban roads, typically present between city and highway roads. The shape of the road includes both straights with low curvature and some sharp curves. The speed limit in inter urban area is considered as 70 km/h. The road is composed with two lanes. The lanes are separated by a dashed line and each lane has a width of 4m. At the beginning of the simulation, the car is placed in the middle of the lane with an initial velocity equal to 0 km/h.
- **Scenario 3, Berlin Race Track:** The path considered is the one used in the *Formula Student Germany competition* in 2018. The shape of the road includes both straights and some very sharp turns. There is only one lane and it has a width of 4m. At the beginning of the simulation, the car is placed in the center line with an initial longitudinal velocity equal to 0 km/h.

Scenario 1, Highway

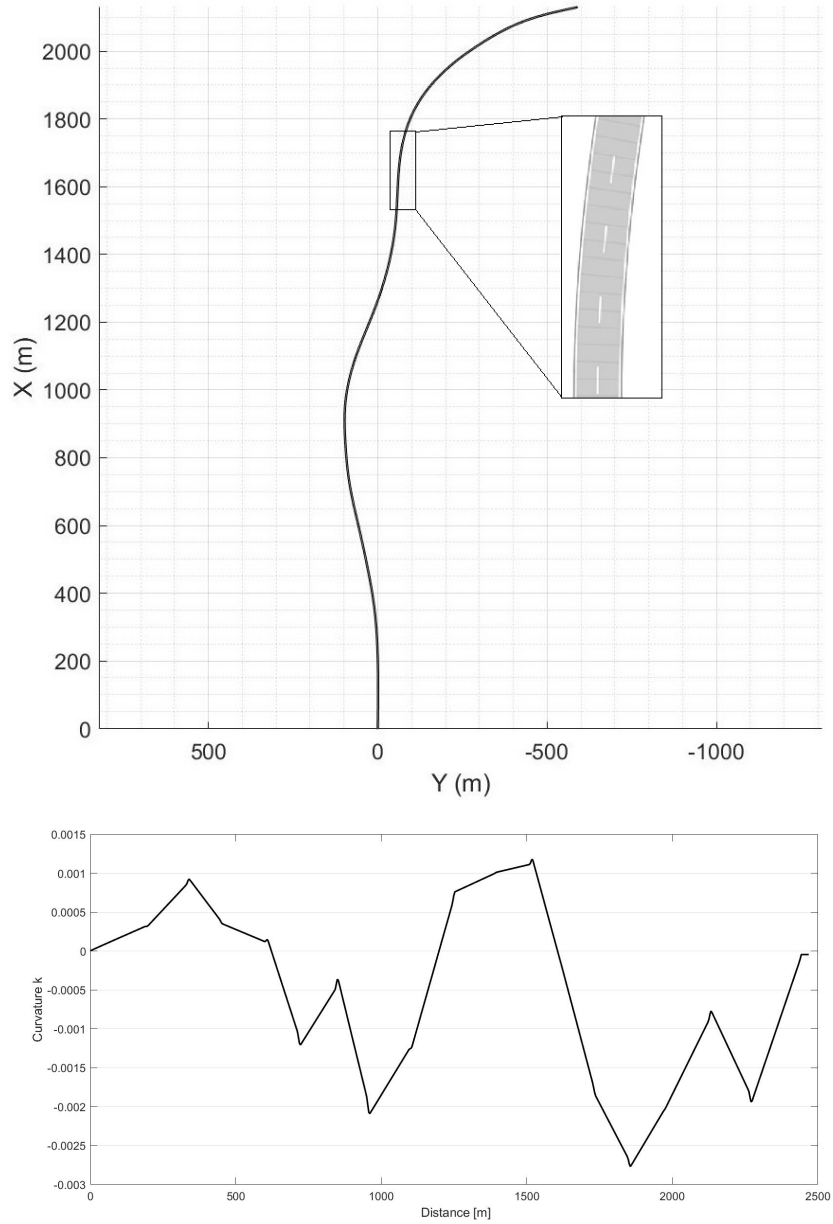


Figure 5.1: Highway scenario and road curvature κ

Scenario 2, Inter Urban

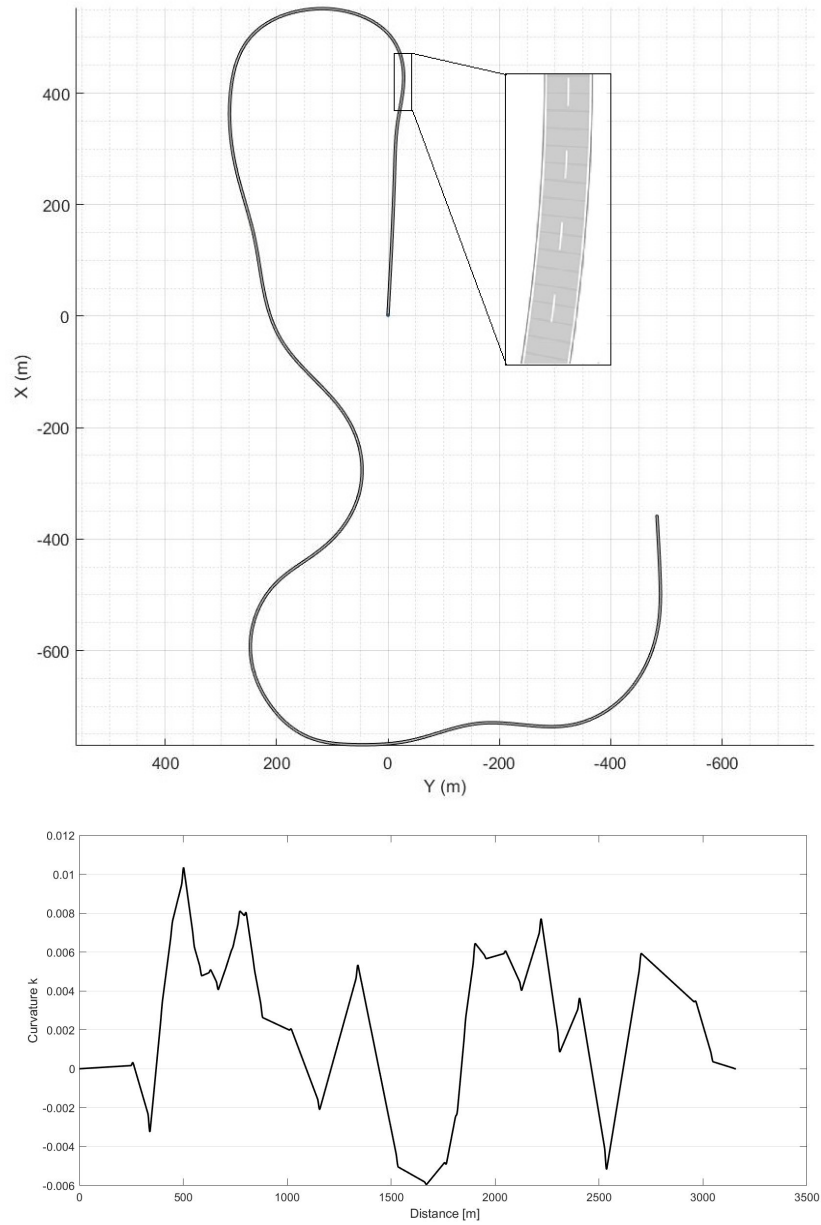


Figure 5.2: Inter Urban scenario and road curvature κ

Scenario 3, Berlin Race Track

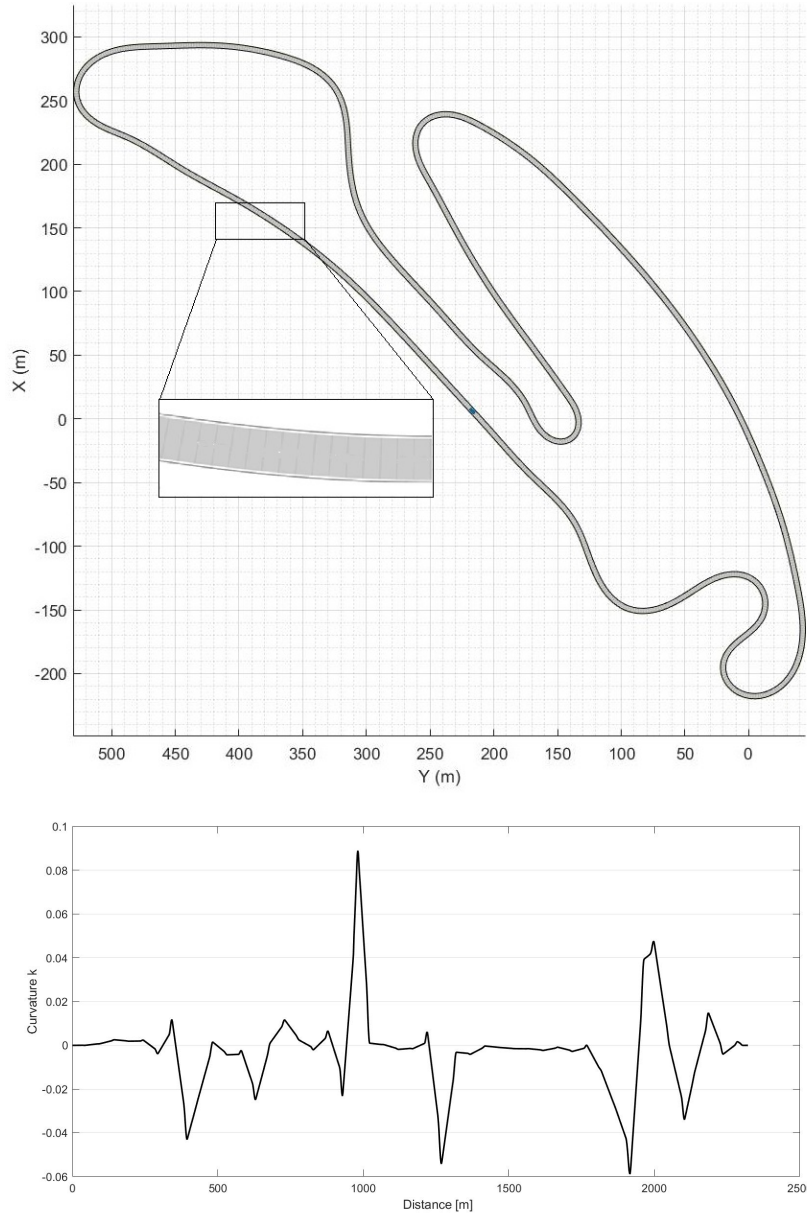


Figure 5.3: Berlin Race Track scenario and road curvature κ

In the figures above, all the three driving scenarios with their road curvature are illustrated. The Berlin Race Track scenario in Figure 5.3 is characterized by higher values of curvature relative to sharp curves, while the highway scenario in Figure 5.1 has lower curvature values. Inter-urban scenario in Figure 5.2 lies between these two with intermediate curvature values. Together, they form a comprehensive set of key environments for the evaluation of the fuzzy comfort-oriented speed profile generator that is proposed in this thesis work.

5.2 3 Degrees of Freedom vehicle model validation and results

In this section, the results acquired from the simulations with the simple three degrees of freedom model are reported. The results obtained using the fuzzy comfort-oriented speed profile generator developed in this thesis work are compared with the classical approach that does not take care of comfort performances. In the classical approach, the reference velocity is computed just considering the road curvature parameter. The figures below are presented in this way: (a) results obtained with the Fuzzy Logic Controller, (b) results obtained with the classical approach (without Fuzzy Logic Controller).

Highway scenario, results (3 DOF):

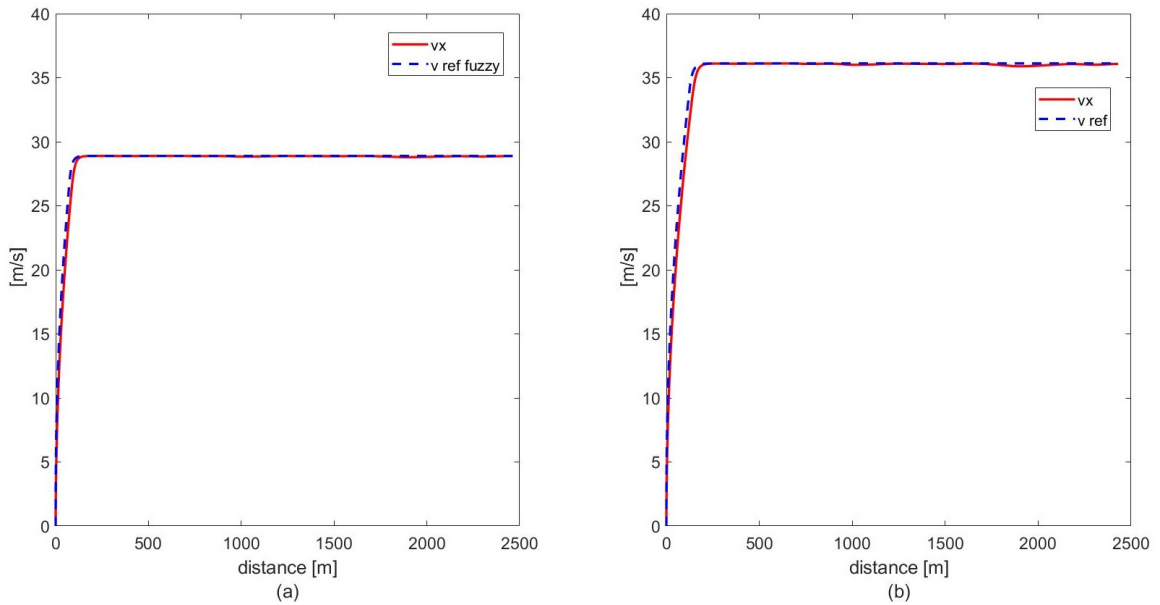


Figure 5.4: Reference velocity and Longitudinal Actual velocity; (a) With Fuzzy Controller (b) Without Fuzzy Controller -*Highway scenario(3 DOF)*

The Figure 5.4 illustrates the actual longitudinal velocity of the vehicle (solid red line) and the Reference velocity (dashed blue line) computed in (a) with the Fuzzy Controller and in (b) without it. As can be seen, the reference velocity computed with the method proposed in this thesis work is lower with respect to the one computed with the classical approach. This is established by the rules present in the Fuzzy Controller in order to optimize the passengers' comfort.

The behaviour of the longitudinal acceleration and lateral acceleration are shown below.

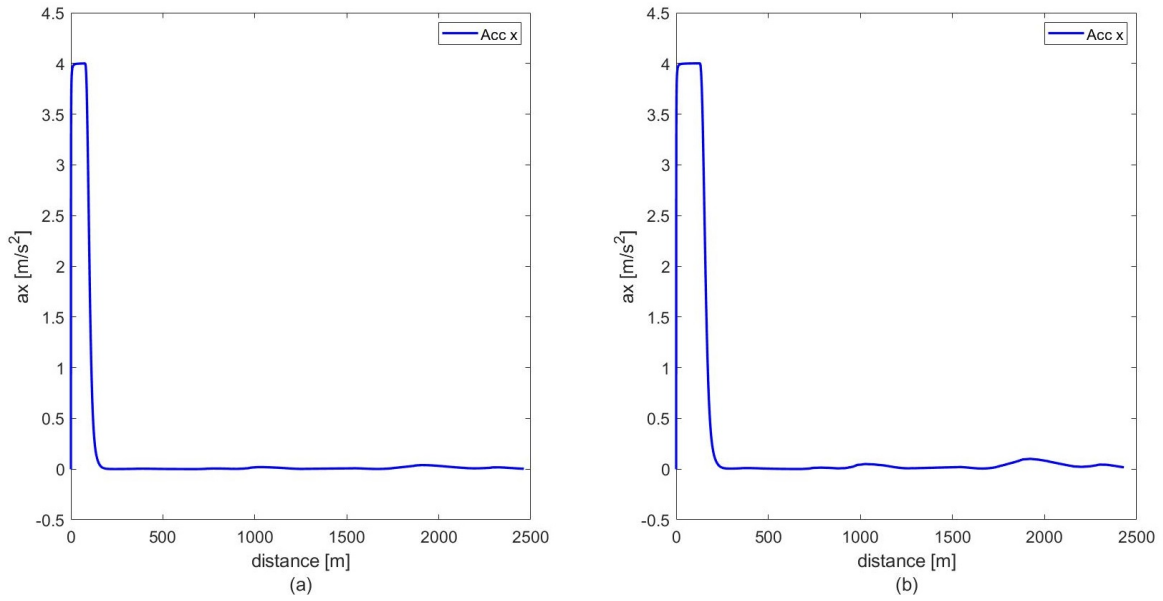


Figure 5.5: Longitudinal Acceleration; (a) With Fuzzy Controller (b) Without Fuzzy Controller -Highway scenario (3 DOF)

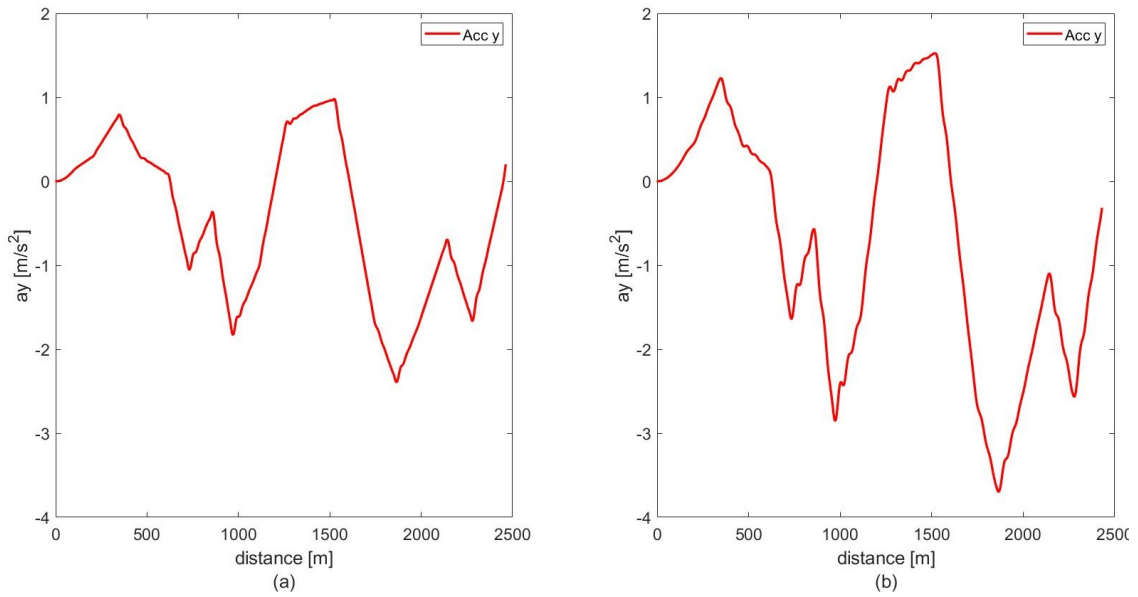


Figure 5.6: Lateral Acceleration; (a) With Fuzzy Controller (b) Without Fuzzy Controller -Highway scenario (3 DOF)

As can be seen in Figure 5.6, the lateral acceleration obtained with the proposed method has lower magnitude values with respect to the one computed with the classical approach. This will have a positive significant impact on the comfort of the passengers.

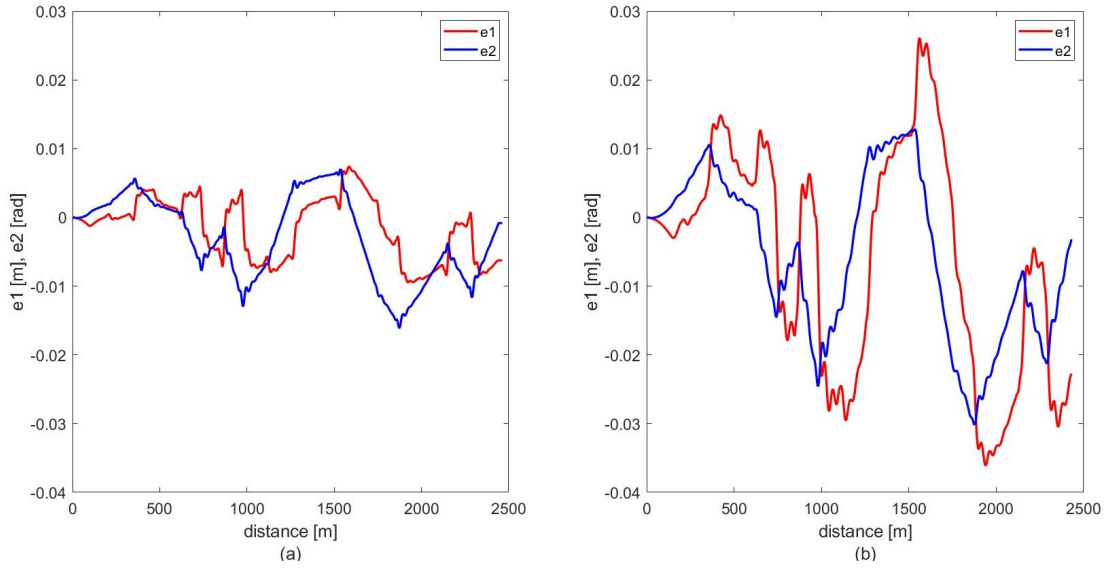


Figure 5.7: Lateral deviation e_1 and relative yaw e_2 ; (a) With Fuzzy Controller (b) Without Fuzzy Controller -*Highway scenario (3 DOF)*

It can be seen that the Fuzzy Logic Controller generates a reference velocity that leads to better control performances. The lateral deviation e_1 and the relative yaw e_2 are quite smaller compared to the case without the Fuzzy controller.

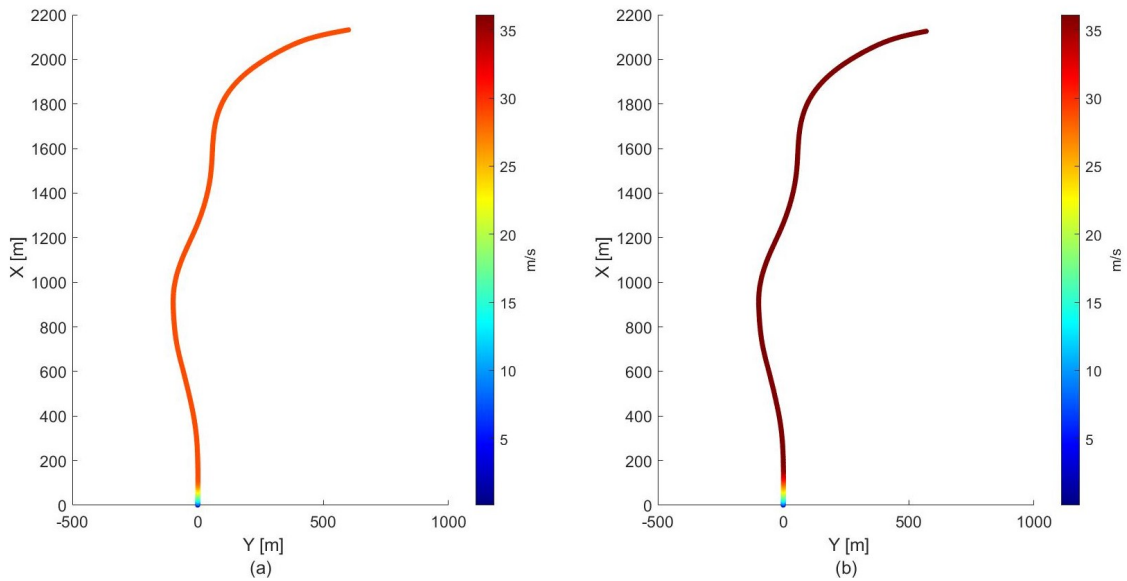


Figure 5.8: Colormap of the longitudinal velocity; (a) With Fuzzy Controller (b) Without Fuzzy Controller -*Highway scenario (3 DOF)*

Table 5.1: Highway scenario results (3 DOF)

	With Fuzzy Controller	Without Fuzzy Controller
a_{eq} coefficient	0,068 m/s^2	0,092 m/s^2
Likely Reaction	'not uncomfortable'	'not uncomfortable'
$MSDV$	7,1 %	11,9 %
Maximum velocity	130 km/h	130 km/h
Simulation time	90 s	73 s

The comfort optimization method results in a lower percentage of people who may experience nausea ($MSDV$) and in a lower value of equivalent acceleration a_{eq} perceived by the passengers compared with the classical approach. In both cases, the a_{eq} index values are 'not uncomfortable'.

Inter-Urban scenario, results (3 DOF):

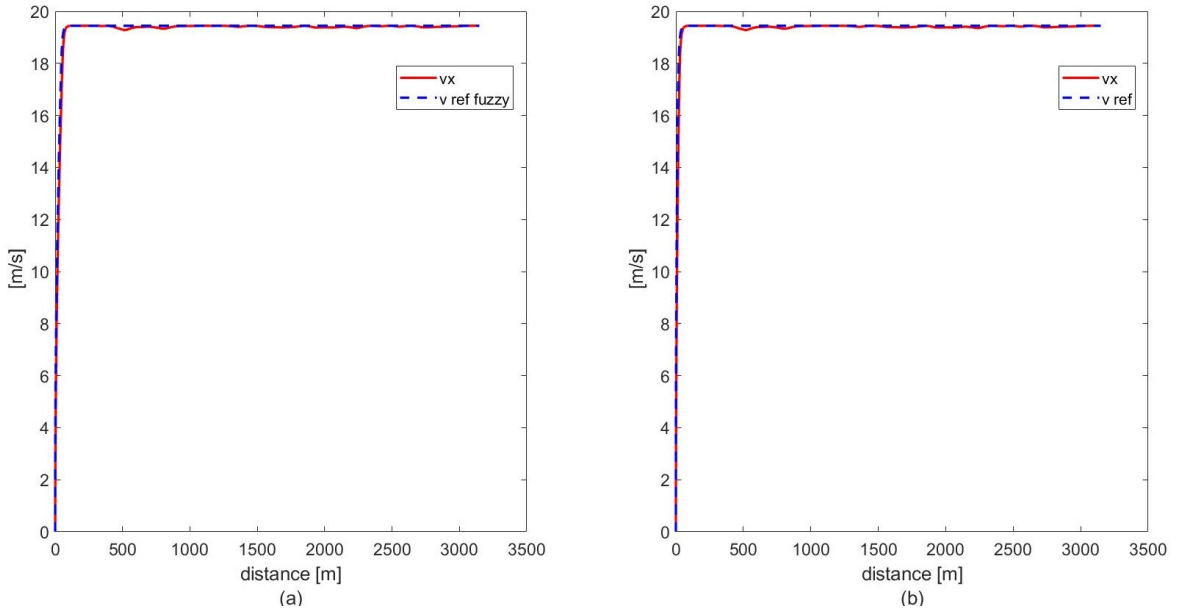


Figure 5.9: Reference velocity and Longitudinal Actual velocity; (a) With Fuzzy Controller (b) Without Fuzzy Controller -*Inter-Urban scenario (3 DOF)*

The Figure 5.9 illustrates the actual longitudinal velocity of the vehicle (solid red line) and the Reference velocity (dashed blue line) computed in (a) with the Fuzzy Controller and in (b) without it. The reference velocity are similar due to the fact that in this scenario the speed limits and the road curvature values don't create an uncomfortable driving experience even in the case without the Fuzzy Logic Controller. However, as shown in the following figures the accelerations values are lower in the case of the comfort oriented method than in the classical approach.

The behaviour of the longitudinal acceleration and lateral acceleration are shown below.

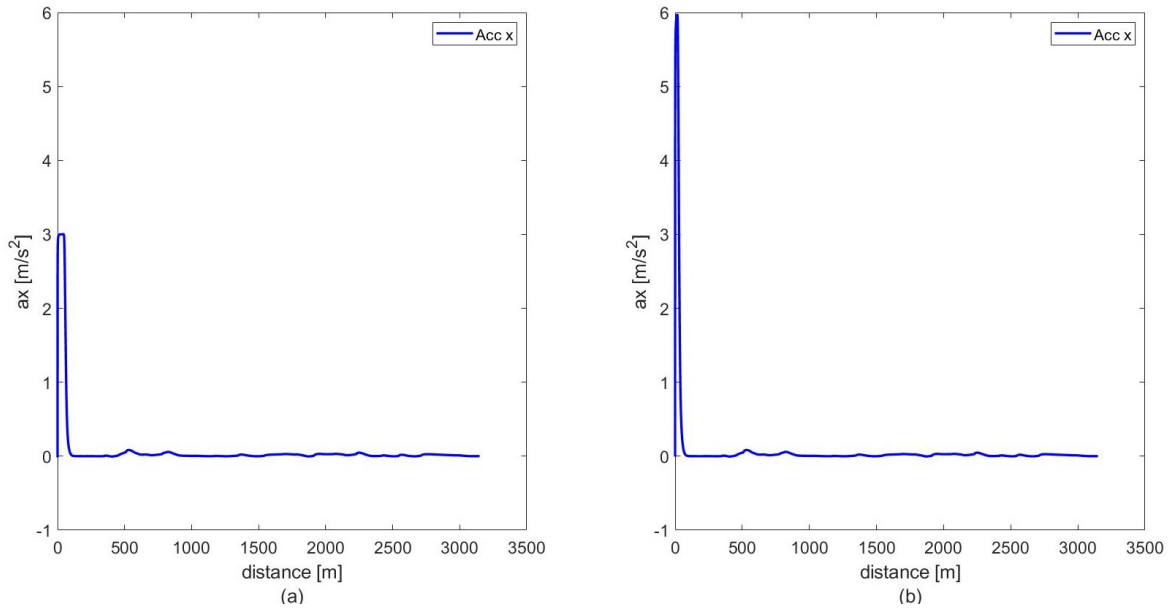


Figure 5.10: Longitudinal Acceleration; (a) With Fuzzy Controller (b) Without Fuzzy Controller -*Inter-Urban scenario (3 DOF)*

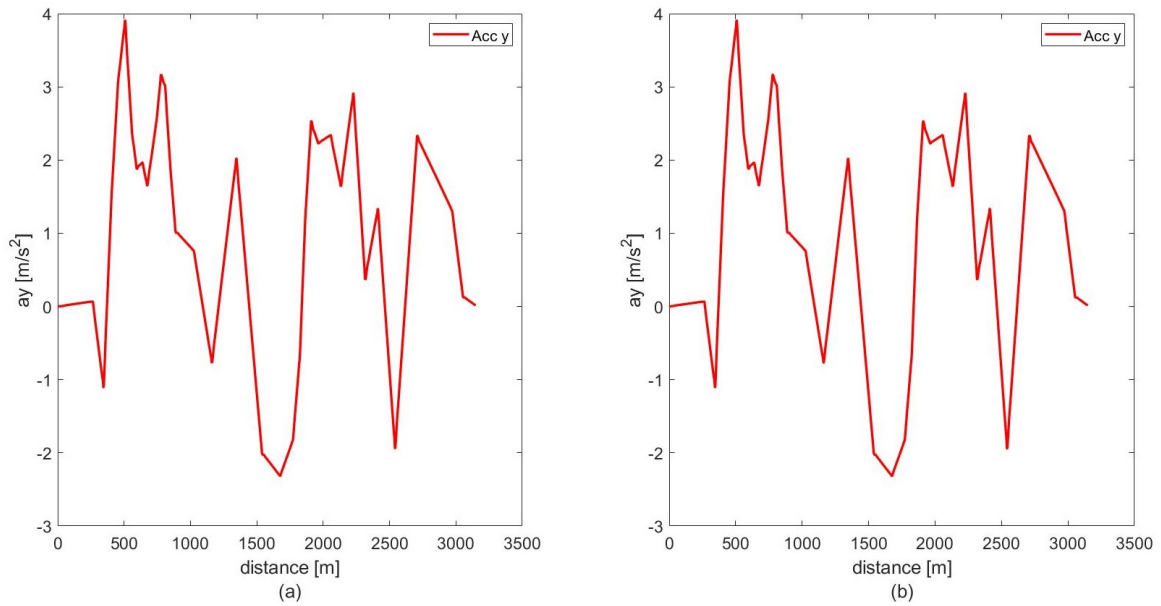


Figure 5.11: Lateral Acceleration; (a) With Fuzzy Controller (b) Without Fuzzy Controller -*Inter-Urban scenario (3 DOF)*

As shown in Figure 5.10, the longitudinal acceleration reaches a maximum value of 3 m/s^2 in the case with the Fuzzy Controller and 6 m/s^2 in the case without the Fuzzy Controller. In the first case, the starting phase will be smoother than the second one, leading to a more comfortable driving.

The following figure shows the lateral deviation e_1 and relative yaw angle e_2 values.

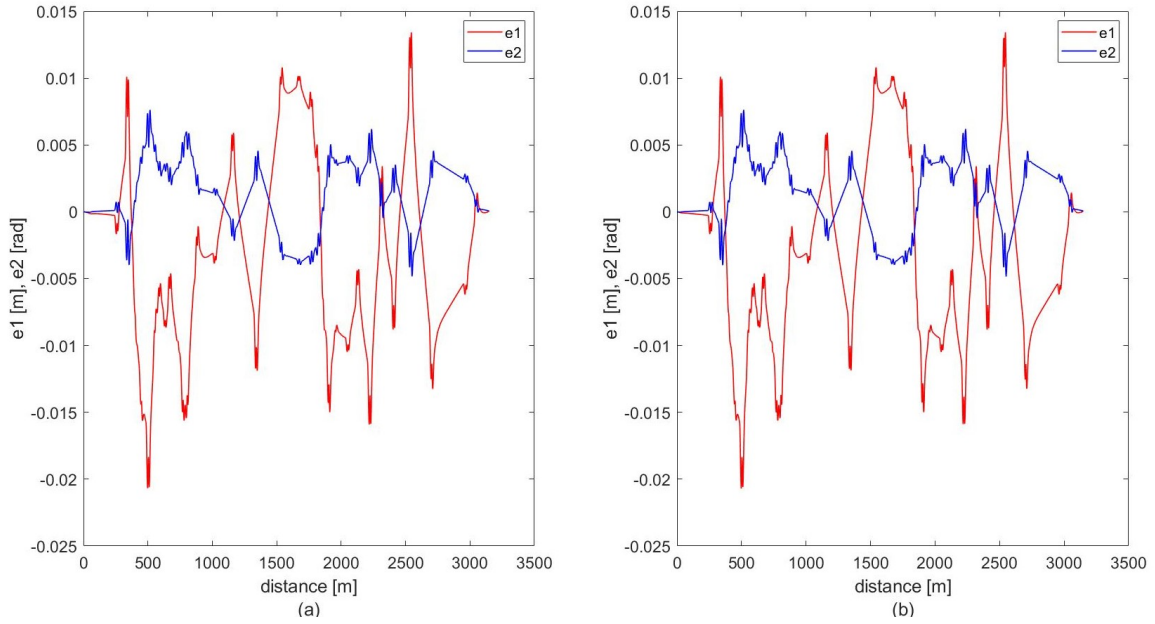


Figure 5.12: Lateral deviation e_1 and relative yaw e_2 ; (a) With Fuzzy Controller (b) Without Fuzzy Controller -*Inter-Urban scenario (3 DOF)*

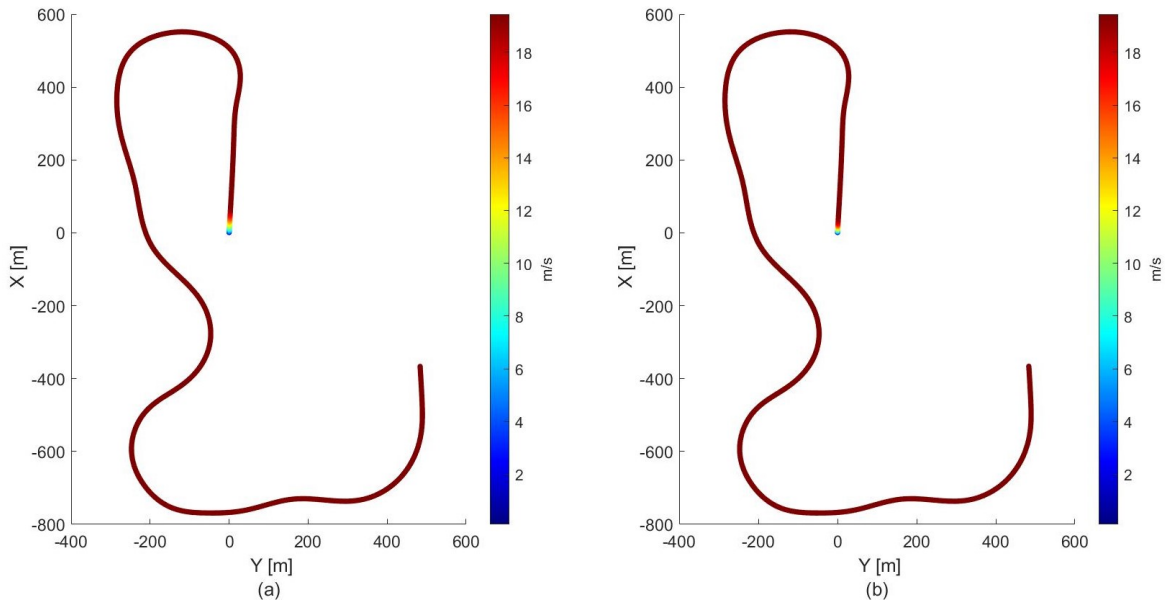


Figure 5.13: Colormap of the longitudinal velocity; (a) With Fuzzy Controller (b) Without Fuzzy Controller -*Inter-Urban scenario (3 DOF)*

The longitudinal velocities are pretty similar in both methods. The only significant different lies in the starting phase where, in the first case, the longitudinal acceleration value is lower compared to the case without Fuzzy Controller.

Table 5.2: Inter-Urban scenario results (3 DOF)

	With Fuzzy Controller	Without Fuzzy Controller
a_{eq} coefficient	0,050 m/s^2	0,068 m/s^2
Likely Reaction	'not uncomfortable'	'not uncomfortable'
$MSDV$	8.5 %	8.7 %
Maximum velocity	70 km/h	70 km/h
Simulation time	163 s	163 s

In this scenario the comfort optimization method results in a slightly lower percentage of people who may experience nausea ($MSDV$) and in a slightly lower value of equivalent acceleration a_{eq} perceived by the passengers compared with the classical approach. In both cases, the a_{eq} index values are 'not uncomfortable'.

Berlin Race Track scenario, results (3 DOF):

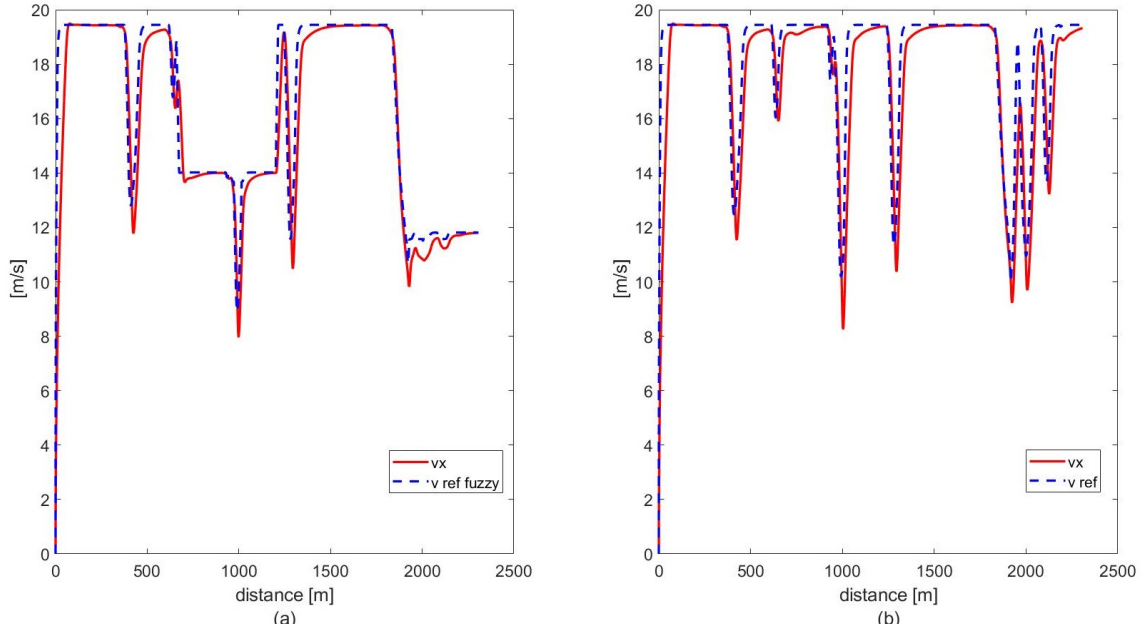


Figure 5.14: Reference velocity and Longitudinal Actual velocity; (a) With Fuzzy Controller (b) Without Fuzzy Controller -Berlin Race Track scenario (3 DOF)

The Figure 5.14 illustrates the actual longitudinal velocity of the vehicle (solid red line) and the Reference velocity (dashed blue line) computed in (a) with the Fuzzy Controller and in (b) without it. As can be seen, the reference velocity computed with the method proposed in this thesis work is in some case lower with respect to the one computed with the classical approach. This is established by the rules present in the Fuzzy Controller.

In particular, after forty seconds, the longitudinal and lateral accelerations are gathered in a buffer and the comfort coefficient a_{eq} is computed as described in section 3.3.2. The latter results in a 'Medium' value according to the membership functions (see Membership

functions in section 3.2.2) . Rules 18 and 19 (see Table 3.1) are activated and the reference velocity value is reduced from 'Medium' to 'Low'. The same procedure is repeated every forty seconds and the reference velocity is adjusted according to the rules that are active in the Fuzzy Controller.

The behaviour of the longitudinal acceleration and lateral acceleration are shown below.

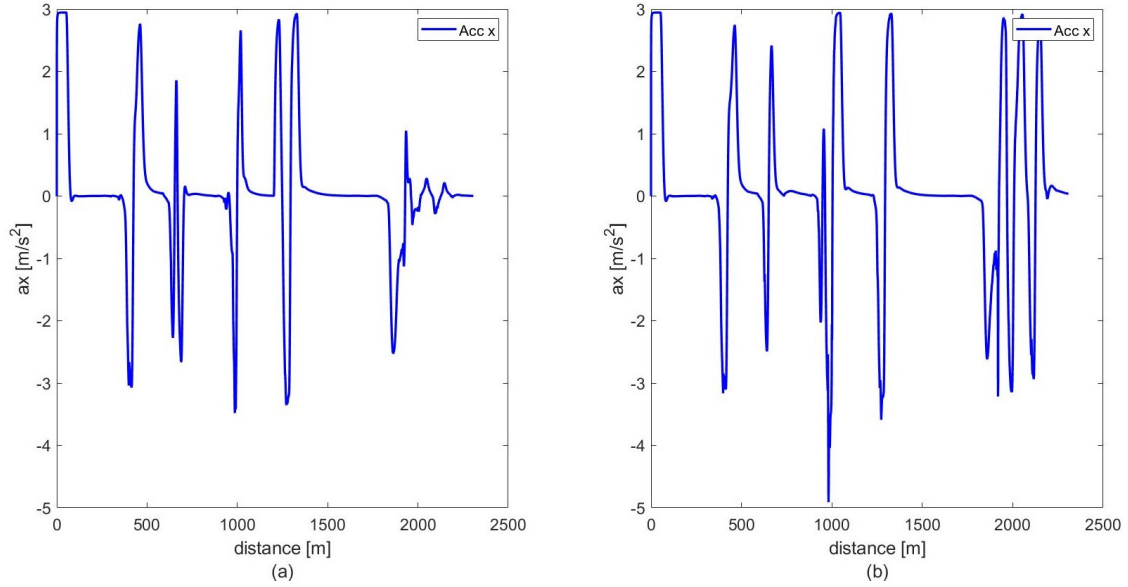


Figure 5.15: Longitudinal Acceleration; (a) With Fuzzy Controller (b) Without Fuzzy Controller -Berlin Race Track scenario (3 DOF)

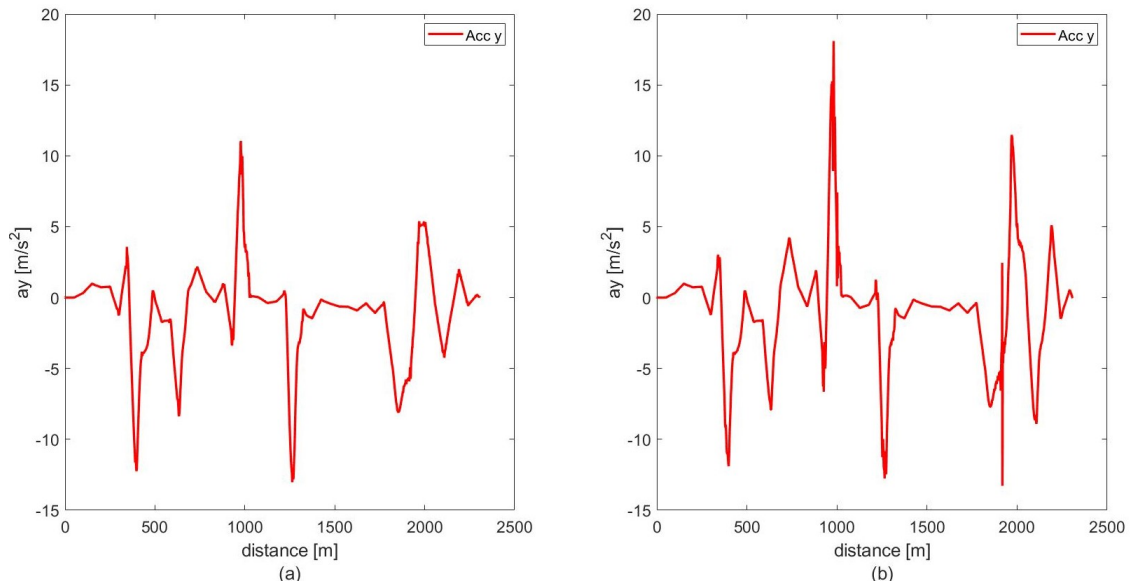


Figure 5.16: Lateral Acceleration; (a) With Fuzzy Controller (b) Without Fuzzy Controller -Berlin Race Track scenario (3 DOF)

As can be seen in Figure 5.15 and 5.16, the longitudinal and lateral accelerations obtained with the proposed method have lower magnitude values with respect to the ones computed with the classical approach. This will have a positive significant impact on the comfort of the passengers.

The following figure illustrates the lateral deviation e_1 and relative yaw angle e_2 values.

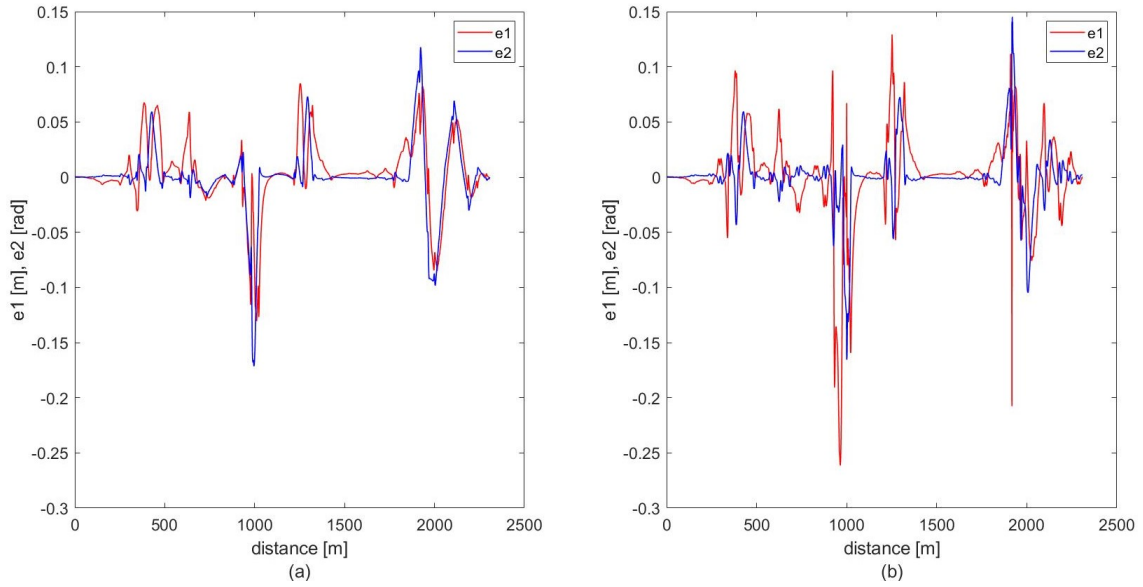


Figure 5.17: Lateral deviation e_1 and relative yaw e_2 ; (a) With Fuzzy Controller (b) Without Fuzzy Controller -*Berlin Race Track scenario (3 DOF)*

It can be seen that the Fuzzy Logic Controller generates a reference velocity that leads to better control performances. The lateral deviation e_1 and the relative yaw e_2 are smaller compared to the case without the Fuzzy controller.

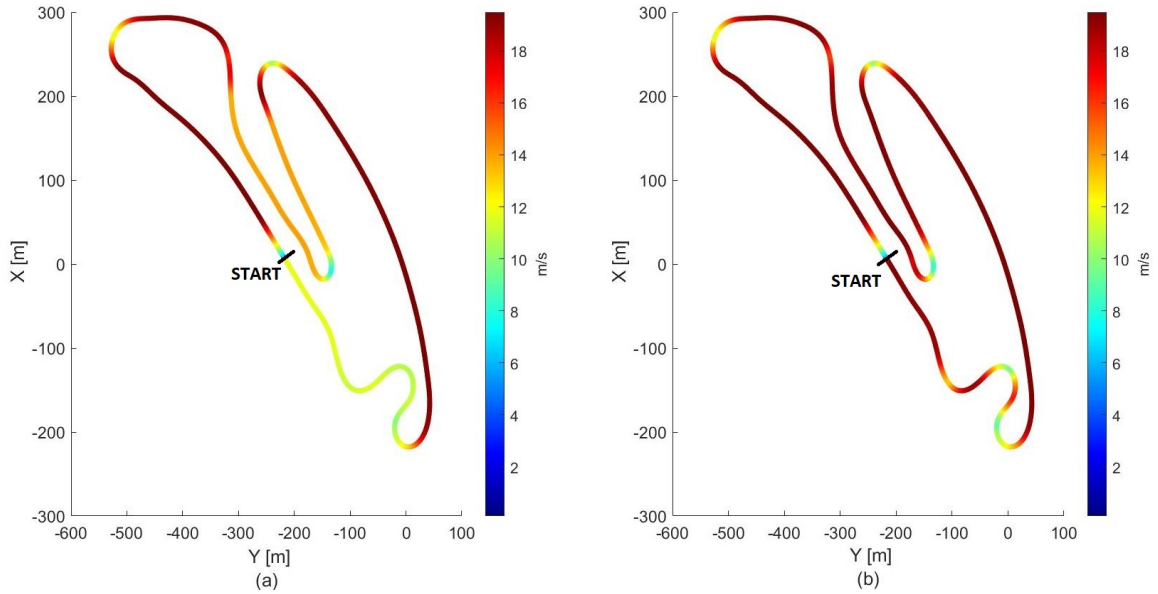


Figure 5.18: Colormap of the longitudinal velocity; (a) With Fuzzy Controller (b) Without Fuzzy Controller -Berlin Race Track scenario (3 DOF)

As can be seen from the colormap in Figure 5.18 the velocity of the vehicle adapts to the scene where it is travelling. In the proximity of a curve, this decreases, while in a straight line, it tends to assume the maximum value of 70 km/h.

Table 5.3: Berlin Race Track scenario results (3 DOF)

	With Fuzzy Controller	Without Fuzzy Controller
a_{eq} coefficient	0,53 m/s^2	0,86 m/s^2
Likely Reaction	'a little uncomfortable'	'uncomfortable'
$MSDV$	45 %	73 %
Maximum velocity	70 km/h	70 km/h
Simulation time	162 s	142 s

In both cases the results of the comfort coefficients are pretty high. This is mostly due to the fact that the scenario is a competition racing track that has very sharp curves with high road curvature value. However, the comfort optimization method results in a lower percentage of people who may experience nausea ($MSDV$) and in a lower value of equivalent acceleration a_{eq} perceived by the passengers compared with the classical approach. The a_{eq} index value changes from 'uncomfortable' to 'a little uncomfortable' using the proposed method.

5.3 15 Degrees of Freedom vehicle model validation and results

After completing the evaluation of the proposed comfort-oriented speed profile generator with the simple three degrees of freedom model, a fifteen degrees of freedom vehicle model, which is imported from Simscape Vehicle Template, was used to obtain very accurate data from simulations.

The figures below are presented in this way: (a) results obtained with the Fuzzy Logic Controller, (b) results obtained with the classical approach (without Fuzzy Logic Controller).

Highway scenario, results (15 DOF):

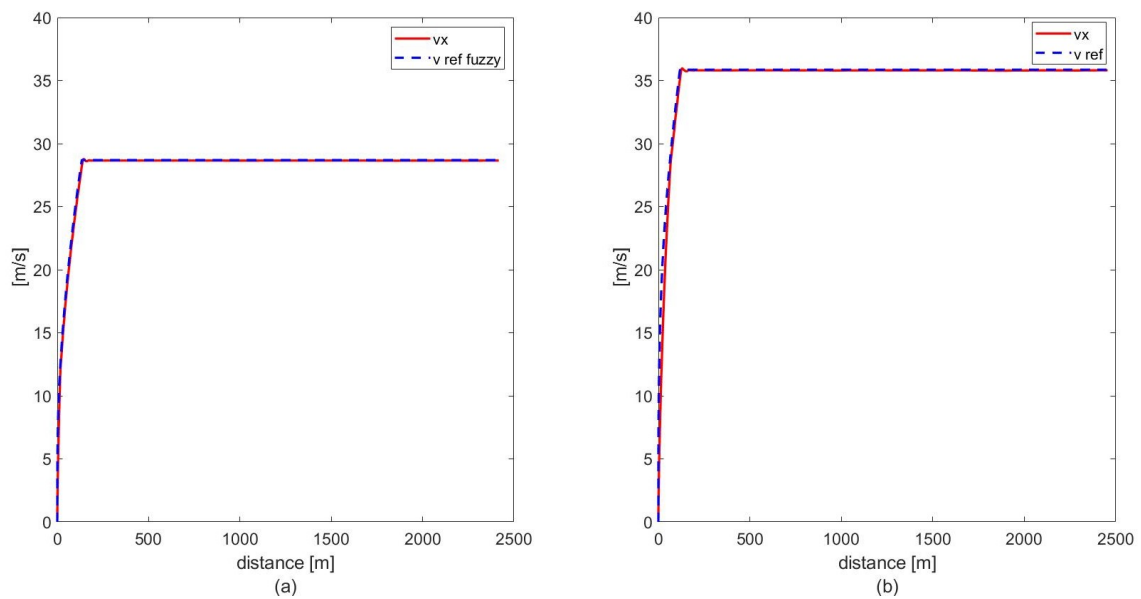


Figure 5.19: Reference velocity and Longitudinal Actual velocity; (a) With Fuzzy Controller (b) Without Fuzzy Controller -*Highway scenario(15 DOF)*

The Figure 5.19 illustrates the actual longitudinal velocity of the vehicle (solid red line) and the Reference velocity (dashed blue line) computed in (a) with the Fuzzy Controller and in (b) without it. As can be seen, the reference velocity computed with the comfort-oriented method proposed in this thesis work is lower with respect to the one computed with the classical approach. This is established by the rules present in the Fuzzy Controller in order to optimize the comfort of the passengers.

The behaviour of the longitudinal acceleration and lateral acceleration are shown in Figure 5.20 and 5.21.

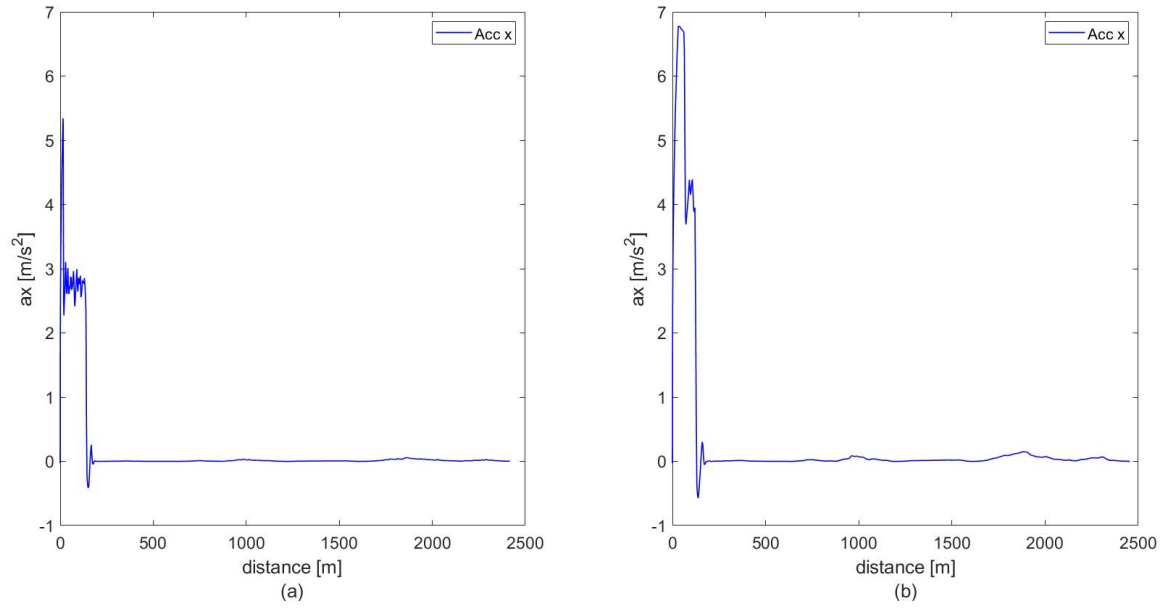


Figure 5.20: Longitudinal Acceleration; (a) With Fuzzy Controller (b) Without Fuzzy Controller -Highway scenario (15 DOF)

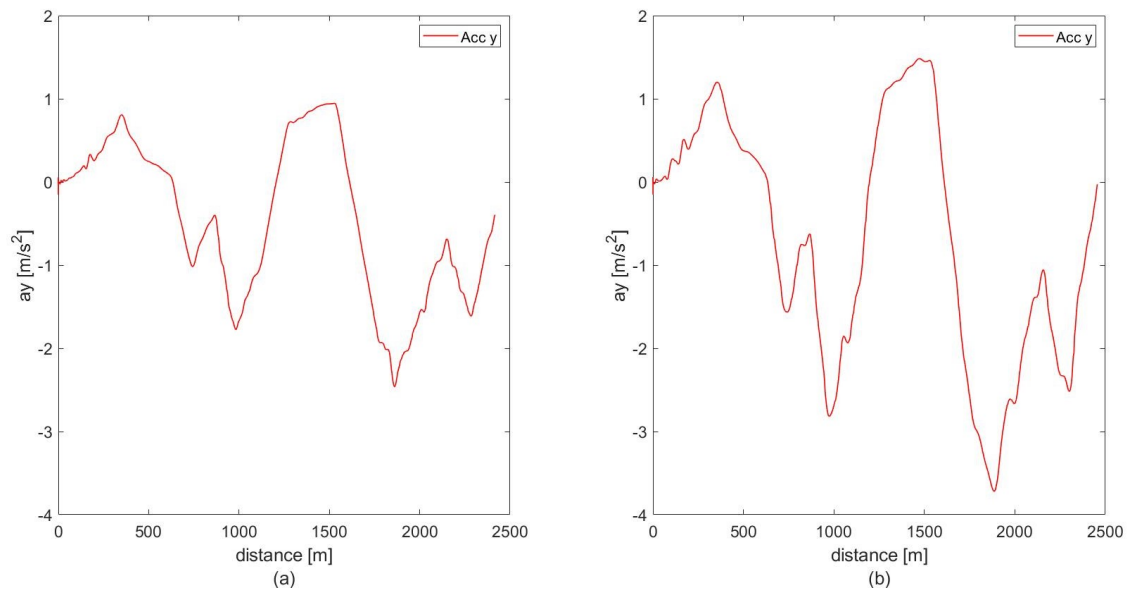


Figure 5.21: Lateral Acceleration; (a) With Fuzzy Controller (b) Without Fuzzy Controller -Highway scenario (15 DOF)

The following figure illustrates the lateral deviation e_1 and relative yaw angle e_2 values.

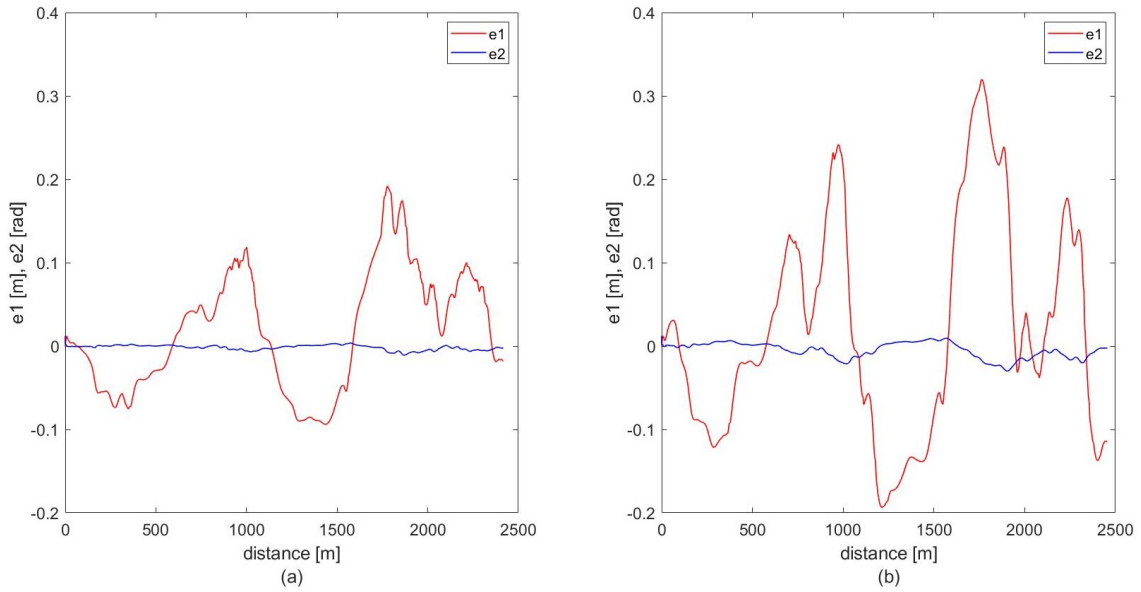


Figure 5.22: Lateral deviation e_1 and relative yaw e_2 ; (a) With Fuzzy Controller (b) Without Fuzzy Controller -*Highway scenario (15 DOF)*

It can be seen that the Fuzzy Logic Controller generates a reference velocity that leads to better control performances. The lateral deviation e_1 and the relative yaw e_2 are smaller compared to the case without the Fuzzy controller.

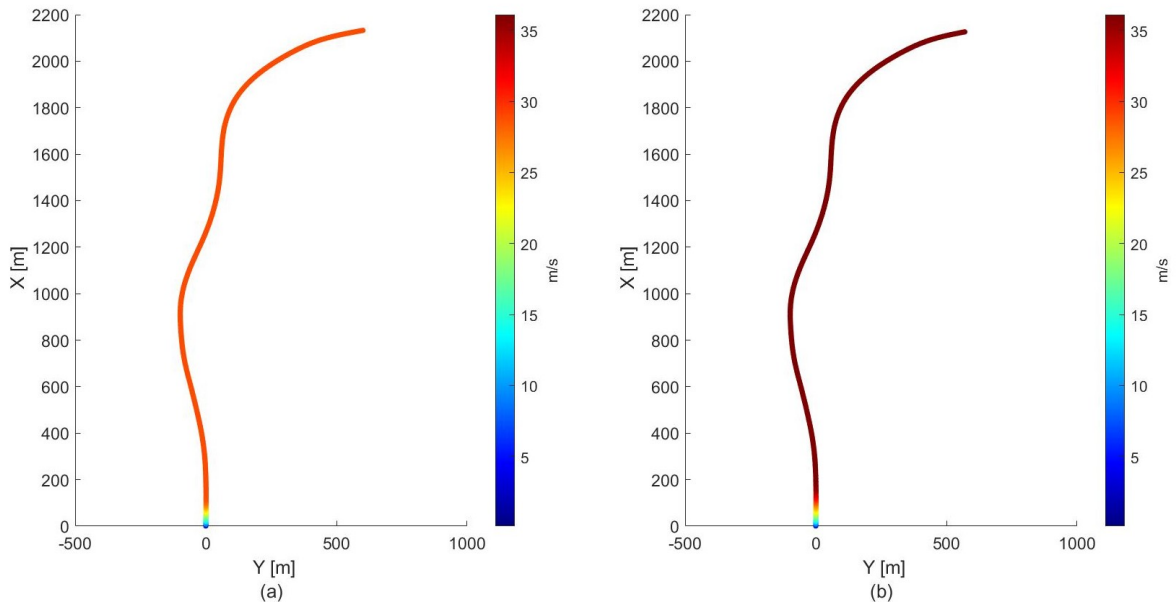


Figure 5.23: Colormap of the longitudinal velocity; (a) With Fuzzy Controller (b) Without Fuzzy Controller -*Highway scenario (15 DOF)*

Table 5.4: Highway scenario results (15 DOF)

	With Fuzzy Controller	Without Fuzzy Controller
a_{eq} coefficient	0,15 m/s^2	0,237 m/s^2
Likely Reaction	'not uncomfortable'	'not uncomfortable'
$MSDV$	7,8 %	12.3 %
Maximum velocity	130 km/h	130 km/h
Simulation time	90 s	74 s

In both cases, the a_{eq} index values are 'not uncomfortable' accordingly to ISO 2631-1. However, the comfort optimization method results in a lower percentage of people who may experience nausea ($MSDV$) and in a lower value of equivalent acceleration a_{eq} perceived by the passengers compared with the classical approach.

Inter-Urban scenario, results (15 DOF):

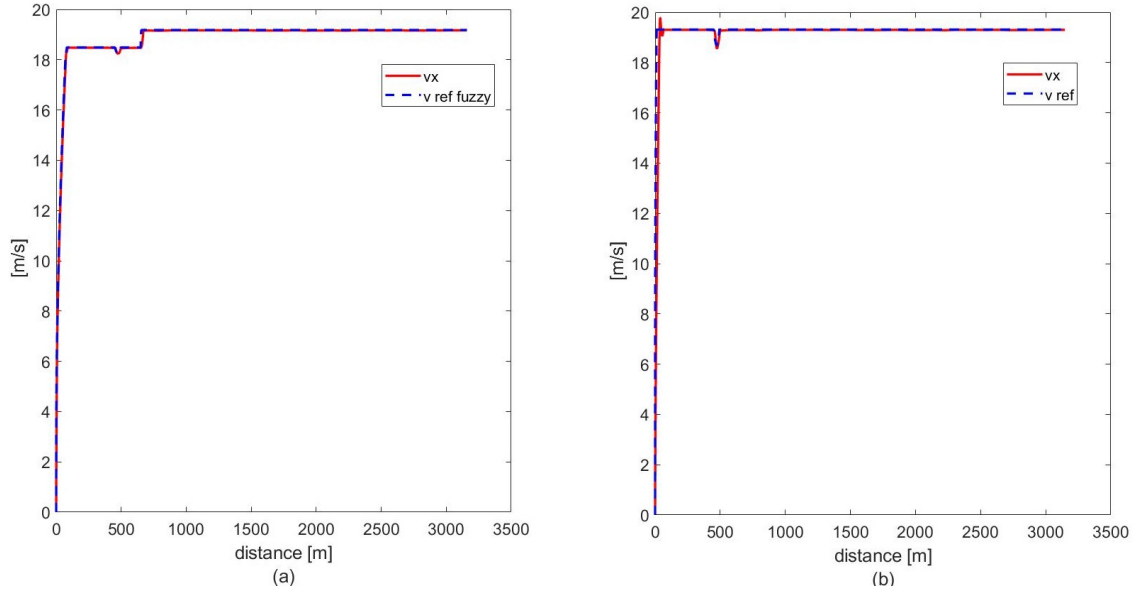


Figure 5.24: Reference velocity and Longitudinal Actual velocity; (a) With Fuzzy Controller (b) Without Fuzzy Controller -*Inter-Urban scenario (15 DOF)*

The Figure 5.24 illustrates the actual longitudinal velocity of the vehicle (solid red line) and the Reference velocity (dashed blue line) computed in (a) with the Fuzzy Controller and in (b) without it. The reference velocity computed with the comfort-oriented speed profile generator is slightly lower in the first part of the track compared to the case without the Fuzzy Controller. The reference velocity is reduced based on the rules established in the Fuzzy Controller, on the values of the longitudinal acceleration and on the comfort coefficient a_{eq} computed in real-time.

The behaviour of the longitudinal acceleration and lateral acceleration are shown below.

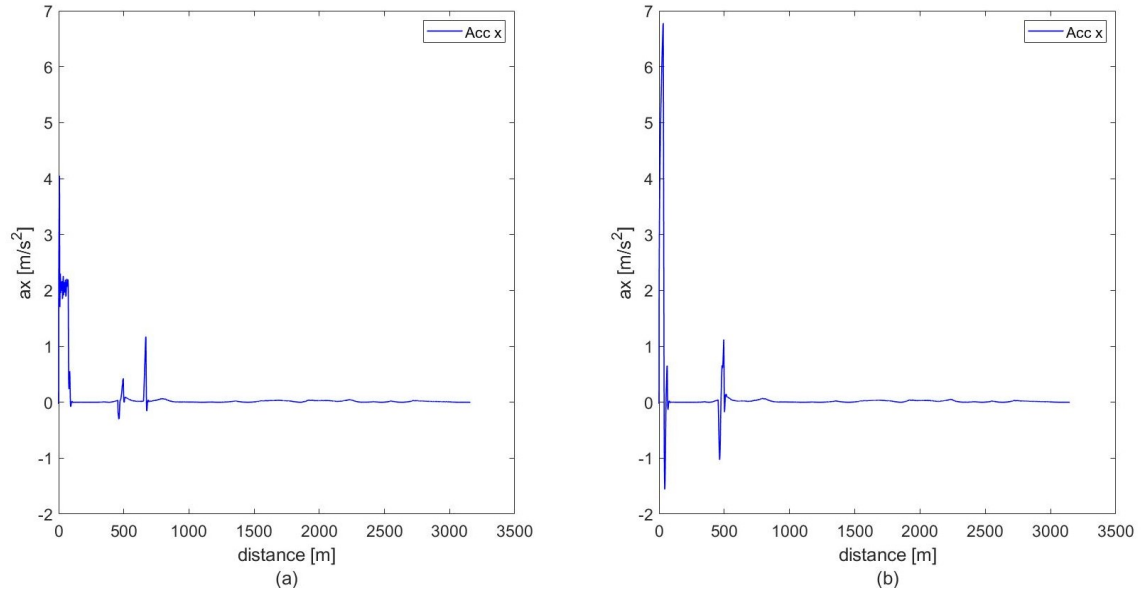


Figure 5.25: Longitudinal Acceleration; (a) With Fuzzy Controller (b) Without Fuzzy Controller -Inter-Urban scenario (15 DOF)

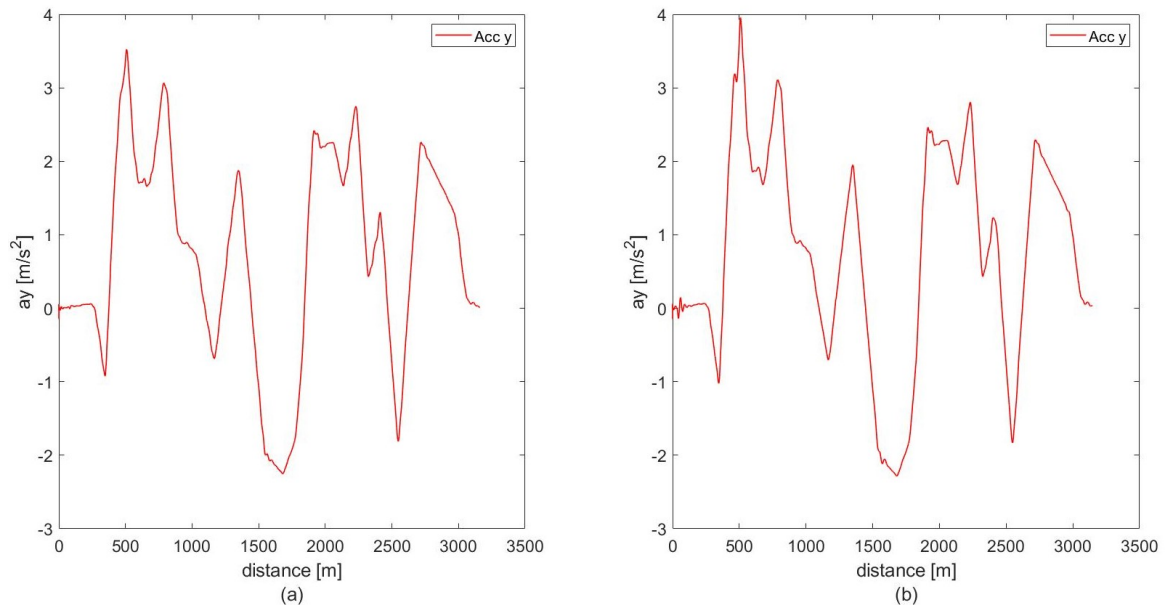


Figure 5.26: Lateral Acceleration; (a) With Fuzzy Controller (b) Without Fuzzy Controller -Inter-Urban scenario (15 DOF)

The figure below illustrates the lateral deviation e_1 and relative yaw angle e_2 values.

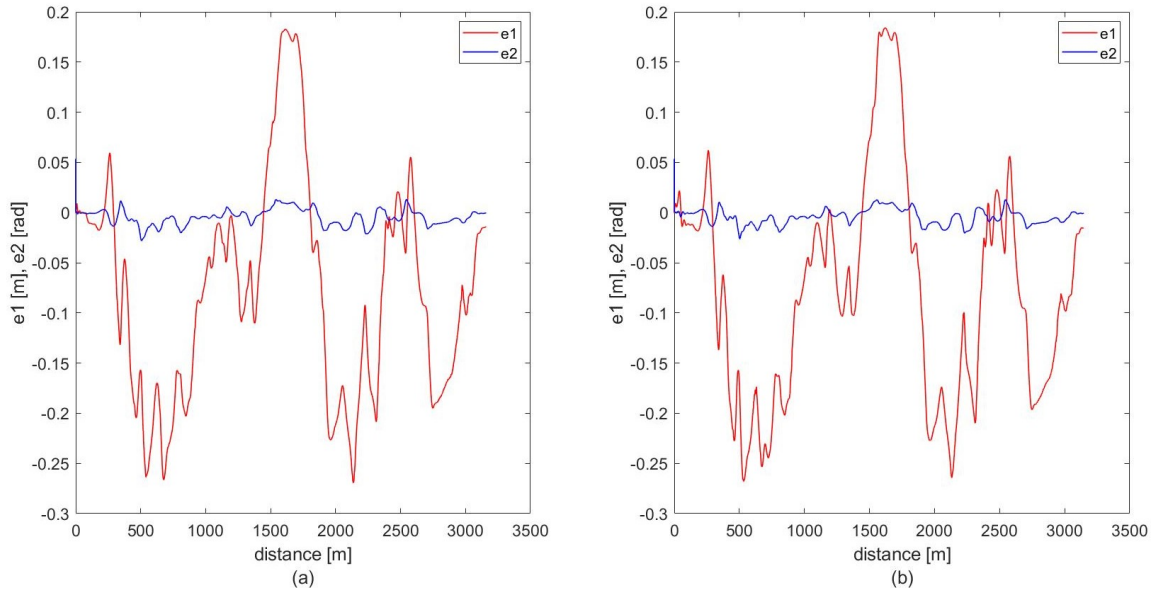


Figure 5.27: Lateral deviation e_1 and relative yaw e_2 ; (a) With Fuzzy Controller (b) Without Fuzzy Controller -*Inter-Urban scenario (15 DOF)*

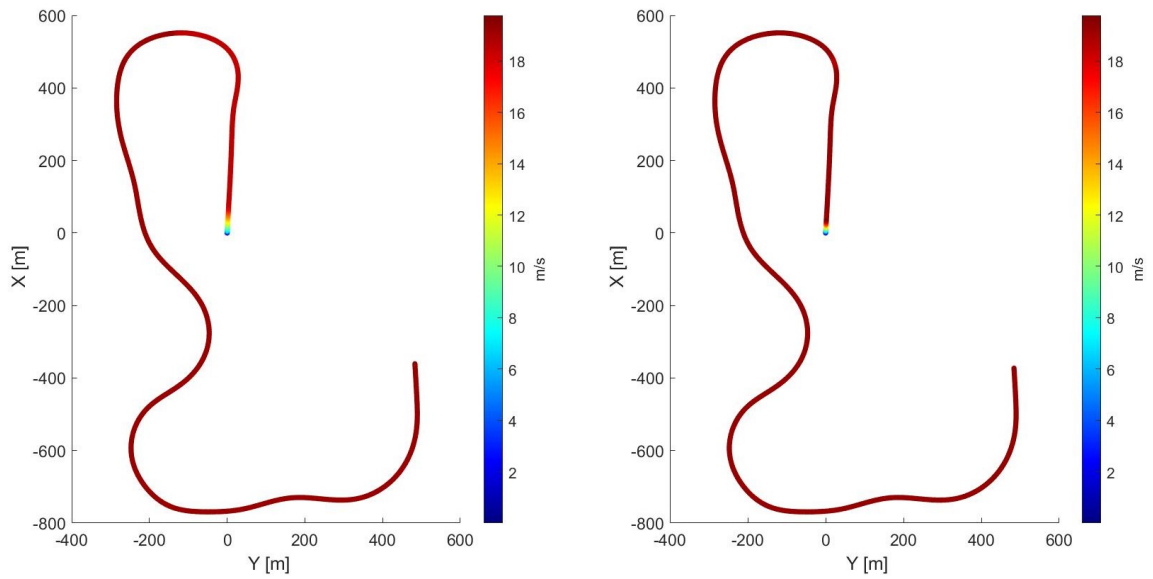


Figure 5.28: Colormap of the longitudinal velocity; (a) With Fuzzy Controller (b) Without Fuzzy Controller -*Inter-Urban scenario (15 DOF)*

The longitudinal velocities of the vehicle are pretty similar in both methods. The only significant different lies in the starting phase where, in the first case, the reference velocity value is slightly lower compared to the case without Fuzzy Controller.

Table 5.5: Inter-Urban scenario results (15 DOF)

	With Fuzzy Controller	Without Fuzzy Controller
a_{eq} coefficient	0,095 m/s^2	0,22 m/s^2
Likely Reaction	'not uncomfortable'	'not uncomfortable'
$MSDV$	7.8 %	10.3 %
Maximum velocity	70 km/h	70 km/h
Simulation time	171 s	167 s

The comfort optimization method results in a lower percentage of people who may experience nausea ($MSDV$) and in a lower value of equivalent acceleration a_{eq} perceived by the passengers compared with the classical approach. In both cases, the a_{eq} index values are 'not uncomfortable'.

Berlin Race Track scenario, results (15 DOF):

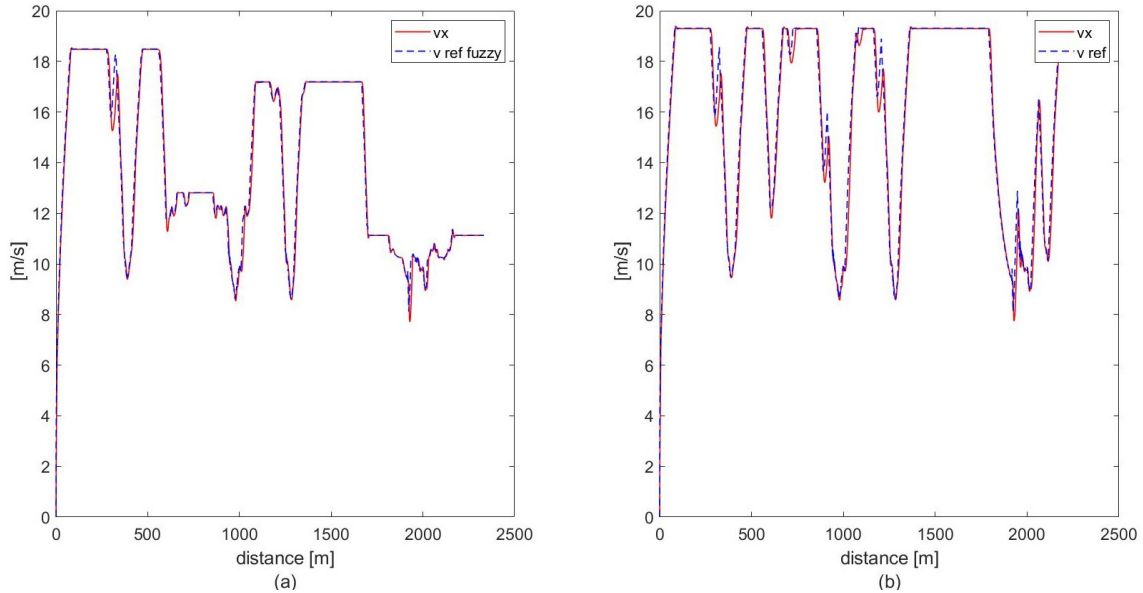


Figure 5.29: Reference velocity and Longitudinal Actual velocity; (a) With Fuzzy Controller (b) Without Fuzzy Controller -Berlin Race Track scenario (15 DOF)

The Figure 5.29 illustrates the actual longitudinal velocity of the vehicle (solid red line) and the Reference velocity (dashed blue line) computed in (a) with the Fuzzy Controller and in (b) without it. As can be seen, the reference velocity computed with the method proposed in this thesis work is in some case lower with respect to the one computed with the classical approach. This is established by the rules present in the Fuzzy Controller.

In particular, after forty seconds, the longitudinal and lateral accelerations are gathered in a buffer and the comfort coefficient a_{eq} is computed as described in section 3.3.2. The latter results in a 'Medium' value accordingly to the membership functions (see Membership functions in section 3.2.2) . Rules 18 and 19 (see Table 3.1) are activated and the reference

velocity value is reduced from 'Medium' to 'Low'. The same procedure is repeated every forty seconds and the reference velocity is adjusted according to the rules that are active in the Fuzzy Controller.

The behaviour of the longitudinal acceleration and lateral acceleration are shown below.

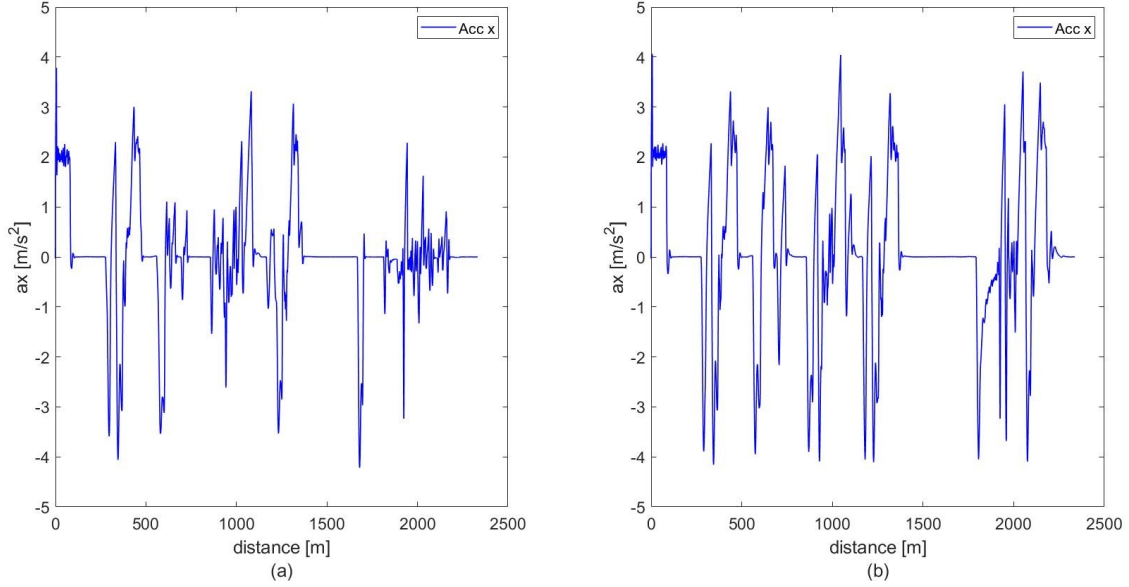


Figure 5.30: Longitudinal Acceleration; (a) With Fuzzy Controller (b) Without Fuzzy Controller -Berlin Race Track scenario (15 DOF)

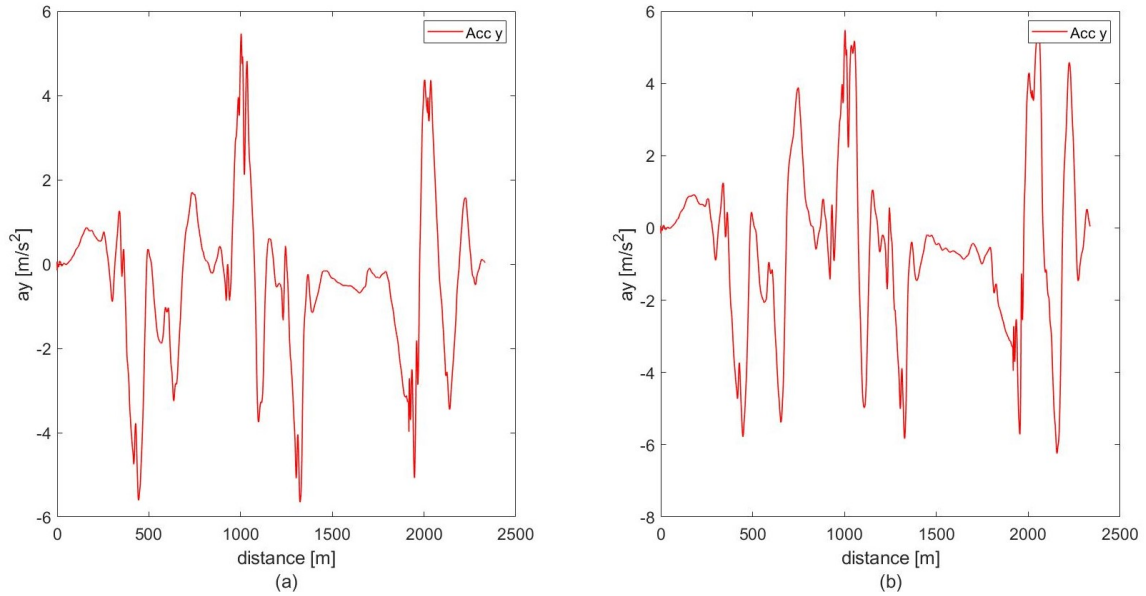


Figure 5.31: Lateral Acceleration; (a) With Fuzzy Controller (b) Without Fuzzy Controller -Berlin Race Track scenario (15 DOF)

The following figure illustrates the lateral deviation e_1 and relative yaw angle e_2 values.

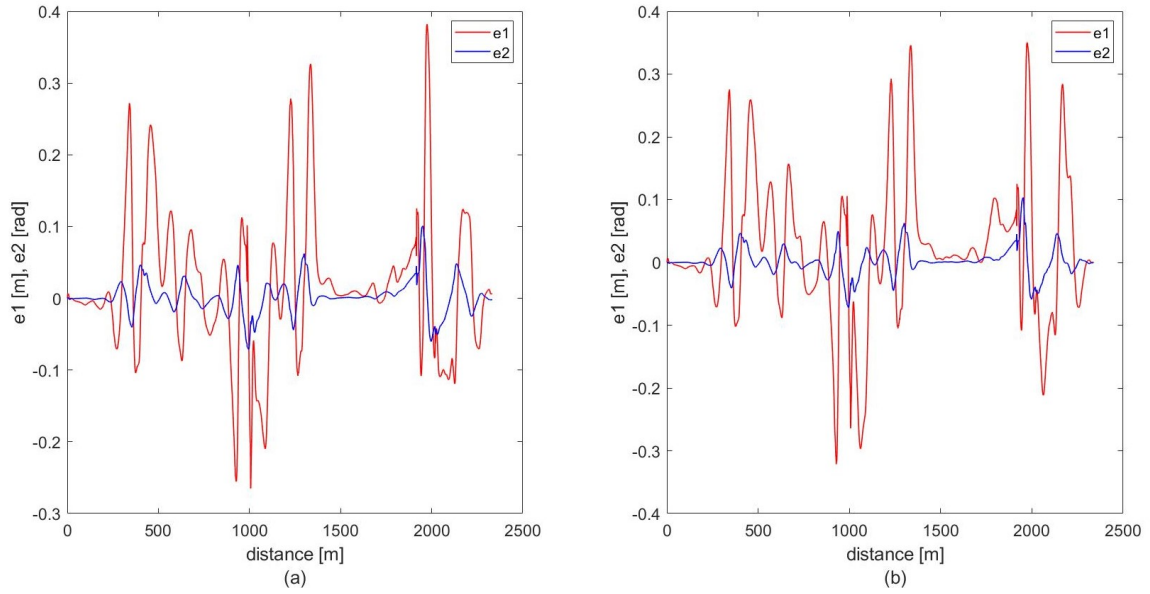


Figure 5.32: Lateral deviation e_1 and relative yaw e_2 ; (a) With Fuzzy Controller (b) Without Fuzzy Controller -*Berlin Race Track scenario (15 DOF)*

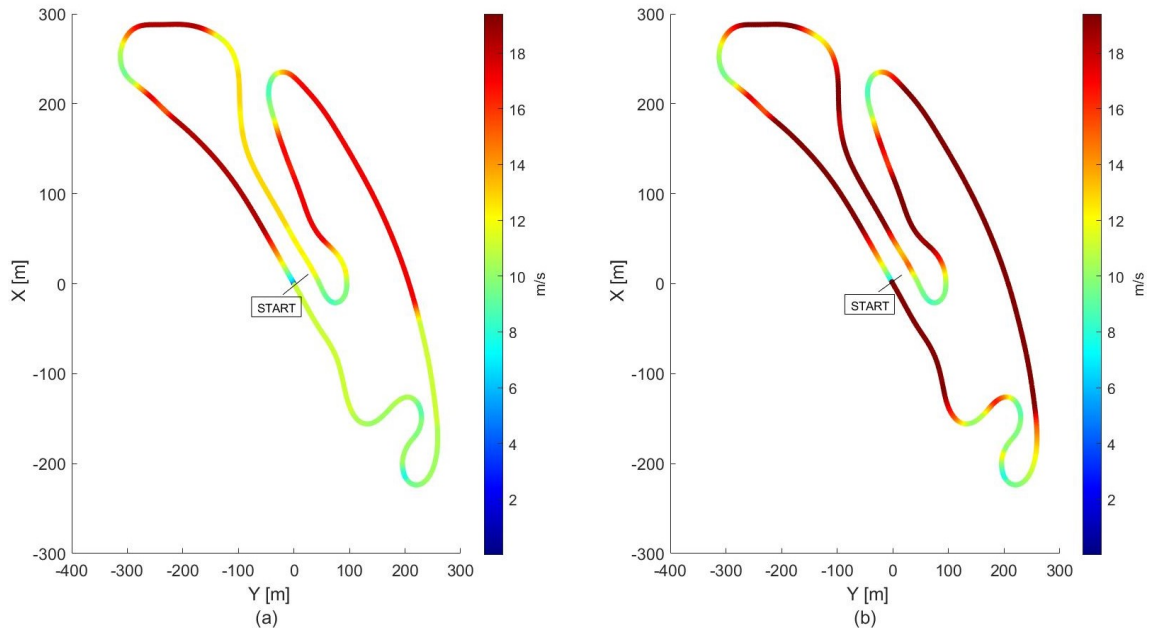


Figure 5.33: Colormap of the longitudinal velocity; (a) With Fuzzy Controller (b) Without Fuzzy Controller -*Berlin Race Track scenario (15 DOF)*

As can be seen from the colormap in Figure 5.33 the velocity of the vehicle adapts to the scene where it is travelling. In the proximity of a curve this decreases, while in a straight line, it tends to assume the maximum value of 70 km/h.

Table 5.6: Berlin Race Track scenario results (15 DOF)

	With Fuzzy Controller	Without Fuzzy Controller
a_{eq} coefficient	0,46 m/s^2	0,81 m/s^2
Likely Reaction	<i>'a little uncomfortable'</i>	<i>'uncomfortable'</i>
$MSDV$	28 %	50.13 %
Maximum velocity	70 km/h	70 km/h
Simulation time	171 s	154 s

In both cases the results of the comfort coefficients are quite high. This is mostly due to the fact that the scenario is a competition racing track that has very sharp curves with high road curvature value. However, the comfort optimization method results in a lower percentage of people who may experience nausea ($MSDV$) and in a lower value of equivalent acceleration a_{eq} perceived by the passengers compared with the classical approach. The a_{eq} index value changes from *'uncomfortable'* to *'a little uncomfortable'* using the proposed method.

5.4 Passengers' comfort results

A deeper analysis of the passengers comfort is presented in this section. In particular, the comfort coefficients a_{eq} and $MSDV$ have been computed for the front passengers and for the rear passengers. The rear passengers, as we will see from the results, are generally less comfortable than front passengers. The simulations are conducted using the fifteen degrees of freedom model in Simscape Vehicle template. In Figure below, the model of the passenger and the body car are illustrated.

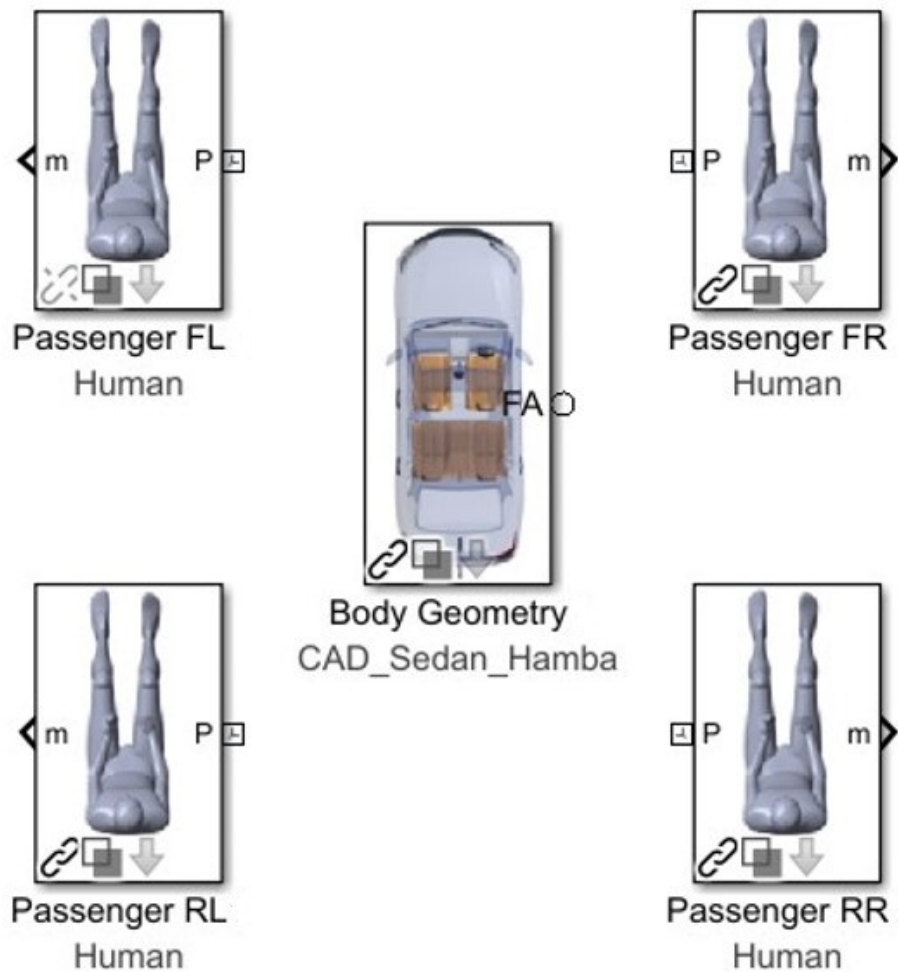


Figure 5.34: Front and rear passengers

In the tables below, the obtained values of the comfort coefficient a_{eq} are presented. The coefficient is computed for the front and rear passengers, in every scenario, and the results obtained with the Fuzzy Controller are compared to the ones obtained without it.

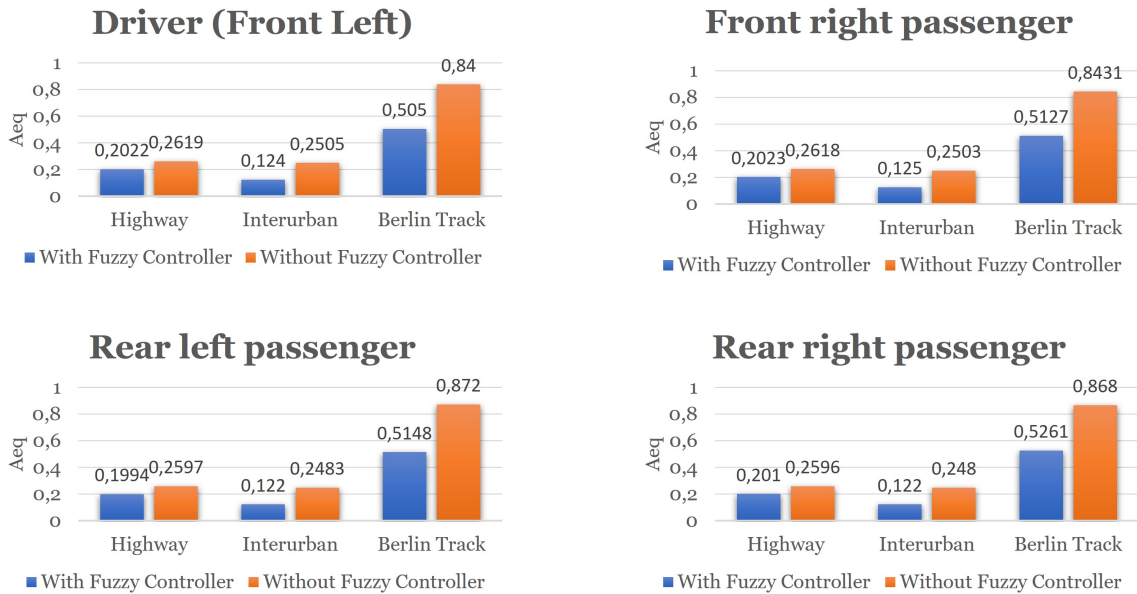


Figure 5.35: Front and rear passengers a_{eq} coefficient

As can be seen from the tables, the rear passengers have slightly greater value of the coefficient a_{eq} and thus they are generally less comfortable than front passengers. Moreover, note that the coefficient a_{eq} is always lower using the Fuzzy Controller than in the case the latter is not considered.

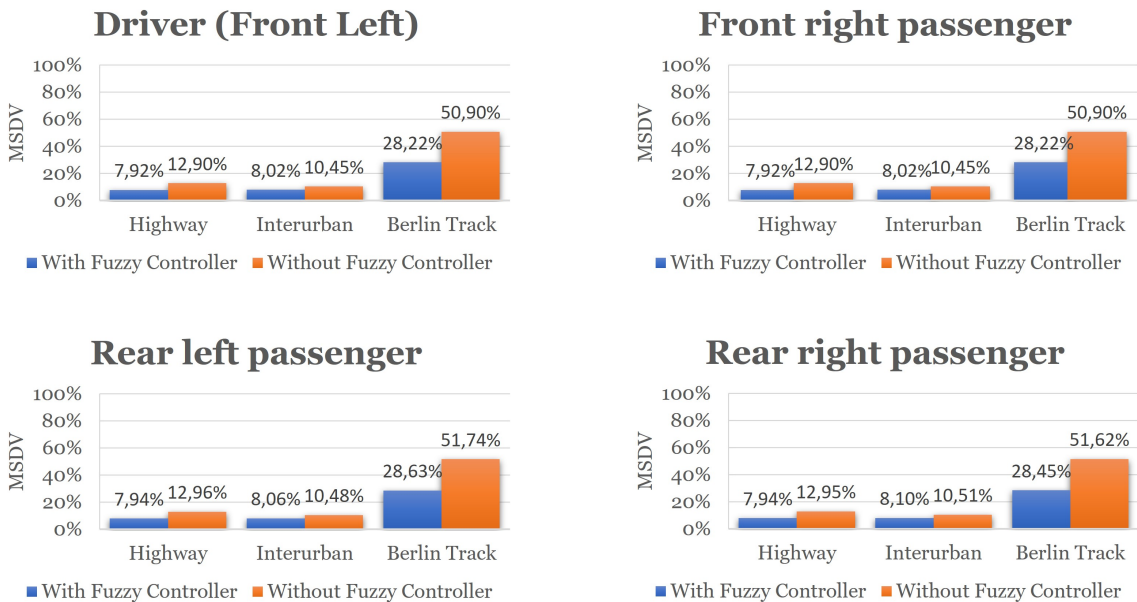


Figure 5.36: Front and rear passengers $MSDV$ coefficient

As in the case of the coefficient a_{eq} , the rear passengers have slightly greater value of the coefficient $MSDV$ and thus they are generally more subject to motion sickness than front passengers. Moreover, note that the coefficient $MSDV$ is always lower using the Fuzzy Controller compared to the case when the latter is not considered.

CHAPTER 6

Conclusions and future works

In this thesis work, a fuzzy comfort-oriented speed profile generator for autonomous passenger cars is presented. After a deep analysis of the state of art and an investigation of the main modules that constitute the overall architecture of an autonomous vehicle, in the first part of the thesis work, the Fuzzy Logic Controller was designed. Fuzzy Logic Controller aims to compute a suitable reference speed profile in order to optimize the passenger's comfort and control performances. To this end, the amount of vibration transmitted to the passengers and the probability to experience motion sickness are evaluated considering two comfort indexes extracted by ISO 2631. These indexes are used to evaluate the performances of the proposed method in the validation phase. The computation procedure of the comfort coefficients is extensively described in this first part of the work.

In the second part of the thesis work, a three degrees of freedom vehicle model is described and used to model the vehicle dynamics. Three different mathematical models have been considered. The first two are related to the kinematic and dynamic model of the vehicle while the third model concerns the linearized model used in the Adaptive Model Predictive Control. Although the 3 DOF model provides low accurate prediction, it is low computationally demanding and for this reason it was used to test the Fuzzy Controller's first design. Afterwards, a fifteen degrees of freedom vehicle model, which is imported from Simscape Vehicle Template, was considered and used to obtain very accurate data from simulations.

In the last part of the thesis work, the results obtained with the Fuzzy Logic Controller are presented and compared to the ones obtained with the classical approach.

Simulations are conducted in virtual scenarios created using Automated Driving Scenario Toolbox[®] on MATLAB[®] and Simulink[®]. Three different scenarios have been considered: an highway scenario where the path has mainly straights and low curvature turns and the maximum speed is set to 130 km/h, an interurban scenario with fairly straight road and slight curves with maximum speed set to 70 km/h and a competition race track with sharp curves and maximum speed set to 70 km/h. Together, they form a comprehensive set of key environments for the evaluation of the proposed method.

The results reported in Chapter 5 shown the effectiveness of the comfort optimization method that results in a lower percentage of people who may experience nausea and in a lower value of equivalent acceleration perceived by the passengers compared to the classical approach. A deeper analysis of the passengers comfort is presented in this chapter. In

particular, the comfort coefficients a_{eq} and $MSDV$ have been computed for both the front and rear passengers. In line with real world experience, the results obtained shown that the rear passengers are generally less comfortable than front passengers.

Regardless of the good results obtained, there are still many possible developments and improvements. The first improvement could be to consider a Neuro-Fuzzy Logic Controller that exploit human driver's velocity planning strategies in straights and curves. Neural network based models can be developed to compute speed profiles under different driving situations.

Another improvement could be to design a Model Predictive Controller that considers the accelerations and jerks in the constrains of the cost function to improve the comfort of the passengers.

Moreover, the model can be implemented in a real-time hardware platform that allows code generation of the model in Simscape.

To conclude, these and other improvements can be made by student that will contribute for autonomous vehicle research at Mechatronics Laboratory LIM.

List of Figures

1.1	History of Autonomous Vehicle Technologies [4]	2
1.2	A self-propelled cart replica at museum Clos Lucé [5]	3
1.3	Wiley Post’s Autopilot “Mechanical Mike” [6]	3
1.4	Ralph R. Teetor’s Cruise Control [7]	4
1.5	James Adams and Les Earnest Stanford Cart [8]	5
1.6	Tsukuba Mechanical, Passenger Vehicle, 1977 [9]	5
1.7	Ernst Dickmanns – VaMoR, 1987 [10]	6
1.8	A LIDAR sensor mounted to an autonomous car [4]	6
1.9	SAE autonomous vehicle standard levels [11]	7
1.10	Timeline of driving assistance technologies[17]	9
1.11	Anti-lock Braking System (ABS) [15]	10
1.12	Electronic Stability Control [16]	10
1.13	Forward collision warning [17]	11
1.14	Lane departure warning [17]	11
1.15	Automatic Emergency Braking [18]	12
1.16	Adaptive Cruise Control [19]	12
1.17	Adaptive Cruise Control [20]	13
1.18	Autonomous vehicle architecture	14
1.19	Fuzzy Logic Controller Architecture	15
1.20	Comfort coefficient computation procedure	16
2.1	Sensors and their range in an autonomous vehicle [21]	21
2.2	The ideal detection result from a 3D LIDAR [22]	22
2.3	LIDAR and RADAR resolution comparison [23]	23
2.4	GPS trilateration principle [24]	24
2.5	Stereo vision working principle [27]	25
3.1	Dubins curves [30]	30
3.2	Osculating circle [31]	31
3.3	Fuzzy Logic architecture	33
3.4	Steps for computing the output [33]	34
3.5	Fuzzy Logic Controller Architecture	35
3.6	Membership function of the first input	36
3.7	Membership function of the second input	36

3.8	Membership function of the third input	37
3.9	Membership function of the output	37
3.10	Comfort coefficient a_{eq} procedure computation	41
3.11	Bode of the High pass filter	42
3.12	Bode of the Low pass filter	42
3.13	Bode of the Acceleration-velocity transition filter	43
3.14	Bode of the band pass filter W_d	44
3.15	Comfort coefficient $MSDV$ procedure computation	45
3.16	Weighting functions; W_f (solid line) for $MSDV$ and W_d (dashed line) for a_{eq} ; ISO 2631-1 [36]	46
4.1	Vehicle Coordinates System [38]	49
4.2	World Coordinates System [39]	50
4.3	Linear single track model [40]	52
4.4	Kinematic of the single track model [40]	52
4.5	Longitudinal vehicle dynamics free-body diagram.[41]	55
4.6	Lateral vehicle dynamics free-body diagram [41]	57
4.7	Relationship between the tire lateral forces and the slip angle [40]	58
4.8	Tires load distribution [40]	59
4.9	Lateral deviation and relative yaw angle errors. [42]	60
4.10	Simscape 15 DoF vehicle model	65
5.1	Highway scenario and road curvature κ	75
5.2	Inter Urban scenario and road curvature κ	76
5.3	Berlin Race Track scenario and road curvature κ	77
5.4	Reference velocity and Longitudinal Actual velocity; (a) With Fuzzy Controller (b) Without Fuzzy Controller - <i>Highway scenario(3 DOF)</i>	78
5.5	Longitudinal Acceleration; (a) With Fuzzy Controller (b) Without Fuzzy Controller - <i>Highway scenario (3 DOF)</i>	79
5.6	Lateral Acceleration; (a) With Fuzzy Controller (b) Without Fuzzy Controller - <i>Highway scenario (3 DOF)</i>	79
5.7	Lateral deviation e_1 and relative yaw e_2 ; (a) With Fuzzy Controller (b) Without Fuzzy Controller - <i>Highway scenario (3 DOF)</i>	80
5.8	Colormap of the longitudinal velocity; (a) With Fuzzy Controller (b) Without Fuzzy Controller - <i>Highway scenario (3 DOF)</i>	80
5.9	Reference velocity and Longitudinal Actual velocity; (a) With Fuzzy Controller (b) Without Fuzzy Controller - <i>Inter-Urban scenario (3 DOF)</i>	81
5.10	Longitudinal Acceleration; (a) With Fuzzy Controller (b) Without Fuzzy Controller - <i>Inter-Urban scenario (3 DOF)</i>	82
5.11	Lateral Acceleration; (a) With Fuzzy Controller (b) Without Fuzzy Controller - <i>Inter-Urban scenario (3 DOF)</i>	82
5.12	Lateral deviation e_1 and relative yaw e_2 ; (a) With Fuzzy Controller (b) Without Fuzzy Controller - <i>Inter-Urban scenario (3 DOF)</i>	83

5.13	Colormap of the longitudinal velocity; (a) With Fuzzy Controller (b) Without Fuzzy Controller - <i>Inter-Urban scenario (3 DOF)</i>	83
5.14	Reference velocity and Longitudinal Actual velocity; (a) With Fuzzy Controller (b) Without Fuzzy Controller - <i>Berlin Race Track scenario (3 DOF)</i>	84
5.15	Longitudinal Acceleration; (a) With Fuzzy Controller (b) Without Fuzzy Controller - <i>Berlin Race Track scenario (3 DOF)</i>	85
5.16	Lateral Acceleration; (a) With Fuzzy Controller (b) Without Fuzzy Controller - <i>Berlin Race Track scenario (3 DOF)</i>	85
5.17	Lateral deviation e_1 and relative yaw e_2 ; (a) With Fuzzy Controller (b) Without Fuzzy Controller - <i>Berlin Race Track scenario (3 DOF)</i>	86
5.18	Colormap of the longitudinal velocity; (a) With Fuzzy Controller (b) Without Fuzzy Controller - <i>Berlin Race Track scenario (3 DOF)</i>	87
5.19	Reference velocity and Longitudinal Actual velocity; (a) With Fuzzy Controller (b) Without Fuzzy Controller - <i>Highway scenario(15 DOF)</i>	88
5.20	Longitudinal Acceleration; (a) With Fuzzy Controller (b) Without Fuzzy Controller - <i>Highway scenario (15 DOF)</i>	89
5.21	Lateral Acceleration; (a) With Fuzzy Controller (b) Without Fuzzy Controller - <i>Highway scenario (15 DOF)</i>	89
5.22	Lateral deviation e_1 and relative yaw e_2 ; (a) With Fuzzy Controller (b) Without Fuzzy Controller - <i>Highway scenario (15 DOF)</i>	90
5.23	Colormap of the longitudinal velocity; (a) With Fuzzy Controller (b) Without Fuzzy Controller - <i>Highway scenario (15 DOF)</i>	90
5.24	Reference velocity and Longitudinal Actual velocity; (a) With Fuzzy Controller (b) Without Fuzzy Controller - <i>Inter-Urban scenario (15 DOF)</i>	91
5.25	Longitudinal Acceleration; (a) With Fuzzy Controller (b) Without Fuzzy Controller - <i>Inter-Urban scenario (15 DOF)</i>	92
5.26	Lateral Acceleration; (a) With Fuzzy Controller (b) Without Fuzzy Controller - <i>Inter-Urban scenario (15 DOF)</i>	92
5.27	Lateral deviation e_1 and relative yaw e_2 ; (a) With Fuzzy Controller (b) Without Fuzzy Controller - <i>Inter-Urban scenario (15 DOF)</i>	93
5.28	Colormap of the longitudinal velocity; (a) With Fuzzy Controller (b) Without Fuzzy Controller - <i>Inter-Urban scenario (15 DOF)</i>	93
5.29	Reference velocity and Longitudinal Actual velocity; (a) With Fuzzy Controller (b) Without Fuzzy Controller - <i>Berlin Race Track scenario (15 DOF)</i>	94
5.30	Longitudinal Acceleration; (a) With Fuzzy Controller (b) Without Fuzzy Controller - <i>Berlin Race Track scenario (15 DOF)</i>	95
5.31	Lateral Acceleration; (a) With Fuzzy Controller (b) Without Fuzzy Controller - <i>Berlin Race Track scenario (15 DOF)</i>	95
5.32	Lateral deviation e_1 and relative yaw e_2 ; (a) With Fuzzy Controller (b) Without Fuzzy Controller - <i>Berlin Race Track scenario (15 DOF)</i>	96
5.33	Colormap of the longitudinal velocity; (a) With Fuzzy Controller (b) Without Fuzzy Controller - <i>Berlin Race Track scenario (15 DOF)</i>	96
5.34	Front and rear passengers	98
5.35	Front and rear passengers a_{eq} coefficient	99

5.36 Front and rear passengers <i>MSDV</i> coefficient	99
--	----

List of Tables

3.1	Rule base	38
3.2	Classification of likely reactions in terms of comfort based on a_{eq} values. [36]	40
3.3	Parameters for the frequency weighting filters of ISO 2631-1	44
4.1	3 DOF vehicle model parameters	64
4.2	15 DOF vehicle model parameters	70
5.1	Highway scenario results (3 DOF)	81
5.2	Inter-Urban scenario results (3 DOF)	84
5.3	Berlin Race Track scenario results (3 DOF)	87
5.4	Highway scenario results (15 DOF)	91
5.5	Inter-Urban scenario results (15 DOF)	94
5.6	Berlin Race Track scenario results (15 DOF)	97

References

- [1] Digital Watch, *The rise of autonomous vehicles*
Available: <https://dig.watch/trends/rise-autonomous-vehicles>
- [2] Pete Goldin, February 20, 2018; *10 Advantages of Autonomous Vehicles*
Available: <https://www.itsdigest.com/10-advantages-autonomous-vehicles>
- [3] Ohio University’s Online Master of Science in Civil Engineering, *The Future of Driving*
March 2, 2021
Available: <https://onlinemasters.ohio.edu/blog/the-future-of-driving/>
- [4] *What are the most important technologies that led to autonomous transportation?* By Adam Kimmel;
Available: <https://www.prescouter.com/2017/11/autonomous-technologies-timeline/>
- [5] Wikipedia,
Available: https://en.wikipedia.org/wiki/Leonardo%27s_self-propelled_cart
- [6] Smithsonian’s National Air and Space Museum, *Wiley Post’s Autopilot “Mechanical Mike”*
Available: <https://airandspace.si.edu/multimedia-gallery/5074hjpp>
- [7] David Sears, *The Sightless Visionary Who Invented Cruise Control*; March 8, 2018
Available: <https://www.smithsonianmag.com/innovation/sightless-visionary-who-invented-cruise-control-180968418/>
- [8] WIRED, *A brief history of autonomous vehicle technology*
Available: <https://www.wired.com/brandlab/2016/03/a-brief-history-of-autonomous-vehicle-technology/>
- [9] Ronan Glon, 4 December 2018; *Journey: the picture history of the driverless car*
Available: <https://www.autocar.co.uk/slideshow/journey-picture-history-driverless-car#10>
- [10] Sommer, Torsten. (2021). *Physics for a 3D Driving Simulator*.
- [11] SAE International “SAE J3016”,
Available: <https://www.sae.org/news/press-room/2018/12/sae-international-releases-updated-visual-chart-for-its-%E2%80%9Clevels-of-driving-automation%E2%80%9D-standard-for-self-driving-vehicles>

- [12] The 6 Levels of Vehicle Autonomy Explained
Available: <https://www.synopsys.com/automotive/autonomous-driving-levels.html>
- [13] Adam Kaslikowski; June 30, 2019 *Everything you need to know about autonomous vehicles*
Available: <https://www.digitaltrends.com/cars/the-current-state-of-autonomous-vehicles/>
- [14] 2021 Robert Bosch GmbH, *Antilock braking system* 25 February 2021 <https://www.bosch-mobility-solutions.com/en/solutions/driving-safety/antilock-braking-system/>
- [15] Shakti Nath Jha, 25 February 2021 *Types of Anti-lock Braking System (ABS) Used in Cars - All Details*
Available: <https://www.91wheels.com/news/types-of-anti-lock-braking-system-abs-used-in-cars>
- [16] 2021 Robert Bosch GmbH, *Electronic stability program*
Available: <https://www.bosch-mobility-solutions.com/en/solutions/driving-safety/electronic-stability-program/>
- [17] National Highway Traffic Safety Administration, *Driver Assistance Technologies*,
Available: <https://www.nhtsa.gov/equipment/driver-assistance-technologies#collision-warning-30631>
<https://www.nhtsa.gov/technology-innovation/automated-vehicles-safety>
- [18] 2021 Robert Bosch GmbH, *Automatic emergency braking* Available: <https://www.bosch-mobility-solutions.com/en/solutions/assistance-systems/automatic-emergency-braking/>
- [19] Volvo Car Group, feb 10, 2004 *Controllo di crociera adattativo (ACC, Adaptive Cruise Control)*
Available: <https://www.media.volvocars.com/it/it-it/media/photos/8158>
- [20] Quattroruote, *Cos'è e come funziona il lane assist*
Available: <https://www.quattroruote.it/guide/Guida-assistita/cos-e-e-come-funziona-il-lane-assist.html>
- [21] Paul Christianson; Sep 30, 2020 *Billions of Miles of Data: The Autonomous Vehicle Training Conundrum*
Available: <https://blog.cloudfactory.com/autonomous-vehicle-training-conundrum>
- [22] Pendleton, Scott & Andersen, Hans & Du, Xinxin & Shen, Xiaotong & Meghjani, Malika & Eng, You & Rus, Daniela & Jr, Marcelo. (2017). Perception, Planning, Control, and Coordination for Autonomous Vehicles. *Machines*. 5. 6. 10.3390/machines5010006.
- [23] Swarit Dholakia Mar 14, 2019 *Perception: How Self-Driving Cars 'See' the World*
Available: <https://swarit.medium.com/perception-how-self-driving-cars-see-the-world-ae630636f4c>

- [24] *Do You Know How GPS Works? (It Might Surprise You)*
Available: <https://gpstracker-malaysia.com/do-you-know-how-gps-works/>
- [25] *How does a vehicle GPS work?*
Available: <https://www.gpstracker.at/how-does-a-vehicle-gps-work/>
- [26] *Difference Between GPS and DGPS*
Available: <https://grindgis.com/blog/difference-between-gps-and-dgps>
- [27] Available: <https://github.com/bkaas/active-stereo-distance>
- [28] Luciani, Sara & Bonfitto, Angelo & Amati, N. & Tonoli, Andrea. (2020). Model predictive control for comfort optimization in assisted and driverless vehicles. *Advances in Mechanical Engineering*. 12. 2020. 10.1177/1687814020974532.
- [29] L. E. Dubins. On curves of minimal length with a constraint on average curvature, and with prescribed initial and terminal positions and tangents. *American Journal of mathematics*, 79(3), 497-516, (1957).
- [30] Yardimci, Ahmet & Karpuz, Celal. (2019). Shortest path optimization of haul road design in underground mines using an evolutionary algorithm. *Applied Soft Computing*. 83. 10.1016/j.asoc.2019.105668.
- [31] Wikipedia
Available: https://en.wikipedia.org/wiki/Curvature#Osculating_circle
- [32] Irfan Khan, *Combined lateral and longitudinal control for autonomous driving based on Model Predictive Control*
- [33] Wikipedia
Available: https://en.wikipedia.org/wiki/Fuzzy_control_system#Fuzzy_control_in_detail
- [34] Thomas G. Dobie *Motion Sickness , A Motion Adaptation Syndrome 2019, Volume 6*
- [35] Wikipedia
Available: https://en.wikipedia.org/wiki/Motion_sickness#Cause
- [36] ISO 2631
- [37] Jenny Eriksson Lars Svensson *Tuning for Ride Quality in Autonomous Vehicle Application to Linear Quadratic Path Planning Algorithm*
- [38] Kissai M., Monsuez B., Mouton X., Martinez D. and Tapus A., *Adaptive robust vehicle motion control for future over-actuated vehicles*, *Machines*, 7(2), 26, 2019.
- [39] Matlab,
Available: <https://it.mathworks.com/help/driving/ug/coordinate-systems.html>
- [40] Schramm, Dieter. *Vehicle Dynamics. Springer Berlin Heidelberg, 2018*

- [41] Samak, Chinmay and Samak, Tanmay and Kandhasamy,Sivanathan. (2020). *Strategies for Autonomous Vehicles*.
- [42] [Website], *Lane Keeping Assist System Using Model Predictive Control*, Available: <https://it.mathworks.com/help/mpc/ug/lane-keeping-assist-system-using-model-predictive-control.html>

